PHYSIK-DEPARTMENT

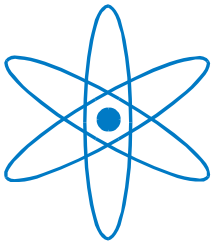

Modeling cell adhesion and its control mechanisms with a vesicle-substrate system

Dissertation

von

Ana-Sunčana Smith

TECHNISCHE UNIVERSITÄT

MÜNCHEN

Physik-Department
Der Technischen Universität München
Lehrstuhl für Biophysik

Modeling cell adhesion and its control mechanisms with a vesicle-substrate system

Ana-Sunčana Smith

Vollständiger Abdruck der von der Fakultät für Physik der Technischen Universität München zur Erlangung des akademischen Grades eines

Doktors der Naturwissenschaften (Dr. rer. nat.)

genehmigten Dissertation.

Vorsitzender:

Univ.-Prof. Dr. R. Netz

Prüfer der Dissertation:

1. Univ.-Prof. Dr. E. Sackmann em.
2. Univ.-Prof. Dr. U. Seifert, Universität Stuttgart

Die Dissertation wurde am 22.11.2004. bei der Technischen Universität München eingereicht und durch die Fakultät für Physik am 16.12.2004. angenommen.

kćerima i majkama

Acknowledgments

I extend my thanks to all the people who helped me in my professional, personal and any other life during my Doctorate degree. Many, however, warrant special mention:

Firstly, I would like to extend my sincerest thanks to my Doktorvater, Professor Erich Sackmann for the unconditional trust he has placed in me. His contagious passion for Biological Physics, great ideas, and the beautiful working environment that he created in E22, were my driving forces. His ability to recognize and provide the support and understanding which I needed, when I needed, has left me with a feeling of being an extremely well-managed student. Danke für alles.

I am very lucky to have had the privilege to work with Professor Udo Seifert. Although staying behind the scenes, he provided me with unrestrained supervision, and introduced me to the field of theoretical biophysics. His sound advice and always immediate response to my constant questions are greatly appreciated. Thank you for taking me into your fold.

Dr. Barbara Lorz and Dr. Stefanie Gönnenwein were there when I just started. Their experiments were both the inspiration and the grounding for my beginnings in the field of vesicle adhesion. Equally unforgettable were the little after-hours chats and the coffee breaks which made my days much warmer.

Thanks are extended to past and present members of E22, for the collegial atmosphere, assistance and laughter which they provided in the day-to-day experience. Moments with Dr. Kheya Sengupta and Dr. Gjertrud Maurstad will always be in my memories. I would also like to mention Dr. Wolfgang Feneberg, Dr. Doris Heinrich and Dr. Felix Linke.

I am extremely grateful to the Frauenbeauftragte der Technische Universität München for enabling me to participate in Hochschul- und Wissenschaftsprogramm (HWP II) that awarded me a bursary for postgraduate students in the final stages of a Doctorate degree.

Particular words are also addressed to Christian Daniel, Katrin Prechtel, Jörg Uhde and their partners Tina, Schüssel and Sabine for being much more than colleges - for being

friends. Thank you for opening the door to the German culture and helping with the sometimes bewildering aspects of a life as a foreigner. To this end, my special thanks are extended to the Oberschleissheimer Families Međugorac and Pejačević and also to Frau Christine Singer for giving me and my family the impression of being welcomed and home.

Somewhat strange paths took me to Australia for five months during my Doctorate. The welcome extended to me by the entire Department of Applied Mathematics at the Australian National University, Canberra, ACT is greatly appreciated. Especially, Dr. Tim Senden, Dr. Gerd Schröder, Dr. Anke Karlsson with her partner Dr. Simon Bennett, and Mr Holger Averdunk helped to make this visit a pleasant experience.

In the final months of my Doctorate, I spent extensive periods of time at the Institute for Physics of the University of Zagreb, Croatia. Assoc. Professor Katarina Uzelac and her Group provided support during this stage and for this I am very grateful. Dr. Davorin Lovrić, and the other members of the institute were a source of great cheering and fun.

With warmth in my heart, I have to thank my mother Solange Barišić and my sister Ivana Tanovitski as well as all other members of my family for helping unconditionally and decreasing the load whenever possible. Wherever you are, in Croatia, Russia, Switzerland, Australia or France, you are in my thoughts.

At last, but as great as to the first, much praise must go to David and Lana: The sacrifices you made enabled me to come to the point where I can write these final words. For this and for the life you are sharing with me, thank you.

Table of Contents

Abstract

In order to study the process of cell adhesion and its underlying mechanisms, a theoretical model system has been developed. The model consists of a functionalized vesicle capable of interacting with an activated substrate. More specifically, mobile ligands incorporated into the vesicle membrane can undergo specific interactions with receptors immobilized on the surface of the substrate. Under suitable conditions, a zone of contact is formed between the vesicle and the substrate, and a process known as adhesion ensues.

The model is simply constructed yet conceptually rich. In particular, explicit consideration is given to the following factors: (*i*) the enthalpy of binding (*ii*) the mobility of the ligands through a contribution to the mixing entropy, (*iii*) the bending energy of the vesicle shape, (*iv*) the finite number of ligands contained in the vesicle, and (*v*) the constant density of receptors on the substrate. The equilibrium conditions of such a canonical ensemble is studied in detail and several adhesion regimes, dependent upon the densities of the system constituents and the binding strength of the ligand-receptor pair, are identified.

Of the many interesting outcomes emerging from the model, the most important can be hierarchically laid out as follows: (*i*) The explicit treatment of the bending energy shows that the determination of the vesicle shape can be decoupled from the equilibration of ligand-receptor binding in the contact zone. (*ii*) The density of bonds formed is found never to decrease in response to a reduced size of the contact zone. (*iii*) The formation of bonds results in an effective adhesion strength which acts as a spreading pressure. This key parameter, which has been calculated and analyzed in considerable detail, provides a bridge between the discrete model elaborated herein and the standard continuous models for the calculation of vesicle shapes. The model as a whole is shown to provide an extremely useful “toolkit” for the direct interpretation of experiments concerning vesicle adhesion. Furthermore, its natural extensions are found to provide a new window through which to view several mechanisms for adhesion control.

The first such control mechanism investigated is the competitive binding of ligand antagonists that are dissolved into the solution surrounding the vesicle. The analysis of recent experiments, in which adhered vesicles were treated with antibodies and observed with reflection interference contrast microscopy, results in the identification of two distinct unbinding mechanisms. In combination with the adaptation of the above theoretical model for basic vesicle adhesion, consideration of these data gives rise to a

self-consistent picture. When the vesicle-substrate contact zone is densely packed with ligand-receptor bonds, antagonists are unable to penetrate the zone. Instead they exert a two-dimensional lateral osmotic pressure that results in the retraction of the rim of the adhesion plate. The resulting reduction of the contact-zone size is accompanied by a heightened binding of ligands to receptors and an associated increase in the density of bonds within the zone. Not surprisingly, the effective adhesion strength is enhanced as a result. The latter quantity is capable of resisting the antagonistic pressure and the balance between the two results in a new equilibrium state. The second unbinding mechanism takes place when antagonists penetrate the vesicle-substrate contact zone without influencing its size. The antagonists are then in direct competition with the mobile ligands for the stationary receptors. Both experiment and theory provide a sigmoidal dependence of the equilibrium number of ligand-receptor bonds on the logarithm of the antagonist concentration. The qualitative agreement regarding both unbinding mechanisms suggests that the underlying physical phenomena are well-accounted for in this work.

The second control mechanism explored herein is the influence of a force externally exerted upon the vesicle membrane. The force opposes the vesicle spreading pressure and is found to serve as a requisite for maintaining a particular size of the contact zone. Within a contact zone constrained thus, the equilibrium number of formed bonds can be determined by the use of the basic adhesion model, which also provides the appropriate effective adhesion strength. The latter can be used as an input parameter for continuous models that result in vesicle shapes. However, in order to determine the shape under these circumstances, the continuous calculations needed to be expanded to explicitly account for a force in geometrical opposition to the contact zone. For weakly adhered vesicles, continuous deformations are found to precede a discontinuous unbinding transition in which the vesicle disengages from the substrate while still in possession of a finite contact zone. In contrast, strongly bound vesicles are found to undergo a transition to a tethered shape, which continuously detaches from the surface. The implications of both adhesion regimes on the equilibrium number of ligand-receptor pairs are elucidated.

As was the case for the antagonist-induced unbinding, the experimental and theoretical advances combine synergistically once again. This time the result is an explanation of the adhesion equilibrium under constant force. The favorable comparison between the theoretically calculated shapes and those obtained from confocal fluorescence measurements, supports the strategy of decoupling of the shape from the equilibrium in the contact zone. Reflection interference contrast microscopy measurements, of vesicles pulled with magnetic tweezers, are also in agreement with the predictions of the model.

Zusammenfassung

Ein theoretisches Modell zum Verständnis von Zell Adhäsionsprozessen und der zugrunde liegenden Prozesse wurde entwickelt. Es besteht aus einem funktionalisierten Vesikel, das mit einer aktiven Membran interagieren kann. Mobile Liganden, die in die Vesikelmembran eingebunden sind, können spezifische Bindungen mit immobilisierten Rezeptoren auf der Substratoberfläche eingehen. Unter günstigen Bedingungen wird eine Kontaktzone zwischen Vesikel und Substrat gebildet, ein Prozess, der als Adhäsion bezeichnet wird.

Das Modell ist einfach aufgebaut aber konzeptuell vielseitig. Folgende Faktoren wurden speziell berücksichtigt: (*i*) die Bindungsenthalpie (*ii*) Die Ligandenmobilität aufgrund eines Beitrags der Mischungsentropie (*iii*) die Biegeenergie der Vesikelform (*iv*) die finite Anzahl von Liganden im Vesikel und (*v*) die konstante Rezeptordichte auf dem Substrat. Die Gleichgewichtsbedingung eines solchen kanonischen Ensembles wird im Detail untersucht und mehrere Adhäsionsregime wurden identifiziert, je nach Dichte der Systeme, der beteiligten Moleküle und der Bindungsstärke der Ligand-Rezeptor Paare.

Von den vielen interessanten Ergebnissen, die aus dem Modell folgen können die wichtigsten wie folgt hierarchisch dargestellt werden: (*i*) Die explizite Untersuchung der Biegeenergie zeigt, dass die Vesikelform unabhängig vom Gleichgewicht der Ligand-Rezeptor Bindung in der Kontaktzone ist (*ii*) Die Bindungsdichte verringert sich nicht falls die Kontaktzone verkleinert wird, (*iii*) Die Bildung von Bindungen resultiert in einer effektiven Adhäsionsstärke die als Spreitdruck fungiert. Dieser fein ausgearbeitete Schlüsselparameter bildet eine Brücke zwischen dem diskreten Modell dieser Arbeit und dem konventionellen Kontinuumsmodell zum Berechnen von Vesikelformen. Das Modell als Ganzes liefert ein extrem nützliches Werkzeug, um Adhäsionsexperimente zu interpretieren. Zusätzlich kann die dieses Modells ein neues Fenster öffnen, durch die mehrere Adhäsionsmechanismen sichtbar sind.

Einer dieser untersuchten Kontrollmechanismen ist das kompetitive Binden von Antagonisten, der Liganden die in der Lösung in der Umgebung der Vesikel zu finden sind. Die Analyse neuer Experimente, in denen die Rezeptor-Liganden-Wechselwirkung durch Zugabe von Antikörpern geschwächt wurde, zeigt zwei distinkte Entbindungsmechanismen. Durch Anwendung des theoretischen Modells Vesikeladhäsion lassen sich die

Daten in selbstkonsistenter Weise interpretieren. Wenn die Kontaktzone zwischen Vesikel und Ligand dicht mit Ligand-Rezeptor-Paaren belegt ist, können Antagonisten nicht eindringen. Stattdessen üben sie einen zweidimensionalen lateralen osmotischen Druck aus, der zu einer Retraktion des Randes der Adhäsionsscheibe führt. Die Verkleinerung der Kontaktzone wird von einer erhöhten Bindung von Liganden an Rezeptoren begleitet und führt außerdem zu einer Erhöhung der Anzahl von Bindungen. Die effektive Bindungsstärke wird dadurch erhöht und widersteht daher dem Antagonistendruck. Dadurch wird eine neuer Gleichgewichtszustand erreicht.

Der zweite Entbindungsmechanismus tritt auf, wenn Antagonisten in die Vesikel-Substrat Kontaktzone eindringen, ohne deren Größe zu verändern. Die Antagonisten stehen dann in direktem Wettbewerb mit den mobilen Liganden um die stationären Rezeptoren. Sowohl Experiment als auch Theorie liefern eine sigmoidale Abhängigkeit der Gleichgewichtsanzahl von Ligand-Rezeptor Bindungen vom Logarithmus der Antagonistenkonzentration. Die qualitative Übereinstimmung zwischen Theorie und Experiment liefert Einblicke in die zugrunde liegenden physikalischen Phänomene.

Der andere hier untersuchte Kontrollmechanismus ist die extern angewandte Kraft auf die Vesikelmembran. Die Kraft wirkt dem Spreitdruck entgegen und dient als Voraussetzung, um eine bestimmte Größe der Kontaktzone beizubehalte. Innerhalb einer begrenzten Kontaktzone kann die Gleichgewichtsanzahl von Bindungen durch die Anwendung des grundlegenden Adhäsionsmodells bestimmt werden, was die Bestimmuzng der effektiven Adhäsionsstärke ermöglicht. Diese kann als Eingangsparmeter für das Kontinuumsmodell zur Vesikelformbestimmung benutzt werden. Um jedoch die Form unter diesen Umständen zu bestimmen, mussten Rechnungen auf der Basis der Kontinuumstheorie erweitert werden um der Kraft rechnung zu tragen die der Kontaktzione entgegen wirkt. Für schwach adhärierte Vesikel geht die kontinuierliche Deformation einer nichtkontinuierlichen Ablösung voraus, wobei das Vesikel sich vom Substrat ablöst obwohl noch eine finite Kontaktzone vorhanden ist. Im Kontrast dazu bilden stark gebundene Vesikel schlauchartige Ausstülpung, wobei sie sich kontinuierlich vom Substrat ablösen. Der Einfluß beider Adhäsionsregime auf die Gleichgewichtsanzahl von Ligand-Rezeptor Paaren wird beleuchtet.

Wie im Fall der Antagonisten-induzierte Entbinden, stehen auch hier Experiment und Theorie im Einklang. Damit läßt sich das Adhäsionsgleichgewichts unter konstanter Kraft interpretieren. Die Übereinstimmung von theoretisch berechneten Formen und

mittels konfokalen Fluoreszenzmikroskopie experimentell bestimmten Formen zeigt den Erfolg meiner Strategie die Vesikel-Form vom Gleichgewicht in der Kontaktzone zu entkopeln. Auch Messungen mit Reflektions-Interferenz-Kontrast-Mikroskopie von Vesikeln, die mit magnetischen Pinzetten verformt werden, sind im Einklang mit den Vorhersagen dieses Modells.

CHAPTER 1

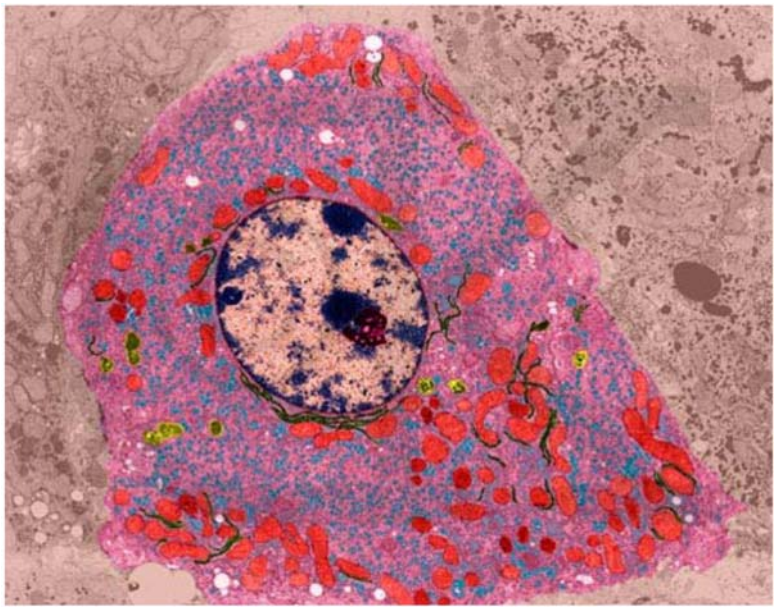

PHYSICAL ASPECTS OF CELL ADHESION 2

Above: Human kidney cell. Picture from wwww.Dennis.Kunkel.com

Chapter 1

PHYSICAL ASPECTS OF CELL ADHESION

Biological cells can be considered to be small-scale machines that have a permanent need to process a large amount of input signals in order to perform their normal function. As well as having to be capable of functioning in widely varying circumstances, they are required to cope with an extremely noisy environment. For these reasons, the control mechanisms of most biological processes have had to develop so as to be able to permanently monitor and correct cellular performance.

The structures from which cells are comprised can be, at least from a simplistic point of view, divided into two groups. The first group is responsible for cell functioning and consists of various small molecules, proteins and nucleic acids. Interactions between molecules belonging to this group are the foundation of every action performed by the cell. In order for the system to function properly, a highly sophisticated set of chemically and physically induced signaling pathways has had to develop. The understanding of this signal transmission, along with structures of the proteins and the details of gene expression, falls mainly within the realms of biology and biochemistry. The investigations in these fields have, to date, revealed an amazing complexity in the cellular response system.

The second of the two groups provides structural integrity to cells and consists mainly of membranes and the cytoskeleton. It is these components that initially caught the attention of the physicist. Apart from having amazing material properties that can be exploited beyond pure biological aspects, the membranes and polymers comprising the cytoskeleton provide a working environment for the first group of molecules. For example, in contrast to the situation in solution, molecules which connect to membranes and the cytoskeleton can sustain force. Furthermore, due to the strong coupling of the biochemical reactions to the spatial coordination provided by membranes and the cytoskeleton, biological signaling is subject to a plethora of physical constraints. Indeed,

many signaling pathways, particularly those involving the adhesion of cells, involve protein diffusion and aggregation guided by these cellular structures. It is this aspect of cell recognition by adhesion that can be understood by means of statistical physics and enables the treatment of membrane-embedded polymer and protein interactions that is undertaken in this thesis.

1.1 The cell

As a consequence of a common heritage, certain physical properties and biochemical processes are common to virtually all forms of life, from single-cell organisms such as bacteria to multi-cellular plants and animals. This attribute implies that a great technical advantage may be attained if these universal processes can be conveniently studied in simple organisms such as bacteria [1] or even further, in artificial cells [2].

Cells are categorized into two types: nucleus-containing (or eukaryotic) cells are the building blocks for all multi-cellular organisms as well as some single-cell organisms (Figure 1.1). Cells with no nucleus, called prokaryotic cells, are the second type and are characteristic for bacteria. From the physical point of view, a eukaryotic cell can be presented as a system of four elastic shells. The inner shell is the hardest and consists of a nucleolus, where the ribosomes are formed, which is embedded in a nucleus. The cytoplasm forms the second shell that houses a large number of organelles, such as the endoplasmic reticulum, lysosomes, mitochondria, golgi body etc., that are essential for cell function. Within the cytoplasm, numerous fibrous proteins (actin and intermediate filaments as well as microtubuli) form an entangled network referred to as the cytoskeleton (Figure 1.2). The cytoskeleton maintains the shape of a cell as well as serving to anchor the organelles. It also regulates the cell motility and controls internal structural movements [1]. The actin filaments in the outer part of the cytoplasm form a cortex and are the main ingredient of the third shell.

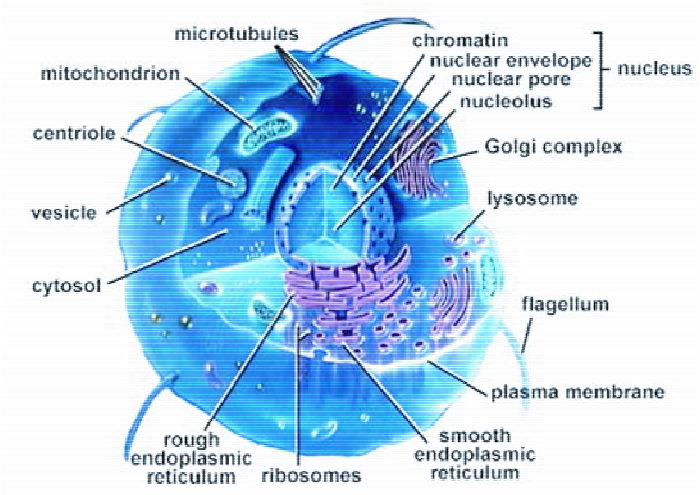

Figure 1.1: Diagram of a eukaryotic cell.
Figure obtained from: http://www.biosci.uga.edu/almanac/bio_103/notes/may_15.html

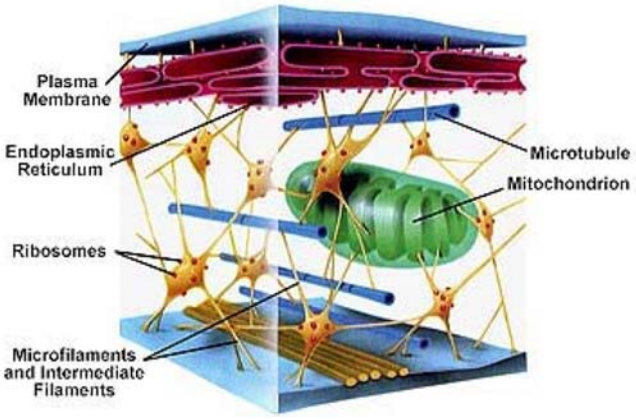

Figure 1.2: Schematic view of the cytoskeleton. Image from Prentice Hall.

The outermost of the four shells consists of a membrane encasing the cell. This membrane physically and chemically isolates the cell from its environment. In order to control the passage of water and salt between the interior and the exterior of the cell, the membrane must contain a variety of channels, carriers, and pumps which are modulated by signaling molecules such as hormones and whose transport is controlled by several classes of physiochemical variables [3]. Membranes also house signaling molecules through which intracellular sites can receive information about the extracellular environment without the signal-carrying molecules actually entering the cell [4]. This generally occurs by the activation of GTPases, through a conformational change that takes place in response to the binding of extracellular material. In addition, enzymes tethered in membranes catalyze reactions that occur on the membrane surface [1]. As this outer shell is the one responsible for cell adhesion, several details relevant to cell membrane structure will be outlined in the following section.

1.1.1 Cell Membrane Structure

All cell membranes are constructed from phospholipids and proteins (Figure 1.3) and can be generally described by the fluid mosaic model introduced by Singer and Nicolson [5]. Lipids provide the basic confinement function of membranes. Due to the amphiphilic nature of phospholipids, which allows them to self-assemble in water, the plasma membrane (but also intracellular membranes) is in the form of bilayer (Figure 1.4). Furthermore, measurements of lateral diffusion properties of phospholipids, by the introduction of markers, have furnished a diffusion constant between 10^{-7} and 10^{-9} cm^2/sec [6,7]. Although this diffusion constant is less than in water, it is several orders of

magnitude larger than the diffusion between the inner and outer leaflets. Such, "flip-flopping" of lipids between two leaflets of the bilayer takes place on a time-scale of hours due to the large activation barrier for dragging a polar head group through the hydrocarbon chain region [8]. The low solubility of lipids in water (10^{-12} molar) makes the bilayer very stable [9]. Consequently, the number of lipids within the bilayer and bilayer leaflets is constant on the time scales of an experiment. For a constant temperature, the total area of the bilayer is constant, since it can adjust to its optimal value.

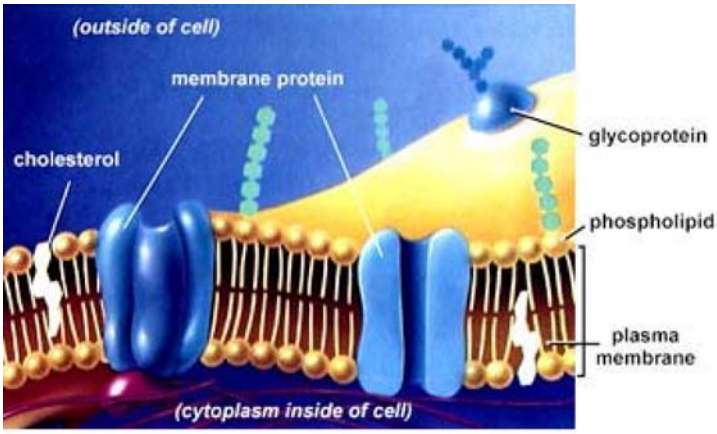

Figure 1.3: Diagram representing the cell membrane. The figure is obtained from: http://www.biosci.uga.edu /almanac/bio_103/notes /may_15.html

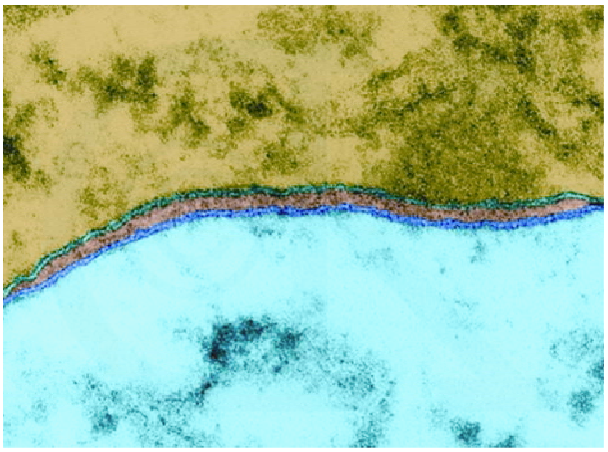

Figure 1.4: Electron micrograph of cell membranes from opposing neurons stained in blue and green. (TEM x436,740). Because the electron-opaque heavy metals combine strongly with the polar heads and much less with the hydrocarbon chains of phospholipids, the outer leaflets of the membrane appear dark, whereas the central portion appears light. The brown stained area between two membranes consists of the glycocalix embedded into the extracellular matrix. This image is from: www.DennisKunkel.com.

A very important aspect of the biological function of fluid membranes is their elastic properties. Any shear deformation relaxes by flow within the membrane resulting in a vanishing zero-frequency shear modulus. Thus, fluid membranes exhibit only two types of elastic deformations [10,11]. The stretching of a lipid bilayer is limited to small deformations characterized by a compressibility modulus of the order of 200 mJ/m^2. However, membranes tend to rupture as soon as their surface area is increased by about 4%. Bending deformations of membranes are governed by the low bending rigidity κ~10-100 k_bT. Furthermore, the bending properties of membranes are regulated by the intrinsic presence of cholesterol. The role of this small steroid alcohol is to increase the membrane fluidity but it also increases the bending stiffness of the phospholipids bilayer considerably.

The fluidity of the membrane is, however, strongly dependent on the types of phospholipids as well as on the temperature [9]. Several phases of lipids can be observed by a decrease of temperature. Typically, fluid lamellar phases at higher temperatures are replaced by gel phases at lower temperatures. At low concentrations of lipid, cubic and hexagonal-liquid-crystalline phases can be observed [12]. However, for cells, the fluidity of the plasma membrane is essential for normal function.

The diffusion of proteins, ions and sugars across the membrane is very unlikely. Thus osmotic conditions within the membrane are maintained by the relatively fast diffusion of water molecules. However this implies that special mechanisms have had to be developed in order to transport the material between the outer region and the region that the membrane is enclosing.

The lipids and cholesterol provide a matrix for embedding the proteins that impart membranes with their specialized functions such as transport, signaling, catalysis etc. Due to the fluidity of the matrix, large proportions of proteins are able to diffuse laterally in the bilayer with a characteristic diffusion constant of 10^{-10} cm^2/sec [6]. Some membrane proteins, on the other hand, appear to be relatively immobile in the membrane, presumably because they are tethered to the cytoskeleton. Furthermore, there are two types of proteins that differ in their disposition in the membrane. The ones associated with the hydrophilic surface of the membrane are called peripheral proteins. Such proteins are water soluble and easy to extract. Proteins anchored in the lipid bilayer are called integral proteins. Their diffusion is somewhat slower. Rather than being water

soluble, integral proteins are soluble in detergents and are thus relatively difficult to extract from the membrane.

In addition to lipids and proteins, some membranes contain carbohydrates. The carbohydrates are, in many cases, attached to lipids in order to form glycolipids (Figure 1.3). The carbohydrates can also be part of so-called glycoproteins, which are membrane spanning proteins exposing several oligosaccharides on their outer leaflet domain toward the cell exterior. Both glycolipids and glycoproteins participate in the glycocalix which is a macromolecular film that covers the cell surface and plays a critical role in the processes of cell recognition and protection [13,14].

The proportions of lipids, proteins and carbohydrates vary among different types of cells and are in accordance with the cell function (Table 1.1). For example, a major function of myelin is to provide electrical insulation of neurons, which is consistent with the high proportion of lipid relative to protein. On the other hand, the erythrocyte travels a long way through blood vessels and the large fraction of carbohydrates serves to provide a substantial glycocalix so as to prevent unwanted interaction with other floating cells.

Table 1.1: Percentage composition by weight of proteins, lipids, and carbohydrates in cellular membranes for different types of cells. Adapted from Darnell *et al.*[15].

Membrane type	%protein	%lipid	%carbohydrate
Myelin	18	79	3
Mouse liver	44	52	4
Human erythrocyte	49	43	8
Amoeba	54	42	4
Halobacterium purple membrane	75	25	0

The salient feature that arises from the previous discussion is that the cell membrane can be described as a two-dimensional fluid structure in which diffusible membrane components are relatively free to move laterally, but whose diffusion in the orthogonal direction is much more restricted. This outcome has a crucial impact on the theoretical approach to cell membranes. In particular, the above properties allow membranes to be

modeled as two-dimensional elastic sheets embedded into a three-dimensional space [10,11,16].

1.2 Cell adhesion

Cell adhesion may be considered as a wetting process of a complex fluid droplet which is governed by the interplay of many factors, such as numerous generic interfacial forces [13,17] and membrane elasticity [18,19]. However, the key to the high specificity of cell recognition relies on the topological and chemical complementarities of proteins interacting at the interface of two cells. These interactions, also called *lock and key forces*, can be formed by bonds between identical (homophilic) receptors embedded in opposing membranes, or between receptors and conjugate ligands exposed on the surface of the cell [20]. The generic forces are controlled by the glycocalix. This film can extend up to 40 nm into the extracelluar space and can exert strong steric repulsive forces between the adhering interfaces. The constituents of this film can thus fulfill a repelling function, counteracting the formation of adhesive bonds [18].

The mobility of at least one binding partner involved in the specific linkages is essential for the strengthening of adhesion by the formation of adhesion patches (also called immunological synapses). These patches allow cells to form very strong adhesion sites which can also act as focal points for the formation of stress fibers and muscle-like actin-myosin assemblies (Figure 1.5.). Such strengthening is essential for cells subjected to strong hydrodynamic forces, as is the case for the endothelial cells lining the inner surface of blood vessels.

Figure 1.5: Focal adhesion points can be seen at the contact between the cells. Actin filaments stabilize the adhesion contacts. This picture is obtained from: www.helthsystem.virginia.gov

Focal adhesion points have both structural and signaling functions. From a structural point of view, they act as pinning sites and are needed by the cell in order to spread on

the surface. On the other hand, a lack of different pathways signaling successful adhesion to the cell can cause death [21].

Given that the presence of only 10^4 specific adhesive molecules on the cell surface is sufficient for the normal functioning of the cell [19], the efficiency of the cell adhesion mechanism is indeed stunning. In order to enable such sophistication in the very noisy environment typical for the cell surrounding, several control mechanisms for cell adhesion must act.

1.2.1 Control mechanisms

Key control parameters in the process of cell adhesion are the densities of the membrane-bound receptors (or ligands) and the repelling molecules. The latter can either be embedded in one of the membranes or it can reside in the tissue. An example of the former type of repelling molecule is the glycoprotein CD43 expressed at the surface of human leucocytes [22,23]. Hyaluronic acid, a highly charged giant polysaccharide, is an example of the latter type of repelling molecule. This species can act as repulsive spacer between cells thus impeding their adhesion but it can also act as attractive buffer between cells if these carry the appropriate polysaccharide receptors such as CD44 [19].

The density of membrane-bound receptors and ligands in the plasma membrane (and thus the adhesion strength) is controlled, firstly, by depletion through internalization of receptor- (or ligand-) loaded vesicles budding from the plasma membrane (endocytosis) or, secondly, by enhancement through the fusion of vesicles carrying newly synthesized adhesion molecules within the plasma membrane [24]. Another possible control mechanism is the suppression of the cell adhesion by molecules that compete with the ligands for receptor binding sites [25].

Many cellular programs such as the division of cells, their motility, locomotion and adhesion generate, and rely upon, physical force. For example, leukocytes use the blood flow in their search for inflammation, and are thus submitted to large shearing forces while adhering and rolling along the blood vessel. Fibroblasts which structure the connective tissue, on the other hand, are able to pull strongly on their surroundings when participating in the recovery process of wounded tissue. Therefore, both internally produced and externally exerted forces are necessary for normal cell functioning.

1.3 Model systems

Many features of cell-to-cell and cell-to-substrate adhesion have been, and continue to be, studied using cells [26,27,28]. However, due to the complexity of the cell and the natural regulation mechanisms, it is often difficult to reproduce experimentally the exact same conditions for the purposes of adhesion experiments. This was the main incentive for the development of a variety of model systems in which "ideal conditions" could be achieved. These ideal conditions comprise (at least) a smooth fluid membrane, strong ligand-receptor interactions, and the ability to mimic the control of the glycocalix. At least one of the participants in the specific interaction should be mobile and the total number of ligand and receptors constant.

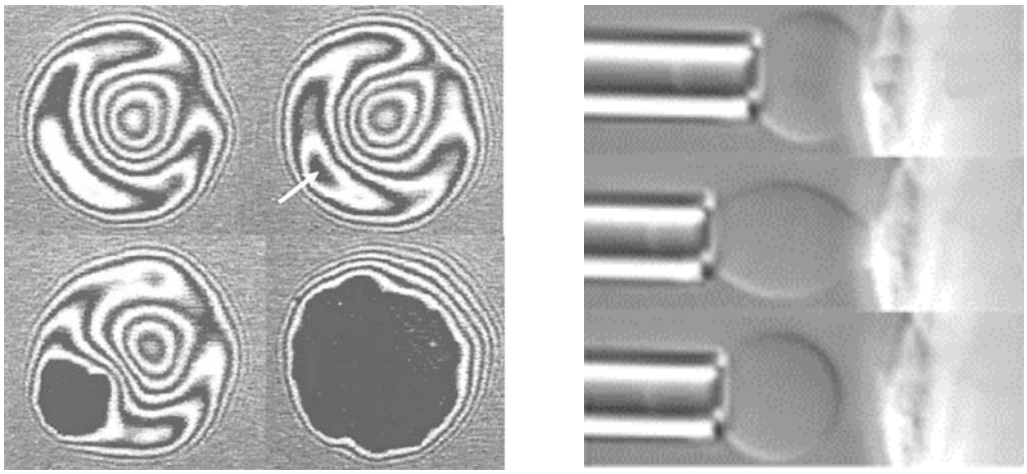

Figure 1.6: Left: Interference contrast reflection microscopy pictures of an adhering vesicle. The dark patch in a contact zone is a result of specific bindings. Picture from Boulbitch *et al*. [29]. **Right:** Unbinding of a vesicle specifically adhered to a cell, manipulated by the micropipette technique and observed in a phase contrast. Picture from Prechtel *et al*. [30].

To achieve these goals, giant liposomes known as vesicles are used to simulate the cell plasma membrane. The second cell can be simulated by another vesicle as, for example, in the case of experiments with micropipettes [31,32]. This technique allows for a macroscopic view of the adhering vesicles whereas the information about adhesion events is obtained from the response function of the applied suction (right panel in Figure 1.6). Interference contrast reflection microscopy can be used when the vesicle is brought in contact to a flat substrate (left panel in Figure 1.6) and is more appropriate for detailed studies of the adhesion zone [33]. Due to a very good height resolution of such setups, fluctuations of the membrane in the contact zone can be recorded in real-time. This

allows the determination of the mean-square amplitude of the fluctuations and thus the distinction between weakly and strongly adhered (the growing dark patch in the left panel of Fig. 1.6) parts of the membrane can be obtained [34]. The drawback of this technique is that the tension in the vesicle can not (presently) be directly controlled and the reconstruction of the macroscopic shape of the vesicle is limited to only several hundreds of nanometers above the substrate. However, both these techniques have provided important insights into the general underlying physics of cell and membrane adhesion. In concert with theoretical advances, it was possible to clarify some important questions concerning vesicle adhesion mechanisms.

Although the experimental methods for studying free or adhering membranes in three dimensions are quite limited, the variety of surface sensitive optical techniques and electrical measurements that can be applied to planar system is vast. Furthermore, in planar membranes, the contribution to the tension induced by the enclosure into a three-dimensional shape does not play a role and thus is somewhat more approachable by theoretical tools. This is the reason that flat bilayers are often used to study interacting surfaces.

1.3.1 Adhesion of flat membranes

1.3.1.1 Development of solid supported bilayers

The development of solid supported membranes [35,36] has enabled the identification of several issues relevant to the physics of interacting membranes. It has also permitted the measurement of the diffusion constants of membrane ingredients [6], the determination of binding energies of specifically interacting proteins [37,38], and provided insight into lateral interactions between different species in the membrane resulting in phase separation [39].

Flat bilayers can be assembled by rupturing of pre-tensed unilamellar vesicles on hydrophilic surfaces [40,41]. When a bilayer is deposited directly on the surface, only a thin film of lubricating water (thickness of ~1 nm) will form to separate the membrane from the support. This layer is sufficient for preservation of matrix fluidity and does not influence the diffusion of lipids. However, large trans-membrane proteins such as integrins become immobile (left panel in Figure 1.7). The interaction of these (and other)

proteins with the substrate can result in their denaturing the concomitant loss of their ability to perform as partners for specific interactions [42].

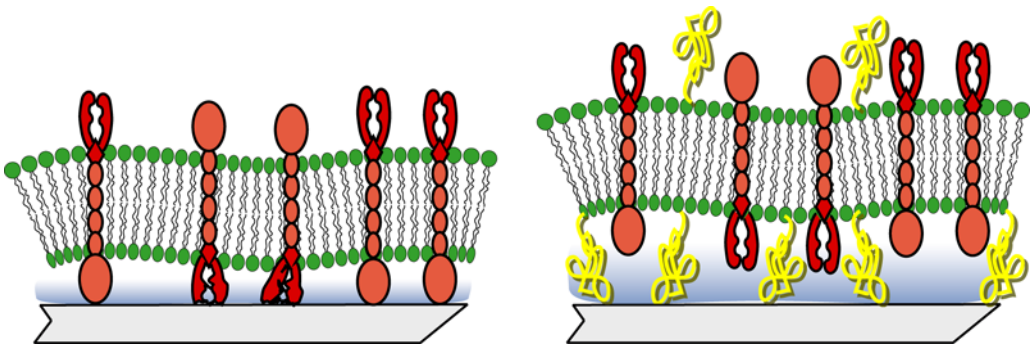

Figure 1.7: Left: Cartoon of a solid supported membrane deposited directly on a surface. Incorporated proteins adhere to the substrate and lose their functionality. Presentation of a solid supported membrane with incorporated polymers. **Right:** Repulsion of the polymeric molecules is capable of maintaining a sufficiently large separation between the substrate and the membrane so as to enable diffusion and functioning of embedded proteins.

A different strategy for separating the membrane from the substrate involves the inclusion of intercalating water-swelling polymers. This film can be achieved by the chemical grafting of water soluble proteins such as dextran or hyaluronic acid [43,44,45], the reconstitution of lipopolymers covalently bound to the lipid in the bilayer [46,47] as shown in the right panel in Figure 1.7, or by the deposition of multilayers of amphiphilic molecules such as cellulose with alkyl side chains [48,49]. Though somewhat more elaborate for preparation and control, these systems ensure that a large proportion of proteins remain mobile and fully functional, and are hence suitable for adhesion experiments.

1.3.1.2 Mechanics of interacting surfaces

Studies of lamellar membranes have resulted in important advances in the understanding of specific and nonspecific forces acting between two surfaces as well as clarifying the concept of an effective potential. Generally, the effective potential represents an average of nonspecific interactions acting between two bodies. It is constructed from interactions such as hydration forces, van der Waals and electrostatic interactions as well as thermal fluctuations of the surface.

Instinctively, one would think that the effective potential is simply a superposition of the different contributions. According to Helfrich, the energy of a membrane is the sum of the external potential and the cost of bending [50]. However, at finite temperature, the potential determines the spectrum of fluctuations, according to the equipartition of energy. In turn, the entropy costs of fluctuations contribute to the free energy and determine the average position of the membrane with respect to the substrate. If the effective potential depends on the position, then the effective potential felt by the membrane depends on how the membrane explores the space around its equilibrium position [51]. The effective potential, the average position and the fluctuation amplitude are thus coupled quantities and must therefore be determined self-consistently. However, different contributions to the effective potential need to be evaluated first:

- Hydration forces

Strong repulsive forces between bilayers in a multilayer system have been determined by exerting pressures of up to 10^8 Pa in order to bring the bilayers to separations in the nanometer range [52]. One of the mechanisms causing such an observation is the hydration of the bilayers. Due to the distortion of water molecules in the vicinity of polar lipid head-groups, the interaction between two bilayers increases exponentially with decreasing membrane distance [53]. The decay length is measured to be of the order of 10^{-1} nm while the pressure amplitude is of the order of 10^7-10^9 Pa [54].

- Van der Waals interaction

Relevant studies have also been undertaken to understand intrinsic van der Waals interactions between two flat lipid bilayers. In the geometry of flat immobilized membranes, the van der Waals potential has a crossover from h^{-4} at large separation distances to h^{-2} at distances of the order of the bilayer thickness [55]. The strength of such potential is given by the Hamaker constant which results from the effective polarizability of the membranes. In the biologically relevant case of high salt concentration (resulting in a low Debye screening length of about 1 nm) such calculations predict the Hamaker constant for lipid membranes to be of the order of 10^{-21}-10^{-22} J. Subsequent measurements on membranes immobilized on mica surfaces, with the surface force apparatus, have confirmed such values [56].

- Thermal fluctuations

Enhanced by the typically small bending rigidities of the bilayers, membranes undergo thermally exited fluctuations. These out-of-plane undulations result in an effective repulsion which can drive the membranes to infinite separation with a sufficient increase of temperature [57]. The first to address these entropic contributions to the overall interactions was Helfrich [50] who derived an overall steric repulsion for flat membranes, under the assumption that the membranes do not interact by any other force. The simple superposition of this repulsion with the van der Waals potential and hydration forces, results in a first order unbinding transition and a divergent mean spacing between the membranes. Lipowsky and Leibler [51] later employed the functional renormalization group and an approximate recursion relation, in the limit of large distances and large fluctuations, to derive a second-order unbinding transition. In this case, the mean bilayer spacing is determined as a function of the Hamaker constant, and is found to diverge as the Hamaker constant approaches a critical value. For homogeneous membranes, this critical value is later found to be a universal quantity [58]. Small angle X-ray diffraction on stacked lamellar bilayers has confirmed this theory, albeit with a discrepancy in the value of the critical Hamakar constant [59]. A different self-consistent theory for the case of moderate undulations, much below the unbinding transition, has been developed in which the average membrane position could be calculated for arbitrary substrate potentials [60,61].

- Electrostatic interactions

As a significant number of phospholipids in plasma membranes bear a net negative charge, electrostatic interactions often play a significant role. By 1879, Hemholtz had already recognized that fixed charges at a surface attract counter-ions from aqueous solution [62]. A major advance was made by Gouy [63] and, independently, by Chapman [64] who used the Poisson equation to describe the electrostatic attraction of the counterions to the surface and the Boltzmann relation to describe the statistical tendency of the counterions to diffuse away from the region of high concentration. Although the Guy-Chapman theory was developed in the beginning of last century, surface force measurements have demonstrated that it predicts the potential profile at distances larger than 2 nm [65,66]. However, this mean field theory breaks down for very low concentrations of ions in the membrane. In addition, it does not take into account size effects, specific binding of ions, or the many-body ion-ion correlations [67]. Finally, as pointed out by Andelman and Paregian, the cancellation of different effects not

considered by Guy-Chapman theory can still result in the correspondence of theory and experiment [68,69]. Recently, by use of field theory techniques this problem was addressed systematically [70,71].

- Specific ligand-receptor interaction

The incorporation of molecules (ligands and receptors) which are capable of selective binding allows one to mimic cell adhesion as well as to investigate enzyme reactivity. However, as depicted in Figure 1.8, the interaction between two distinct molecules usually relies on the interplay of numerous weak bonds [72]. It is due this fact that numerous low energy interactions are ordinarily required in order to produce a binding that is sufficiently strong to be useful in the recognition process. The weakness of the individual interactions also conveys the ability to spontaneously dissociate without the need for further control mechanisms to be developed by the cell.

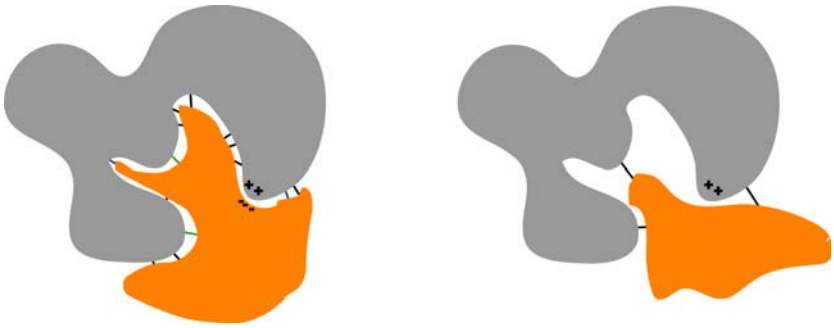

Figure 1.8: Cartoon of a strongly bound aggregate composed from complementary molecules **(left)** and a sketch of weakly bound complex of mismatching molecules **(right)**. The recognition is established by formation of weak bonds (depicted with lines). These bonds dissociate due to thermal excitations. Hence, the complex on the left should have a life-time much longer than the complex on the right.

The weak bonds can be formed by different mechanisms. As such, electrostatic interactions between two complementarily charged domains in molecules lead to binding energies of 2-4 k_bT. Hydrogen bonds are somewhat weaker and contribute with energies of 1-2 k_bT. Furthermore, van der Waals contacts induced by the complementarities of shapes, although associated with low energies on the atomic level (0.2-0.5 k_bT), can, due to the large number of contacts, amount to considerable contributions. Finally, as the proteins are exposed to water, domains in molecules with similar affinity to water will feel attractive forces due to the hydrophobic effect.

- Repulsion of the glycocalix

Molecules that possess long chains above the membrane surface are submitted to large, thermally excited conformational changes. If the gyrational space of such molecules is reduced by the presence of a substrate, a net repulsion arises between the polymer cushion and the imposed surface. This effect is generally well described by the mean-field Flory theory which shows that the strength of the repulsion depends on elements such as the density of polymers, the strength of the attractive van der Waals potential and, in particular, the average height of the membrane above the substrate [34].

When two cells are brought into close contact, the molecules from the glycocalix produce the above described repulsion [34]. Furthermore, in order to form a close contact between the cells, the molecules from the glycocalix must be expelled from the contact zone. This will occur naturally as there is a strong energy penalty for having the gyration space reduced to less than the gyration radius of the polymer. However, there is an entropy cost due to the reduction of area accessible to the polymers. Hence, a competition between the specific binding and the polymeric repulsion is associated with the presence of glycocalix-like molecules.

1.3.2 Membranes in three dimensions

1.3.2.1 Vesicles as enclosed surfaces

Due to the amphiphilic nature of phospholipids, as soon as their concentration in aqueous solution exceeds a critical value, lipid molecules assemble in supramolecular structures built from bilayers. These structures are a result of the hydrophobic effect that forces the lipid bilayers to arrange in such a way that they have no edges and thus form closed vesicles or liposomes. Production of unilamellar vesicles requires either sonification of structures obtained by the self-assembling process [73] or preparation by the electroswelling technique [74]. The sonification results in a relatively narrow size-distribution of vesicles, but the vesicles are also too small to be seen in optical microscopes. The electroswelling technique, however, produces large unilamellar vesicles with sizes ranging from 5 to 20 μm in radius.

A major step forward for the field of vesicles was the successful elucidation of free vesicle shapes obtained from a minimal continuum model [75]. Shortly afterwards, these

shapes received experimental confirmation [76]. Together, these works show that the shape of a vesicle freely suspended in solution can be understood as arising from the minimization of the bending energy under constraints on the total area and volume. At a given temperature, the area is constant because the exchange of molecules between the membrane and the solution can be neglected. The volume of the vesicle is determined by the osmotic pressure difference between the solution used for the construction of vesicles and the buffer used for suspending the vesicles. If these two solutions possess the same numbers of osmotically-active molecules, the vesicle assumes a shape of a sphere. However, if the osmolality of the surrounding buffer is larger than the one associated with the swelling solution, the water from inside of the vesicle will be expelled in order to balance the number densities of solutes in the two solutions. This results in a reduction of volume and the formation of excess free area. The time scale for this equilibration is defined by the diffusion constant of the water through a bilayer and is very short. Any further deformation of a vesicle is constrained to the resulting reduced volume and area.

The area of the bilayer can be altered by manipulating the temperature (Figure 1.9). From the theoretical point of view, the change in temperature can be understood as a change in the area to volume ratio. With a change of a control parameter (such as the temperature or the osmotic pressure), the shape with the minimal bending energy usually evolves in a smooth manner.

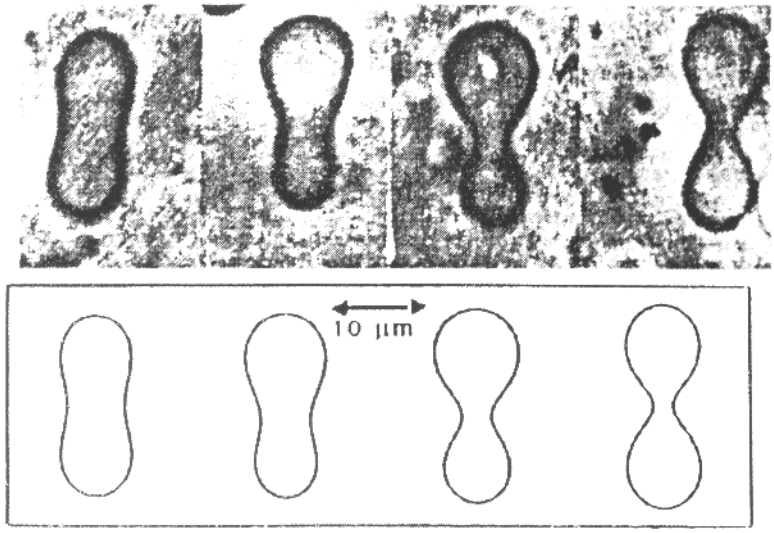

Figure 1.9: Shape transformation of a single vesicle as observed by phase contrast microscopy. The transformations were induced by an increase of temperature that leads to an increase of surface are of the vesicle. Pictures taken from Berndl *et al.* [77].

Properties of bilayers, beyond the local curvature and the area and the volume constraints are responsible for a variety of shapes that can be observed in experiments. For example, even a tiny asymmetry in the membrane, which can be treated through constant mean curvature (bilayer coupling model [77, 78]), leads to a considerably different temperature evolution of the shape. A more sophisticated, area-difference elasticity model couples the curvature directly to the density difference between two leaflets of the bilayer [79]. Both models provided solution for a budding transition and the transition to pear like shapes. The phase diagrams for these models show a variety of continuous and discontinuous transitions between different families of shapes [80].

Minimization of the total curvature energy can be performed for topologies different than the spherical one. Henceforth, toroidal shapes of genus 1 have been predicted theoretically [81] and then confirmed experimentally [82]. For vesicles with more than one handle or hole (genus larger or equal to 2), the degeneracy of the ground state can occur as calculated first by Jürlicher and his coworkers [83] and measured by Michalet and Bensimon [84].

1.3.2.2 Vesicles as models for cell adhesion

Although the biochemical and biofunctional aspects of cell adhesion have been intensively studied for many years [20,85,86], our knowledge of the physical basis of this extremely complex wetting process is still rudimentary. Several important revelations in understanding the foundation of cell recognition processes emerged from studies on model systems containing the essential ingredients of adhesion. These consist of giant vesicles containing artificial or natural receptors (or ligands) that act as test (or toy) cells interacting with solid supported membranes or polymer cushions that expose the conjugate ligand (or receptor) and thus can mimic the target cell or tissue. The effect of the glycocalix is accounted for by the incorporation of lipopolymers (lipids exposing hydrophilic macromolecular chains) into the test cell. In absence of the ligand from the surface of the molecule, the dynamic demixing of cholesterol and repellers could be observed and coupled to the shape fluctuations [87]. In the presence of ligands, binding events take place. The adhesion process is evaluated by reflection interference contrast microscopy (RICM), a micro-interferometric technique enabling the reconstruction of the surface profiles of adhering soft shells. By analyzing these surface profiles in terms of the theory of wetting of planar surfaces by partially wetting fluid droplets exhibiting surface

(bending) elasticity, the free energy of adhesion can be estimated [88,89]. These studies have resulted in new insight into the physical basis of cell adhesion and provided experimental evidence for theoretical predictions based on the original work of Bell [90].

The major results of the model membrane studies can be summarized as follows: Adhesion inevitably leads to receptor segregation resulting in the spontaneous formation of adhesion plaques. The free energy of adhesion is determined by the (non-ideal) lateral osmotic pressure exerted by the repelling molecules of the glycocalix and the unbound receptors (or ligands). The glycocalix plays a key role in the suppression of unwanted adhesion through the regulation of the surface density of the receptors and the repelling molecules. It enables the establishment of a situation near a wetting transition, thus allowing nature to optimize the density of adhesion molecules. This suggests that the adhesion strength can be controlled by modification of features such as (i) the lateral densities of the receptors and repelling molecules in the cell surface, (ii) the ratio of the hydrodynamic radii of the repelling molecules to that of the receptors and (iii) the bending stiffness of the membrane.

These experimental studies have revealed and addressed a variety of physical phenomena but they have also served as a source of motivation for many theoretical advances. Concerning vesicle adhesion, one of the first models was based on the continuum approach and provided vesicle shapes bound in a contact potential [91]. This study gave rise to the standard boundary condition which shows that, at the contact of the vesicle with the substrate, the membrane is closing a zero contact angle but of finite curvature. The continuum approach has later been extended to account for the influence of gravity [92], as the inner solution of a vesicle usually has a higher mass density that the outer buffer to enable the sinking of vesicles from the bulk solution to the substrate. Recently, a continuum path has also been undertaken to explore the influence of vertically exerted local force on a vesicle [93,94]. These models are very successful in explaining stationary stable shapes on the mesoscopic scale. They rely on an average adhesive potential acting on the vesicle that can, in some cases, be extracted for experimental comparisons. However, continuous models do not explain the microscopic nature of the vesicle-substrate interaction, nor do they account for details of the vesicle composition which can be essential for the understanding of the adhesion processes.

Several theoretical models that take the discrete nature of specific binding into account have been developed over time. The thermodynamic considerations of Bell, Dembo and

Torney [90,95,96] have had a major impact on the understanding of the origins of cell to cell adhesion. Their models were primarily concerned with the balance between the repulsive potentials accorded to the glycocalix, the binding enthalpy and the mixing entropy. Somewhat later, Zuckerman and Bruinsma discussed the influence of fluctuations and membrane-mediated long-range attractions and mapped the statistical model for ligand-receptor interactions to Coulomb plasma. As a result, they found the ideal mixing state assumed by Bell and co-workers to be unstable against the migration of ligands to the rim of the adhesion plate. They also predicted the enhancement of the membrane adhesion due to fluctuations [97,98].

The problem of lateral phase separation for ligand mediated adhesion was first considered by Lipowsky and co-workers for the case of flat membranes [99,100]. In the case of vesicles, Komura and Andelman evaluated the mean separation distances between the membrane and the substrate as well as the changes in the height profile, within the contact zone, from patch-like strong adhesion to weak adhesion [101]. Different scenarios for the dynamics of the adhesion process were identified by de Gennes and co-workers and found to depend on the mobility of ligands and receptors as well as on the reaction time associated with binding [102]. Very recently, Coombs *et al.* have extended previous theoretical approaches of Bell and co-workers to encompass the equilibrium thermodynamics of cell adhesion mediated by two ligand-receptor pairs of different length, resulting in a variety of a regimes dependent on control parameters such the binding constants, length scales and densities [103].

A barrier in the effective potential of a membrane interacting with the substrate was also found to control the phase behavior of membranes that contain both ligands and repelling molecules [104,105] In order to construct an effective potential and explore its influence on specific binding, Bruinsma *et al.* superimposed contributions from the van der Waals potential, average fluctuations, gravity and an effective repulsion due to lipopolymers [34]. Although this model is restricted to low concentrations of membrane constituents and weak interactions with the substrate, it does result in the concept of a double-well effective potential, which appears to be in agreement with the experimental observations as well as highlighting the importance of gravity. However, the shape of the vesicle has not been explicitly treated in any of these models, and therefore the role of the membrane bending and the effects of the finiteness of the vesicle system have not been elucidated.

In summary, by accounting for the numerous factors elaborated in the previous section, many phenomenological aspects vesicle adhesion have now been studied. Unfortunately, however, the results of the theories are often difficult to apply to the actual interpretation of experimental data. The aim of this thesis is therefore to partially rectify this situation. To this end, an attempt is made to provide a set of self-consistent tools that can be directly applied to the measured results. In particular, the task of building a detailed model for vesicle adhesion to a flat substrate will be undertaken. In subsequent steps, the methodology will be extended in order to provide new insight to some of the aforementioned control mechanisms. Accompanying the model development will be the presentation and discussion of several new experimental and theoretical results.

1.4 References

1. Weiss T. F. 1998. *Cellular Biophysics. Volume 1: Transport.* Chap. 1.

2. Limozin, L., and E. Sackmann. 2002. *Phys. Rev. Lett.* **89**:168103.

3. Alberts B., D. Bray, J. Lewis, M. Raff, K. Roberts, and J. D. Watson. 1994. *Molecular biologiy of the cell, 4th edition*.

4. Voet D., J. Voet, and W. Pratt. 1995. *Biochemistry, 2nd edition.*

5. Singer S., and G. Nicolson. 1972. *Science* **175**:720-731.

6. Jain M. K. 1988. *Introduction to biological membranes.*

7. Galla, H.-J., W. Hartmann, U. Theilen, and E. Sackmann. 1979. *J. Membrane Biol.* **48**:215-236.

8. Homan R., and and H. J. Pownall. 1988. *Biochim. et Biophys. Acta* **938**:155-166.

9. Sackmann E. 1995. In *Handbook of Biological Physics*. Chap.5.

10. Canham P. B. 1970. *J. Theoret. Biol*. **26**:61-81.

11. Evans E. A. 1974. *Biophys J.* **14**:923-931.

12. Janiak M. J., D. M.Small, G. G., and Shipley. 1979. *J. Biol. Chem.* **254**:6068-6078.

13. Fisher L. 1993. *J. Chem. Soc. Faraday Trans.* **89**:2567-2582.

14. Coakley W. T, H. Darmani, and A. J. Baker. 1991. *Cell and Model Membrane Interactions.* 25-46.

15. Darnell J., H. Lodish, and D. Baltimore. 1990. *Molecular Cell Biology.*

16. Helfrich W. 1973. *Naturforsch. C* **28**:693-703.

17. Israelachvili J. N., and H. Wennerstrom. 1992. *J. Phys. Chem.-US* **96**:520-531.

18**.** Sackmann E., and R. F. Bruinsma. 2002. *ChemPhysChem.* **3**:262-269.

19. Bruinsma R., and E. Sackmann. 2001. *C. R. Acad. Sci. IV-Phys.* **2**:803-815.

20. Bongrand P. 1989. *Rep. Prog. Phys.* **62**:921-968.

21. Balaban N.Q., U. S. Schwarz, D. Riveline, P. Goichberg, G. Tzur, I. Sabanay, D. Mahalan, S. Safran, A. Bershadsky, L. Addadi, and B. Geiger. 2001. *Nature Cell Bio.* **3**:466-472.

22. Shelley C., N. Da Silva, and J. M. Teodoridis. 2001. *British J. of Hematology* **115**:159-166.

23. Springer T. A. 1994. *Cell* **76**:301-314.

24. Springer T. A. 1990. *Nature* **346**:425-434.

25. Zinkl G. M., A. Zuk, P. van der Bijl, G. van Meer, and S. Matlin. 1996. *J. Cell Biol*. **133**:695-708.

26. Evans E. 1994. In *Handbook of Biological Physics.* 697-728.

27. Tozeren A., K. L. P. Sung, L. A. Sung, M. L. Dustin, P. Y. Chan, T. A. Springer, and S. Chien. 1992. *Cell Biol.* **116**:997-1006.

28. Hochmuth R. M., and W. D. Marcus. 2002. *Biophys. J.* **82**:2964-2969.

29. Boulbitch A., Z. Guttenberg, and E. Sackmann. 2001. *Biophys. J.* **81**:2743-2751.

30. Prechtel K., A. Bausch, V. Marchi-Artzner, M. Kantlehner, H. Kessler, and R. Merkel. 2002. *Phys. Rev. Lett.* **89**:028101.

31. Noppl-Simson D. A., and D. Needham. 1996. *Biophys. J.* **70**:1391-1401.

32. Heinrich V., and R. E. Waugh. 1996. *Ann. Biomed. Eng*. **24**:595-605

33. Ploem J. 1975. *Mononuclear Phagocytes in Immunity, Infelction and Pathology.*

34. Bruinsma R., A. Behrisch, and E. Sackmann. 2000. *Phys Rev E* **61**:4253-4267.

35. Brian A. A., and H. M. McConnell. 1984. *Proc. Nat. Acad. Sci. U.S.A.* **81**:6159-6163.

36. Sackmann E. 1996. *Science* **271**:43-48.

37. Waats T., H. Gaub, and H. McConnell. 1986. *Nature* **320**:179-181.

38. Salafsky J., J. Groves, and S. Boxer. 1996. *Biochem.* **35**:14773-14781.

39. Veatch. S. L., and S. L. Keller. 2002. *Phys. Rev. Lett.* **89**:268101.

40. Kalb E., S. Frey, and L. Tamm.1992. *Biochim. Biophys. Acta* **1103**:307-316.

41. Keller C., K. Glasmästar, V. Zhdanov and B. Kasemo. 2000. *Phys. Rev. Lett.* **84**:5443-5446.

42. Gönnenwein S. 2003. *Generic and specific cell adhesion: Investigations of a model system by Micro-Interferometry.*

43. Küchner M., R. Tampé, and E. Sackmann. 1994. *Biophys. J.* **76**:217-226.

44. Küchner M., and E. Sackmann. 1996. *Langmuir* **12**:4866-4876.

45. Sengupta K., J. Schilling, S. Marx, M. Fischer, A. Bacher, and E. Sackmann. 2003. *Langmuir* **19**:1775-1781.

46. Baeckmark T., G. Elender, D. Lasic, and E. Sackmann.1995. *Langmuir* **11**:3975-3987.

47. Purrucker O., A. Förtig, R. Jordan, and M. Tanaka. 2004. *ChemPhysChem* **5**:327-335.

48. Wegner G. 1992. *Thin Solid Films* **216**:105-116.

49. Goennenwein S., M. tanaka, B. Hu, L. Moroder, and E. Sackmann. 2003. *Biophys. J.* **85**:646-655.

50. Helfrich W. 1978. *Z. Naturforsch.* **33a**:305-315.

51. Lipowsky R., and S. Leibler. 1986. *Phys. Rev. Lett.* **56**: 2541-2544.

52. Rand R. P., and V. A. Parsegian. 1989. *Biochim. Biophys. Acta* **988**:351-376.

53. Marcelja S., and N. Radic.1976. *Chem. Phys. Lett.* 42:129-130.

54. Israelachvilli J. N. 1992. *Intermolecular and Surface Forces. 2nd edition.*

55. Lipowsky R. 1995. In *Handbook of Biological Physics.* 524-596.

56. Marra J., and J. N. Israelachvilli. 1985. *Biochem.* **24**:4608-4618.

57. Mutz R., and W. Helfrich. 1989. *Phys. Rev. Lett.* **62**:2881-2884.

58. Leibler S., and R. Lipowsky. 1987. *Phys. Rev. B* **35**: 7004-7009.

59. Safiniya C., R. Roux, G. Smith, S. Sinha, P. Dimon, N. Clark, and A. Bellocq.1986. *Phys. Rev. Lett.* **57**:2718-2721.

60. Mecke K. R., T. Charitat, and F. Graner. 2002. *Langmuir* **19**: 2080-2087.

61. Fragneto G. T.Charitat, F. Graner, K. Mecke, L. Perino-Gallice, and E. Bellet-Amalric. 2001. *Europhys. Lett.* **53**: 100-106.

62. Helmholtz H. L. 1879. *Ann. Phys. Leipzig* **7**:337-382.

63. Gouy M. 1910. *J. Phys. Paris* 9:457-468.

64. Chapman D. L. 1913. *Philos. Mag.* **25**:479

65. Israelachvili J. N., and G. E. Adams.1976. *Nature* **262**:774-776.

66. Winiski A. P., M. Eisenberg, M. Langner, and S. McLaughlin. 1988. *Biochem.* **27**:386-392.

67. Langner M. , D. Cafiso, S. Marcelja, and S. G. L. McLaughlin. 1990. *Biophys. J.* **57**:335-349.

68. Andelman D. 1995. In *Handbook of BiologicalPhysics.* 605-640.

69. Parsegian V. A, and R. P. Rand.1995. In *Handbook of Biological Physics.* 645-687.

70. Netz R. R. 2001. In *Electrostatic effects in soft matter and biophysics*.

71. Netz R. R. 2001. *Euro. Phys. J. E* **5**:557-574.

72. Bogan B., and K. Thorn. 1998. *J. Mol. Biol.* **280**:1-9.

73. Lasic D. 1993. In *Liposoms, From Physics to Application.*

74. Dimitrow D. S., and M. I. Angelova. 1988. *J.l of Electroanal.l Chem.* **253**:323-336.

75. Seifert U., K. Berndl, and R. Lipowsky. 1991. *Phys. Rev. A* **44**:1182-1202.

76. Käs J., and E. Sackmann. *Biophys. J.* **60**:825-844.

77. Berndl K., J. Käs, R. Lipowsky, E. Sackmann, and U. Seifert. 1990. *Europhys. Lett.* **13**:659-664.

78. Svetina S., A. Ottova-Leitmanova, and R. Glaser. 1982. J. theoret. Biol. **94**:13-23.

79. Seifert U. 1991. *J Phys. A: Math. Gen*. **24**:L573-L578.

80. Seifert U. 1997. *Adv. Phys*. **46**:13-137.

81. Seifert U. 1991. *Phys. Rev. Lett.* **66**:2404-2407.

82. Mutz M., and D. Bensimon.1991. *Phys.Rev. A* **43**:4525-4527.

83. Jürlicher F., U. Seifert, and R. Lipowsky. 1998. *Phys. Rev. Lett.* **71**:452-455.

84. Michalet X., and D. Bensimon. 1995. *Science* **269**:666-668.

85. Grakoui A, S. K. Bromley, C. Sumen, M. M. Davis, A. S. Shaw, P. M. Allen, and M. L. Dustin. 1999. *Science* **285**:221-227.

86. Alon R., and S. Feigelson. 2002. *Semin. Immunol*. **14**: 93-104.

87. Marx S., J Schilling, E. Sackmann, and R. Bruinsma. *Phys. Rev. Lett*. **88**:1380102.

88. Nardi J., R. Bruinsma, and E. Sackmann. 1999. *Phys. Rev. E* **58**:6340-6354.

89. Guttenberg Z., B. Lorz, E. Sackmann, and A. Boulbitch. 2001. *Europhys. Lett*. **54**:826-832.

90. Bell G. I. 1978. *Science* **200**: 618-627.

91. Seifert U., and R. Lipowsky. 1990. *Phys. Rev. A* **42**:4768-4771.

92. Kraus M., U. Seifert, and R. Lipowsky. 1995. *Europhys. Lett.* **32**:431-436.

93. Smith A.-S., E. Sackmann, and U. Seifert. 2003. *Europhys. Lett.* **64**:281-288.

94. Smith A.-S., E. Sackmann, and U. Seifert. 2004. *Phys. Rev. Lett.* **92**:208101.

95. Bell G. I., M. Dembo and P. Bongrand. 1984. *Biophys. J.* **45**:1051-1064.

96. Torney D. C., M. Dembo, and G. I. Bell. 1986. *Biophys. J.* **49**:501-507.

97. Zuckerman D. M., and R. F. Bruinsma. 1995. *Phys. Rev. Lett.* **74**:3900-3903.

98. Zuckerman D. M. and R. F. Bruinsma. 1998. *Phys. Rev. E.* **57**:964-977.

99. Lipowsky R. 1996. *Phys. Rev. Lett.* **77**:1652-1656.

100. Lipowsky R. 1997. *Colloids Surf. A* **128**:255-264.

101. Komura S., and D. Andelman. 2000. *Euro. Phys. J. E* **3**:259-271.

102. Brochard-Wyart F., and P. G. de Gennes. 2002. *Proc. Nat. Acad. Sci. U.S.A*. **99**:7854-7859.

103. Coombs D., M. Dembo, C. Wofsy, and B. Goldstein, 2004. *Biophys. J.* **86**:1408-1423.

104. Weikl T. R., R. R. Netz, and R. Lipowsky. 2000. *Phys. Rev E* **62**: R45-R47.

105. Weikl T. R., and R. Lipowsky. 2001. *Phys. Rev. E* **64**: 011903.

CHAPTER 2

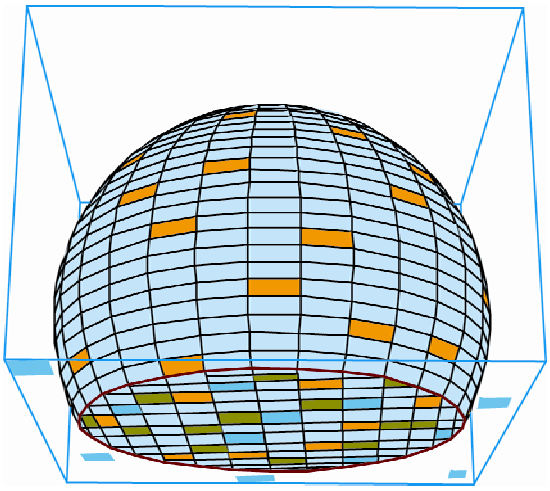

MODELING VESICLE ADHESION 31

Above: Schematic view of a vesicle adhering to the substrate by formation of ligand-receptor bonds. Different colors indicate sites containing different species.

Chapter 2

MODELING VESICLE ADHESION

The aim of the work contained in this chapter is to provide a well defined theoretical model, simple enough to be manageable and applicable to experiments, while at the same time retaining sufficient sophistication to account for the most important factors in the process of vesicle adhesion. To this end, the case of a vesicle adhering to a flat substrate, mediated by the formation of numerous ligand-receptor bonds, has been considered. Ligands embedded into the vesicle membrane are assumed to possess full translational freedom whereas receptors on the substrate are considered to be uniformly distributed and immobile. The task of this work is to determine the equilibrium allocation of bound and free ligands in the vesicle and then calculate the effective adhesion strength, which is often the most important quantity resulting from the relevant experiments [106,107].

The vesicle is treated in a canonical description where the membrane serves to define a two-dimensional surface with a fixed finite number of sites. Ligands are allocated to a certain number of these sites, while the remaining ones are considered to be empty. The size of a single site is defined as the area that the ligand occupies on the vesicle surface. It will be demonstrated that the finiteness of the system has important repercussions on the allocation of bound and free ligands. Furthermore, rather than being restricted to low concentrations of the system constituents, such an approach is suitable for any choice of receptor density on the substrate and any ligand density in the vesicle (as long as the interactions *between* these latter components remains small).

The problem of vesicle adhesion is simplified to its bare minimum. That is, we consider only the mixing entropy of ligands in the vesicle, the enthalpy of ligand-receptor binding and the bending energy of the entire vesicle shape. The vesicle surface is initially separated into a region parallel to the substrate (the contact zone) and a region consisting of the remaining part of the vesicle. We allow the interaction between the ligands and the receptors to take place only within the contact zone. Nevertheless, the ligands in the contact zone are able to exchange with those in the free part of the vesicle.

2.1 Notation

A schematic view of a model vesicle-substrate system is presented in Figure 2.1 where the color of a given site reflects whether it contains a ligand, a receptor, or is an empty site. In addition, a bond is formed if, within the contact zone, a site containing a ligand is positioned above a site occupied by a receptor.

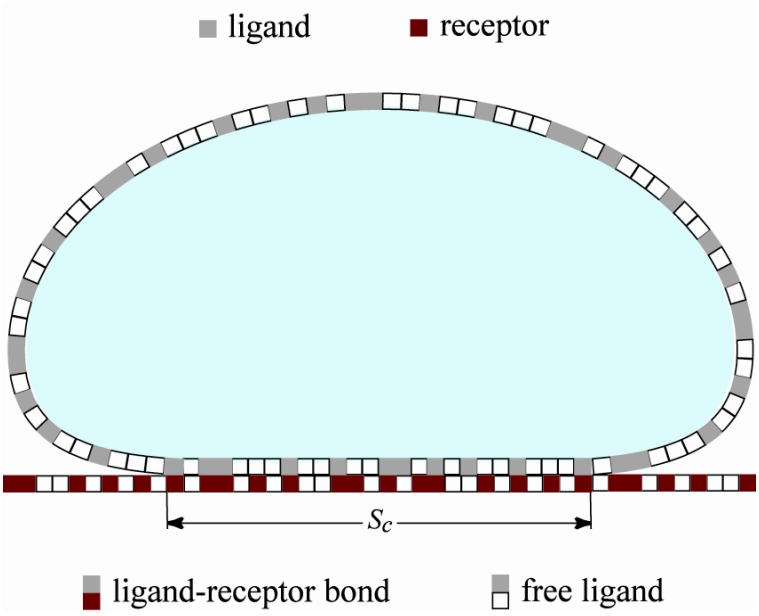

Figure 2.1: A cross-section of a model system depicting the system constituents. There are a total of N_t grey sites in the vesicle. The contact zone S_c is shown as the part of the vesicle at zero distance from the substrate. The black sites appear with the density, ρ_r which results in $\rho_r S_c$ receptors in the contact zone. If, within the contact zone, a grey site is on top of a black site, it contributes to N_b by forming a bond. A grey site over a white site indicates a free ligand in the contact zone that can be associated with N_f.

There are several ways in which the vesicle-substrate system may be parameterized. The simplest such a method is to use the absolute numbers of sites of different occupation. Hence, the following notation is chosen:

- S_t – The total number of sites in the vesicle. One site is of the size of a ligand on the vesicle surface. Within the model, the receptors are of the same size as the ligands.
- S_c – The number of sites forming the contact zone of the vesicle.
- ρ_r – The density of receptors on the substrate. It reflects the extent of surface coverage (*e.g.* for $\rho_r = 1$ the surface is fully covered, while for $\rho_r = 0$, there are no receptors on the surface).
- N_t – The total number of ligands in a vesicle.
- N_b – The number of ligands that are in the contact zone and bound to receptors.
- N_f – The number of ligands that are in the contact zone and free.
- $N_{free} = N_t - N_b$ – The number of free ligands in the vesicle**.**

Although the above presented notation is the one most intuitive when understanding the obtained results, in some cases, it is more applicable to work with fractions:

- s_c – the fraction of the total vesicle area forming the contact zone: $s_c = S_c / S_t$
- n_t – total surface concentration of ligands in a vesicle: $n_t = N_t / S_t$ (*e.g.*, for n_t = 0.1, 10% of the vesicle surface is covered by ligands).
- n_b – fraction of total ligands that are in the contact zone and bound to receptors: $n_b = N_b / N_t$ (*e.g.*, for n_b = 0.1, 10% of ligands in a vesicle are bound to the substrate), $0 \le n_b \le 1$.
- n_f – fraction of total ligands that are in the contact zone and free, $nf = N_f / N_t$, $0 \le n_f \le 1$.

Several other notational marks are used when necessary:

- DN_b – the absolute density of bound ligands in the contact zone, $DN_b = N_b / S_c$.
- DN_f – the absolute density of free ligands in the contact zone, $DN_f = N_f / S_c$.

2.2 The free energy

For a given temperature (T), the free energy of the system is given by $F = U - TS$, where U is the internal energy and S is the entropy of the vesicle-substrate system. In the context of the previously outlined model, several contributions can be identified:

- The internal energy

The internal energy of the system comprises changes in energy due to the formation of bonds. Complexation of two molecules in this way is associated with a gain in enthalpy E_a, which is also a measure of a binding strength of the ligand-receptor pair. It is this quantity that is used to model the formation of the ligand-receptor bond. As every bond formed contributes to the total energy of the system, the internal energy of a vesicle can be written as:

$$U = -N_b \cdot E_a \qquad (2.1)$$

The binding strength is a positive quantity and is expressed in units of $k_B T$ (k_B is the Boltzmann constant). The negative sign thus indicates that bond formation is favorable in terms of the total free energy.

- The entropy

The entropy is calculated by counting all possible conformations (Ω) of the positions of the ligands in the vesicle. Under the previously described assumptions, Ω is the number of combinations in which one can place: $N_t - N_b - N_f$ ligands in the free part of the vesicle on $S_t - S_c$ positions, N_f free ligands on $S_c(1-\rho_r)$ sites not occupied by receptors, and N_b bound ligands on the remaining $\rho_r \cdot S_c$ receptor sites:

$$\Omega = \begin{pmatrix} S_t - S_c \\ N_t - N_b - N_f \end{pmatrix} \begin{pmatrix} S_c(1-\rho_r) \\ N_f \end{pmatrix} \begin{pmatrix} \rho_r \cdot S_c \\ N_b \end{pmatrix}. \qquad (2.2)$$

The entropy is given, in units of k_B by $S = \ln \Omega$, which leads to an expression analogous to the standard mixing entropy term [108]. Application of the approximation given by the Stirling formula for factorials of large numbers ($N! \approx N^N e^{-N}$) yields the following expression:

$$
\begin{aligned}
S = {} & (S_t - S_c)\ln(S_t - S_c) - (N_t - N_b - N_f)\ln(N_t - N_b - N_f) \\
& - (S_t - S_c - N_t + N_b + N_f)\ln(S_t - S_c - N_t + N_b + N_f) \\
& + S_c(1-\rho_r)\ln(S_c(1-\rho_r)) - N_f \ln N_f - (S_c(1-\rho_r) - N_f)\ln(S_c(1-\rho_r) - N_f) \\
& + \rho_r \cdot S_c \ln(\rho_r \cdot S_c) - N_b \ln N_b - (\rho_r \cdot S_c - N_b)\ln(\rho_r \cdot S_c - N_b)
\end{aligned}
\tag{2.3}
$$

The limitation of such a calculation is that the Stirling formula should not be applied to small numbers ($N > 100$).

- The free energy of a shape

The bending energy of an adhered vesicle can be extracted from calculations of shapes bound in a contact potential [109], performed within the continuous approach. Rather than determining the shape of the vesicle and thus the area of contact for a given strength of the contact potential, the problem can be inverted, and the minimum energy shape for a fixed size of the contact zone can be determined. These two problems are equivalent and result in the same well-known shapes. As the details of these calculations can be found elsewhere [109], they will not be presented here. Some insight into such minimization can, however, is obtained from a similar problem that is developed in details in Appendix D. In addition, several aspects of the dependency of the bending energy the size of the contact zone will be discussed.

The calculations within the continuous approach have shown that, due to the constraints on the vesicle area and volume, there exists a shape with a finite maximum contact area $s_c^{\max}$. This area is associated with the shape of a spherical cap and can therefore be calculated exactly (see Table 2.1).

Table 2.1: The maximum area of contact $s_c^{\max}$ for vesicles with volumes reduced to v of the volume of a sphere with same surface area.

v	1.00	0.95	0.90	0.85	0.80	0.75	0.70	0.65	0.60
$s_c^{\max}$	0.00	0.17	0.23	0.28	0.32	0.34	0.37	0.39	0.41

It is for the shape of a spherical cap characterized by $s_c^{\max}$, that the vesicle surface closes a well- defined contact angle with the substrate. In this so-called spherical limit, this finite non-zero angle of contact induces a divergence of the bending energy.

The analysis of aforementioned calculations (see Appendix A) has provided an approximate functional dependence of the bending energy on the size of the contact zone. For a membrane of bending rigidity $\kappa = \alpha \cdot k_B T$, the bending contribution to the free energy arising from the shape can be expressed in units of $k_B T$ as:

$$F_{bend} = \left(-\frac{K_1}{(s_c^{\max} - s_c)} + C_1 (s_c^{\max} - s_c) + C_0 \right) \frac{\alpha}{S_t} \qquad (2.4)$$

The first term in Eq. (2.4) is found to describe the divergence in the spherical limit. The remaining two terms are corrections for small adhesion plates and are found to be more important for more reduced volumes. The coefficients K_1, C_1 and C_0 are functions of the vesicle reduced volume. Equation (2.4) has been displayed in Figure 2.2 together with the solutions of the calculations performed in reference [109], for several reduced volumes.

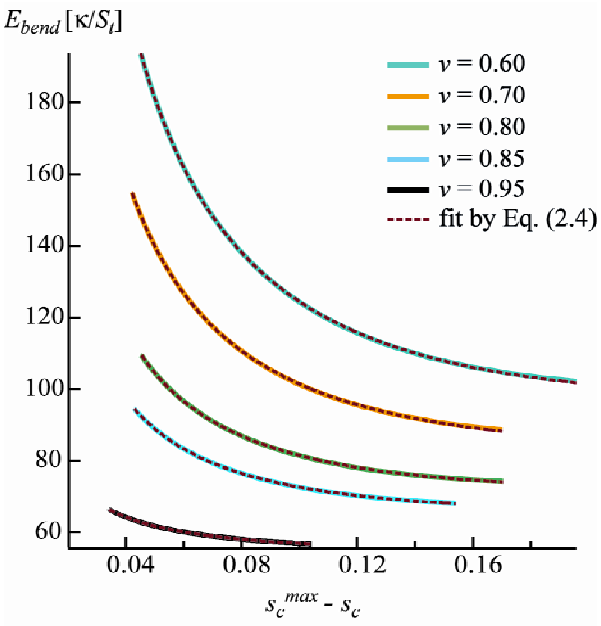

Figure 2.2: The bending energy of a vesicle shape as a function of the fraction of the area used for the formation of the contact zone. The curves are translated in their abscise variable for the maximum size of the contact zone characteristic for the given volume, as shown in Table 2.1. Hence the singularity is at s_c^{max}-s_c=0 for each curve. Data for contact zones that differ from their maximum value by less than 4% of the total vesicle area are not available due to the numerical difficulties involved in generating these shapes.

For standard vesicle membranes, α ranges from 10 to 100, whereas the total number of sites ranges between 10^8-10^{10}, depending of the size of the vesicle and the size of the ligand. The bending energy seldomly exceeds 10^{-5} k_BT per site on a vesicle. On the other hand, the contribution of each ligand is of the order of 1 k_BT. As the number of ligands (even at low concentrations) is very large, the magnitude of the bending energy term is very small in comparison with the internal energy and the entropy, and can generally be omitted from the calculation. The only exception is when the shape of the vesicle approaches the spherical limit when the bending term restricts expansion of the contact zone beyond $s_c^{\max}$.

2.3 Minimizing the free energy

In order to find stationary solutions, minimization of the free energy should be performed with respect to all independent variables. Closer inspection of the contributions to the total free energy reveals that F is a function of two constituent variables: the number of bound ligands (N_b), and the number of free ligands in the contact zone (N_f), and it depends on the size of the contact zone S_c.

2.3.1 Minimization with respect to the constituent variables

Minimizing $F = U - TS$ with respect to N_f and N_b, results in two important relations. The first one can be cast in the form of the "density equation":

$$\frac{N_t - N_f - N_b}{S_t - S_c} = \frac{N_f}{S_c(1-\rho_r)}. \qquad (2.5)$$

The left side of this equation is the density of ligands in the free part of the vesicle. Similarly, the right hand side is the density of free ligands in the adhesion zone over sites not occupied by receptors. As the free energy of a ligand in the upper part of the vesicle is, within the current model, the same as the free energy of an unbound ligand in the contact zone, a violation of the density equation (2.5) would lead to unequal lateral pressures of free ligands inside and outside the contact zone, and hence, to the loss of a stationary solution.

The second important relation resulting from the minimization shows the influence of the binding strength on the allocation of bound and free ligands within the contact zone:

$$\frac{(1-\rho_r)\cdot S_c}{N_f} - 1 = e^{E_a}\left(\frac{\rho_r \cdot S_c}{N_b} - 1\right). \qquad (2.6)$$

On this occasion, it is the densities of the free and bound ligands within the contact zone, (weighed by the Boltzmann factor of each state) which are being equilibrated.

Solving Eq. (2.5) and Eq. (2.6) simultaneously for N_f and N_b results in the optimum allocation of ligands in the vesicle, for a given size of the contact zone:

$$N_b = \frac{N_t + \rho_r S_c}{2} + \frac{S_t}{2\cdot\left(e^{Ea}-1\right)} - \frac{\sqrt{e^{2Ea}\left(N_t-\rho_r S_c\right)^2 - 2e^{Ea}\left[{N_t}^2 + {\rho_r}^2 {S_c}^2 - \left(N_t+\rho_r S_c\right)S_t\right] + \left(N_t+\rho_r S_c - S_t\right)^2}}{2\cdot\left(e^{Ea}-1\right)}, \quad (2.7)$$

$$N_f = \frac{(1-\rho_r)S_c}{S_t-\rho_r S_c}\left(N_t - N_b\right). \quad (2.8)$$

The set of solutions given by Eq. (2.7-2.8) is the physically relevant one of the two sets emerging from the calculation.

2.3.2 Minimization with respect to the size of the contact zone

Minimizing the free energy with respect to the size of the contact zone also results in the density equation (2.5). Consequently, although the free energy depends on three variables, one of the equations emerging from the minimization of the free energy with respect to these three variables is linearly dependent on the remaining two.

Incorporating Eq. (2.7-2.8) into the free energy shows that *F* is a decreasing function of S_c, leading to a boundary minimum with respect to the same variable (see Figure 2.3). In order to reach the thermodynamic equilibrium, the vesicle will thus maximize its area of contact with the substrate. However, the size of the contact zone is restricted by the volume and area constraints and the bending energy of the vesicle. The divergence of the bending energy in the spherical limit induces a stable boundary minimum in the total free energy of the vesicle adhering to the substrate. Thus in the thermodynamic equilibrium, the vesicle shape is always that of the spherical cap, with an optimum number of bound and free ligands in the contact zone given by Eq. (2.7-2.8). Depending on the coverage density and the binding affinity of the ligand-receptor pair, the density of bonds can vary from very low to very high.

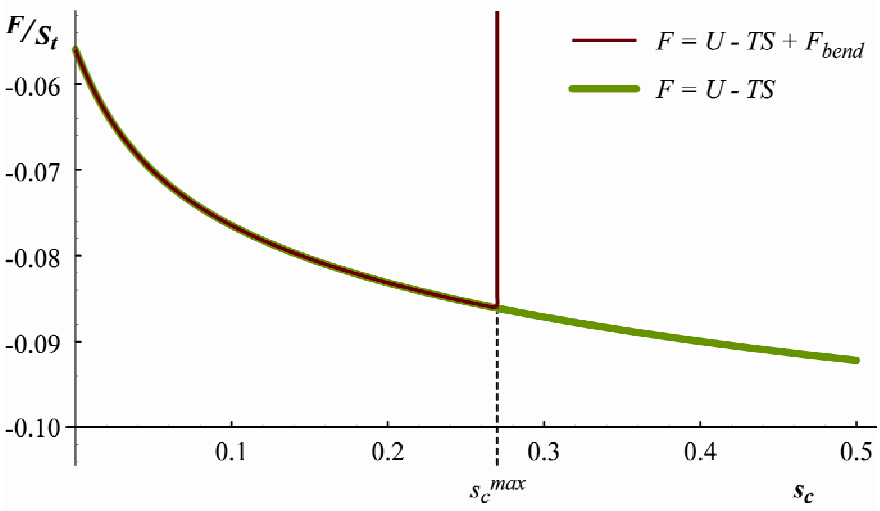

Figure 2.3: Comparison of the free energy including (red line) and omitting (green line) the bending contribution. Curves are shown as a function of the size of the contact zone. The bending energy induces a stable minimum at $s_c = s_c^{max}$.

If, for some reason, the adhesion process is very slow, the free energy will relax with respect to the number of ligands much faster than with respect to the size of the contact zone. Hence, a constrained equilibrium, where the vesicle shape is not that of a spherical cap, can be experimentally observed. In that case, an axially symmetrical shape can in principle be determined with the use of the continuous models [109], where the free energy must be minimized with respect to the given size of the contact zone.

2.4 Allocation of ligands in the contact zone

The allocation functions given by Eq. (2.7-2.8) determine how many ligands are bound and unbound in the contact zone. The total number of free ligands in a vesicle can, considering the definitions given in Section 2.1, be easily determined as $N_{free} = N_t - N_b$. These allocations are sensitive to system parameters such as the density of ligands and of the receptors as well as on the binding strength of the ligand-receptor pair. Several attributes of these functions warrant further discussion.

2.4.1 Limiting behaviors of the allocation functions

If there is no interaction between the ligand and the receptor, *i.e.* $E_a = 0$, the ligands are uniformly allocated over the vesicle. Hence the number of bound and free ligands in the contact zone is scaled by the number of sites containing receptors and the number of empty sites, respectively (first column in Table 2.2). As the binding strength increases, all allocation functions exhibit considerable deviations from their values at $E_a = 0$. However, the allocations reach their saturation values, characteristic for the limit of $E_a \to \infty$ (see columns 2 and 3 in Table 2.2) surprisingly quickly, typically at binding strengths between 10 and 15 $k_B T$. For large binding strengths, the allocation functions are limited by the concentrations of the vesicle and substrate constituents. If there are more ligands available than receptors in the contact zone, all receptors will be bound (see the second column in Table 2.2, and the left panel in Figure 2.4). If, on the other hand, the total number of receptors in the contact zone is larger than the total number of ligands in the vesicle, all of the ligands will be bound (see the last column in Table 2.2 and the right panel in Figure 2.4).

Table 2.2: The limits of the allocation functions.

	$E_a = 0$	$E_a \to \infty$	
		$\rho_r S_c < N_t$	$\rho_r S_c > N_t$
N_b	$\frac{\rho_r S_c N_t}{S_t}$	$\rho_r S_c$	N_t
N_f	$\frac{(1-\rho_r) S_c N_t}{S_t}$	$\frac{S_c (1-\rho_r)(N_t - \rho_r S_c)}{(S_t - \rho_r S_c)}$	0
N_{free}	$\frac{(S_t - \rho_r S_c) N_t}{S_t}$	$N_t - \rho_r S_c$	0

2.4.2 Overall behavior of the allocation functions

All three allocation functions are presented in Figure 2.4 for the case of a vesicle that has 85% of the volume of a sphere with the same surface area. In thermodynamic equilibrium, this leads to a spherical cap with a contact zone that comprises 28% of the total vesicle surface area. Furthermore, if the diameter of the vesicle is 10 μm and the ligand incorporated has the gyration radius of 3.5 nm (as does the commonly used sialyl-Lewis^X-glycosphingolipid) then the total number of sites in the vesicle is about 10^8. If the vesicles are prepared with the number concentration of about 10^{-3} of the ligand with respect to the lipid, 10% of the vesicle surface will be covered by ligands. N_b, N_f, and N_{free} are presented for these parameters, for the cases of surface coverages of 20% and 80%, respectively.

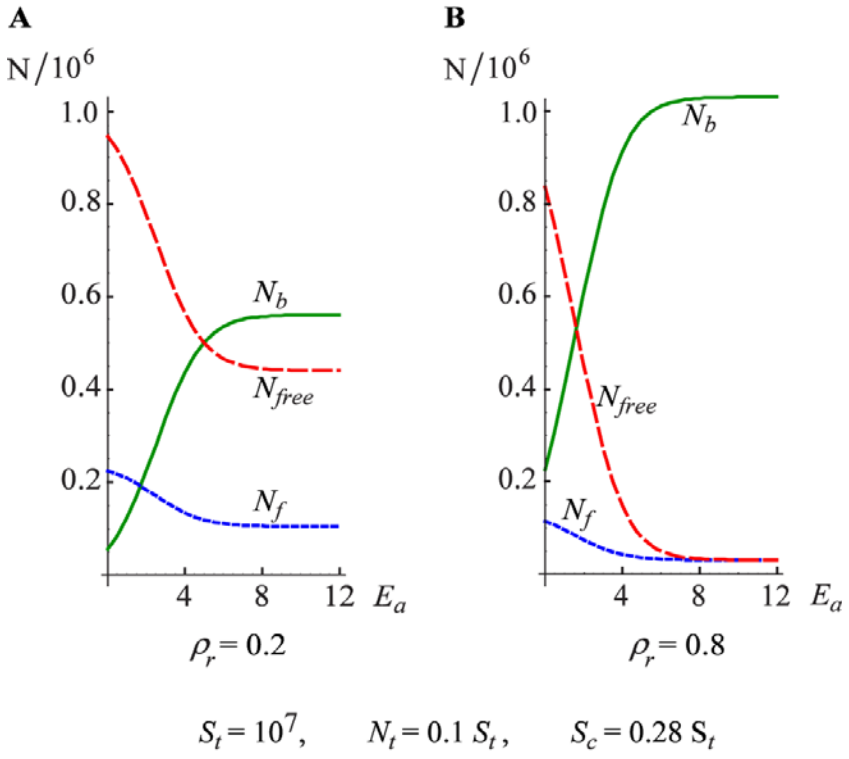

Figure 2.4: The allocation of ligands in a vesicle as a function the binding strength for **(A)** low, and **(B)** high substrate coverage. The allocation in the contact zone of bound (full line) and free ligands (short dotted line) are presented together with the total number of free ligands in the vesicle (long dotted line). The coverages are indicated directly below the graphs whereas the other parameters can be found in the bottom line of the figure.

At small binding strengths, the number of bound ligands in the vesicle is smaller than the number of free ones ($N_b < N_{free}$). As the strength increases, the majority of ligands will

become bound to the receptors. This is a direct consequence of the fact that the total number of ligands in the vesicle is finite. The characteristic binding strength at which the number of bound ligands begins to exceed that of free ligands in the vesicle can be found by solving $N_{free} = N_b = N_t / 2$ which results in:

$$E_a = \ln \frac{2S_t - N_t - 2\rho_r S_c}{2\rho_r S_c - N_t}. \tag{2.9}$$

The crossing will occur as long as $\rho_r S_c > N_t / 2$. At $\rho_r S_c < N_t / 2$ the expression for the number of bound ligands saturates at a value below the limit for the total number of free ligands in the vesicle.

For coverages of the substrate less than $\rho_r = 0.5$, the allocation function for bound molecules (N_b) intersects that for free receptors in the contact zone (N_f). By solving $N_f = N_b$, the following crossover binding strength is obtained:

$$E_a = \ln \frac{S_c(1-\rho_r)(S_t - N_t + (1-2\rho_r)S_c)}{\rho_r S_c(S_t + (1-2\rho_r)S_c) - N_t S_c(1-\rho_r)}. \tag{2.10}$$

This crossover vanishes at $\rho_r = 0.5$ when, due to the equipartition of ligands imposed by the density equation (2.5), $N_f = N_b$ at $E_a = 0$. Furthermore, if the coverage is very low, the expression for the number of bound ligands saturates below that for the number of free ligands in the contact zone and the crossing does not occur for any value of E_a. In this case, the concentration of free ligands in the contact zone is much larger than the concentration of bound ones.

2.4.3 Behavioral regimes of the allocation functions of bound ligands

The expressions governing the numbers of bound and free ligands are functions of four parameters (E_a, ρ_r, S_c, N_t). It is therefore relatively difficult to present all possible regimes for the number of bound and free molecules in a clear and concise manner. However, several relevant cases can be identified from the physical background of the problem. In this sense, Eq. (2.7) should be expected to behave differently in the regimes of weak and strong ligand-receptor binding. Furthermore, the consequences of the existence of two limits for the number of ligands inside and outside the contact zone

when $E_a \to \infty$, must be explored. This is because the path toward these limits (left or right panel in Figure 2.4) will depend on parameters such as the average density of ligands in the vesicle and the density of receptors on the substrate. More importantly, which of the two limits is applicable to a certain composition of the vesicle and the substrate will depend on S_c. In particular, if for a given S_c, there are more ligands in the system than receptors, the number of available receptors will dictate the allocation of ligands over the vesicle. This situation will be referred to as a ***receptor-dominated equilibrium***. On the other hand, the presence of more receptors than ligands leads to a stable solution that is limited by the total number of ligands on the vesicle surface and results in a so-called ***ligand-dominated equilibrium***. Actually, there is a critical size of the contact zone S_c^* for which the number of ligands in the vesicle is same as the number of receptors in the contact zone:

$$S_c^* = \frac{N_t}{\rho_r}. \qquad (2.11)$$

It is for this size of the contact zone that the two limits at $E_a \to \infty$ become equivalent. Specifically, if $S_c < S_c^*$ applies, the system will be found in a receptor-dominated equilibrium whereas in case of $S_c > S_c^*$ the system adopts a ligand-dominated equilibrium. Some transitionary behavior of the allocation functions should thus be expected for $S_c = S_c^*$. Due to the geometrical constraint on the maximal size of the contact zone for a given total area of the vesicle, such transitions should disappear when $S_c^* > 0.5 S_t$ as the system always relaxes in a receptor-dominated equilibrium. In this context, different aspects of Eq. (2.7) will be presented in terms of their dependence on the size of the contact zone and the binding strength of the ligand receptor pair.

2.4.3.1 Dependence on the size of the adhesion plate

If the vesicle has no excess area, it will assume a tense spherical shape and be unable to form a contact zone. On the other hand, a completely deflated vesicle can use, at most, one half of the vesicle area for the purpose of adhesion. For intermediate sizes of the adhesion plate ($0 \le S_c \le 0.5 \cdot S_t$), two distinct types of behavior of the allocation function for the number of bound ligands in Eq. (2.7), can be identified by inspection of the left and the right panels in Figure 2.5, respectively. These behaviors are a direct consequence

of the geometrical constraint on the size of the contact zone and the two classes of equilibria for vesicle adhesion.

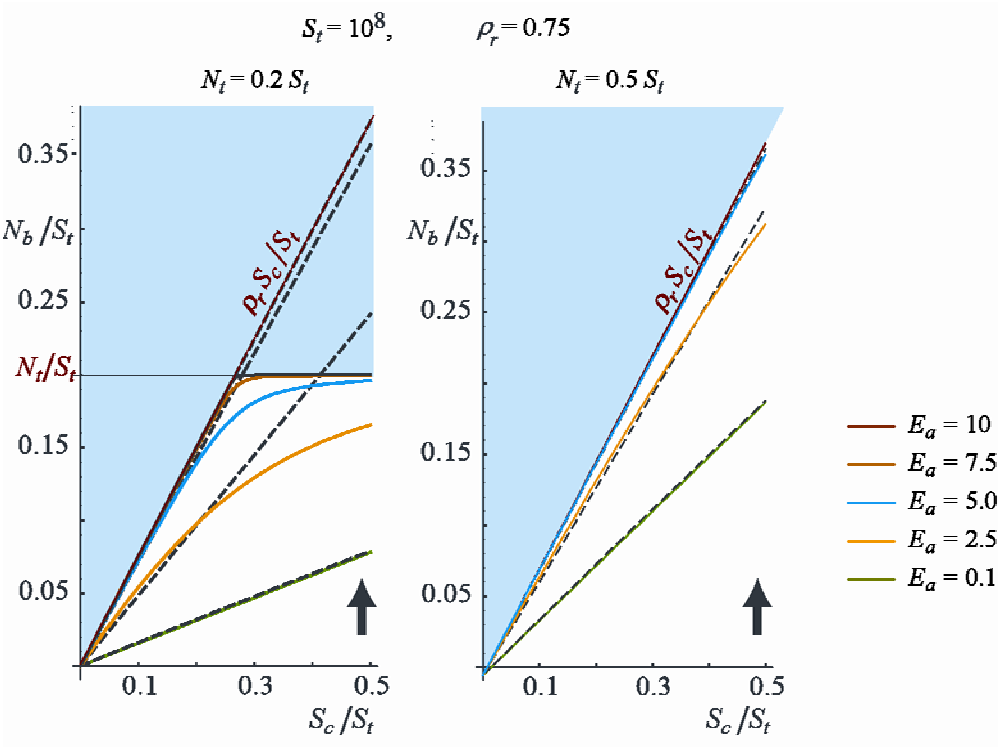

Figure 2.5: The number of bound ligands as a function of the size of the adhesion plate for a set of binding strengths $E_a = 0.1, 2.5,\ 5.0,\ 10.0$. The arrows in the graphs indicate the direction of the increase of the binding strength. The total number of sites in the vesicle and the density of receptors on the substrate are kept constant. Data are presented for two different choices of the total number of ligands as indicated above the left and the right panels respectively. The regions in the graph where N_b has solutions are depicted with a white background, whereas the forbidden regions are shown with shaded backgrounds. The approximate N_b^{LIN} solution (short dotted lines) is presented together with the real solution (full lines). Due to geometrical constraints, S_c is limited to 0.5 S_t.

For several combinations of parameters, the number of bound ligands is found to depend linearly on the size of the contact zone. To approximately determine the nature of these linear relationships, the zero point ($N_b = S_c = 0$) is connected with the point at which $N_b = 0.5 \cdot N_t$. This results in following approximate solution for the number of bound ligands:

$$N_b^{LIN} = \frac{\left(e^{E_a} + 1\right) \cdot N_t}{\left(e^{E_a} - 1\right) \cdot N_t + 2S_t} \cdot \rho_r S_c \quad . \tag{2.12}$$

In order to compare Eq. (2.12) with the full solution from Eq. (2.7), N_b^{LIN} is presented in Figure 2.5 with dotted lines.

Inspection of Figure 2.5 reveals that allocation functions of bound ligands can also be linearized by using their slopes at $S_c = 0$:

$$N_b^0 \equiv S_c \cdot \left.\frac{\partial N_b}{\partial S_c}\right|_{S_c=0} = \frac{e^{E_a} N_t}{S_t - \left(e^{E_a} - 1\right) N_t} \rho_r S_c \,. \tag{2.13}$$

Although N_b^0 is a valid approximation of Eq. (2.7), the approximation given by Eq. (2.12) is found to be the simplest expression that accurately describes the real solution from Eq. (2.7) for the widest choice of system parameters.

a) $S_c^* < 0.5 S_t$ *regime*

This regime is presented in the left panel of Figure 2.5. The solutions for N_b can only be found in the part of the diagram with the white background. The boundaries of this and the forbidden (shaded) region are the horizontal N_t line and the $\rho_r S_c$ line defined by both limits of N_b when $E_a \to \infty$ (Table 2.2). As the binding strength increases, the N_b allocation function approaches both limits. However, a smooth transition from the ligand-dominated to the receptor-dominated type of equilibrium takes place. Hence, for strong binding (e.g. $E_a > 5$ in the case of parameters chosen in Figure 2.5), the N_b allocation function is virtually cornered between the two limits, with a crossover at S_c^*. In the limit of $E_a \to \infty$, the derivative of the allocation function of bound ligands (N_b) with respect to the size of the contact zone has a discontinuity at the boundary between the two types of equilibria.

While $S_c^* < 0.5 S_t$, the N_b functions are linear for small binding strengths ($E_a << 1$). Here, N_b^{LIN} matches the real solution very well. For intermediate binding strengths, N_b^{LIN} is a good approximation only at small sizes of the contact zone. For large binding strengths $N_b^{LIN} \to \rho_r S_c$, so it again becomes representative of the real N_b (until the N_t line is intercepted at S_c^*), as can be seen in the left panel of Figure 2.5.

b) $S_c^* > 0.5S_t$ *regime*

The second regime is presented on the right panel in Figure 2.5. In this case, for any accessible size of the contact zone S_c, the number of available receptors in the system is smaller than the number of ligands in the vesicle ($\rho_r S_c < N_t$). Thus the allocation function of bound ligands is always a solution representing a receptor-dominated equilibrium. Thus the region where solutions for N_b can be found is limited only by the $\rho_r S_c$ line. Furthermore, N_b is almost linear for any choice of parameters. Increasing the binding strength causes the saturation of N_b to the $\rho_r S_c$ line in the whole range of available sizes of the contact zone. An example of this behavior is shown in the right panel of Figure 2.5 where, for the given set of parameters, curves with $E_a > 5$ cannot be distinguished from the $\rho_r S_c$ boundary.

Regardless of the binding strength, when $S_c^* > 0.5S_t$, the approximate solution N_b^{LIN} is a very good representative of the real solution. The maximum deviation of N_b^{LIN} from N_b is found to be less than 5% and arises for binding strengths $E_a \cong 1$ at small sizes of the contact zone. It is in this limit that the approximation given by N_b^0 in Eq. (2.13) can be used as a substitute.

c) *Density of bound ligands in the contact zone*

The dependency of the density of ligands on the size of the contact zone clearly demonstrates the interplay between the entropic contribution to the free energy and the total enthalpy of binding. Thus, in the case of zero binding strength, the density of bound ligands in the contact zone is independent of the size of the contact zone, and results simply from an entropically driven equipartition over the entire surface. For very large binding strengths, the enthalpy completely dominates the free energy and the number of bonds is maximized. Hence, for such E_a (red curve in Figure 2.6) the density saturates to a constant value in a receptor-dominated equilibrium (no further bonds can be formed as all receptors are occupied). For contact zones leading to a ligand-dominated equilibrium, no further bonds can be formed as there are no more ligands at this binding strength. This will lead to an increase of bond density as the contact zone becomes smaller.

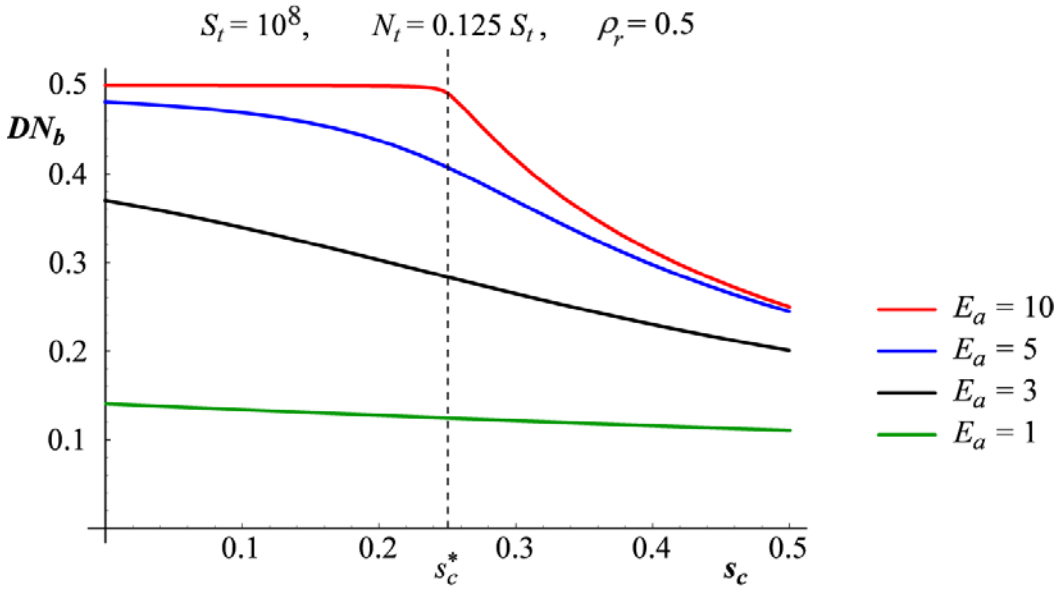

Figure 2.6: The density of ligands in the contact zone for different ligand-receptor binding strengths. Saturation at large binding strength is at $DN_b = \rho_r$.

In the crossover between these two (E_a-based) limits, the density of bonds remains a permanently decreasing function with increasing the size of the contact zone. This fact has important consequences when the size of the contact zone becomes a variable, as in a detachment process induced by the application of a vertical point force (Chapter 4).

2.4.3.2 Dependence on the binding strength of the ligand-receptor pair

In this presentation of the allocation functions, the concentrations of the ligands and the receptors are preset, as is S_c^*. Furthermore, the size of the contact zone must be chosen. The relation between these system parameters, as shown in previous sections, determines whether the system will be in a ligand-dominated or a receptor-dominated equilibrium. Thus when N_b is plotted as a function of the ligand-receptor binding strength, the entire resulting curve is a set of only one type of equilibria.

Two regimes for the number of bound ligands can be seen in Figure 2.7 where the relevant variable is the binding strength of the ligand-receptor pair. For small and intermediate values of the binding strength, the allocation function for bound ligands experiences rapid, almost linear, growth that continuously deviates into a saturation regime defined by one of the two limits at $E_a \to \infty$.

From the mathematical point of view, all allocation functions in Figure 2.4 are almost symmetrical sigmoids with a well-defined linear regime (see also Figure 2.7). To accurately characterize this linearity, the allocation functions should be expanded around the inflection point that signifies the center of the linear part of the curve. However, due to the complexity of the expressions for the full solutions (Eq. (2.7)), such a task is associated with considerable analytical difficulties and unserviceable results. Therefore, a

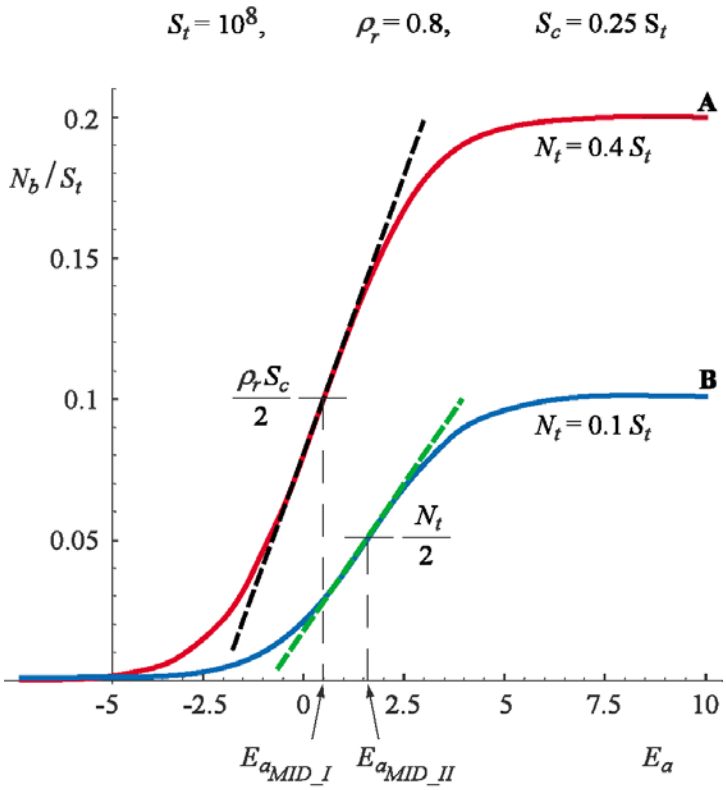

Figure 2.7: The allocation function of bound ligands as a function of the ligand-receptor binding strength. The real solution N_b and the results of the expansion (N_b^{I} and N_b^{II}) are presented with full and short dashed lines, respectively. Points used for the expansion can be associated with the intersection of N_b curves with the long dashed lines. The curve denoted by **A** belongs to the case $S_c < S_c^*$ and is representative of a set of receptor-dominated equilibria. The curve denoted by **B** belongs to the case when $S_c > S_c^*$ and is constructed from a set of ligand-dominated equilibria.

simple but successful procedure has been undertaken for determining the alternative expansion point. The ordinate of this point ($N_b^{\mathrm{I}m}$ and $N_b^{\mathrm{II}m}$) is determined as the value intermediate between the $-\infty$ and $+\infty$ limits. As the allocation function of bound ligands is equal to zero as $E_a \to -\infty$, the ordinate of the expansion point will depend on whether $\rho_r S_c > N_t$ or $\rho_r S_c < N_t$. The abscise of the expansion point can be associated

with the binding strength at which the N_b line crosses the value of the ordinate (see Figure 2.7).

a) Receptor-dominated equilibria.

The coordinates of the expansion point are found to be:

$$N_b^{Im} = \rho_r S_c / 2, \tag{2.14}$$

$$E_a^{I} = \ln \frac{2S_t - 2N_t - \rho_r S_c}{2N_t - \rho_r S_c}, \tag{2.15}$$

which leads to an expansion of N_b in the form:

$$N_b^{I} = \frac{\rho_r S_c}{2} \frac{(2N_t - \rho_r S_c)(2N_t + \rho_r S_c - 2S_t)}{8N_t^2 - 8N_t S_t + 2\rho_r S_c S_t} \left(E_a - E_a^{I}\right) + \frac{\rho_r S_c}{2}. \tag{2.16}$$

For curves representing receptor-dominated equilibria (curve A in Figure 2.7), increasing the number of ligands in the vesicle (N_t) while keeping the coverage density (ρ_r) and the size of the contact zone (S_c) constant, results in a shift of E_a^{I} to smaller energies. As N_b must converge to a constantly maintained value of $\rho_r S_c$, and the slope of N_b^{I} is not significantly altered, N_b also converges to its limiting value at smaller values of E_a. On the other hand, maintaining N_t constant while increasing either ρ_r or S_c leads to a convergence of N_b at increased values, which considerably increases the slope of N_b^{I}. Nevertheless, the saturation of N_b is reached more slowly in both cases. Interestingly, an increase of ρ_r (at constant N_t and S_c) results in a shift of E_a^{I} to smaller values, whereas an increase of S_c (at constant N_t and ρ_r) has the opposite effect.

b) Ligand-dominated equilibria.

The coordinates of the expansion point are found following the same method as previously described:

$$N_b^{\mathrm{II}m} = N_t / 2, \tag{2.17}$$

$$E_a^{II} = \ln \frac{2S_t - N_t - 2\rho_r S_c}{N_t - 2\rho_r S_c}, \tag{2.18}$$

which results in the expansion:

$$N_b^{II} = \frac{N_t}{2} \frac{(N_t - 2\rho_r S_c)(N_t + 2\rho_r S_c - 2S_t)}{8\rho_r^2 S_c^2 - 8\rho_r S_c S_t + 2N_t S_t} \left(E_a - E_a^{II}\right) + \frac{N_t}{2}. \tag{2.19}$$

For this type of equilibrium (curve B in Figure 2.7), the convergence of N_b is governed by the number of ligands in the vesicle. Adding receptors to the surface or increasing the size of the contact zone, while maintaining N_t constant, results in the convergence of N_b to N_t at smaller values of E_a. Although the slope of N_b^{II} remains almost unaltered, raising either ρ_r or S_c results in a shift of E_a^{II} to smaller values. Preparing vesicles with higher ligand concentration while keeping the size of the contact zone (*e.g.* the reduced volume of the vesicle) or the substrate composition constant, will increase the saturation level of N_b. In this case, the convergence is achieved at higher values of both E_a and E_a^{II}. Nevertheless, the slope of N_b^{II} is increased with a higher content of ligands.

2.4.3.3 Relevance to Applications

Together with the convergence limits, which are usually reached at ligand-receptor binding strengths of the order of $10 k_B T$, the developed approximations cover most of the parameter space in which N_b should be determined. As, can be seen from Table 2.3, both expansions N_b^{I} and N_b^{II} are good approximations to N_b and can be used when the somewhat simpler N_b^{LIN} is inappropriate. This is particularly important for the intermediate range of the ligand-receptor binding strengths. Furthermore, for low coverage or small contact zones N_b^{I} and N_b^{II} can be considerably simplified to depend only on the total number of ligands in the vesicle.

Table 2.3: Regions of parameters for the applicability of different approximate relations of the allocation function of the bound ligands. The critical size of the contact zone is a ratio between the total number of ligands in the vesicle and the density of receptors on the substrate ($S_c^*=N_t/\rho_r$). $S_c^*< S_c$ is indicative of a receptor-dominated type of equilibrium whereas $S_c^* > S_c$ results in a ligand-dominated equilibrium**.** N_b^{LIN}, N_b^I, and N_b^{II} are defined in text by Eq. (2.12), Eq. (2.16), and Eq. (2.19), respectively.

E_a	$S_c^* > 0.5S_t$	$S_c^* < 0.5S_t$	
	$S_c < S_c^*$	$S_c < S_c^*$	$S_c < S_c^*$
very low	$N_b^{LIN} \to \rho_r S_c N_t / S_t$		
Low-medium	N_b^{LIN}	N_b^I	N_b^{II}
strong	$N_b^{LIN} \to \rho_r S_c$		N_t

The allocation function for free ligands in the contact zone (N_f) and the allocation function for the total number of free ligands in the vesicle (N_{free}) share the same E_a^I and E_a^{II}. Hence, their expansions can be calculated by the use of the density equation (2.5).

2.5 The effective adhesion strength

Vesicle adhesion is often regarded as a wetting phenomenon where the spreading pressure of a vesicle is determined as the work of the system to induce changes in the contact area with the substrate. Several experimental studies have reported measurements of the adhesion strength of specifically adhered vesicles based on the usage of the Young's law [106,107]. Moreover, previous theoretical investigations have shown that the shape of the vesicle can be understood by adhesion in a continuous (contact) potential [109]. In these models, the average adhesion strength is constant, independent of S_c and given externally. To make a link between the present model and the previously used approaches, it is necessary to calculate the effective adhesive potential (W) resulting from numerous local bindings. Within the canonical approach undertaken herein, the average adhesion strength becomes a function of the size of the contact zone, with a functional dependence that can be obtained by calculating:

$$W \equiv -\frac{1}{a}\frac{\partial F}{\partial S_c}\bigg|_{\rho_r} \equiv \frac{\omega}{a} \quad . \tag{2.20}$$

Here a is the area of a single site and is determined by the size of a ligand. For a chosen value of S_c, it is found that:

$$\omega = \rho_r \cdot \left(\ln \frac{(1-\rho_r)S_c - N_f}{(1-\rho_r)S_c} - \ln \frac{\rho_r S_c - N_b}{\rho_r \cdot S_c} \right) . \tag{2.21}$$

To obtain ω for a given size of the contact zone, N_b and N_f must be calculated from Eqs. (2.7-2.8). The first term on the right hand side of Eq. (2.21) is the natural logarithm of the density of ligand-free sites in the part of the contact zone unoccupied by receptors, whereas the second term is the logarithm of the density of ligand-free sites in the part of the contact zone occupied by receptors. As the chemical potential is the logarithm of a density, ω is the result of an imbalance between two chemical potentials of ***empty*** sites, weighed by the density of receptors.

The dependence of the effective adhesion strength (W) on the ligand size (a) results in ω expressed in units of k_bT. For a ligand with a gyration radius of 3.5 nm, $\omega = 1$ leads to W of the order of 10^{-5} N/m. Moreover, the conversion to adhesion strengths w, as

employed in continuous models [109,110,111,112], can be achieved by using the relation $w = \omega \cdot 4\pi\kappa / S_t \; k_B T$. For a standard bending rigidity of the membrane $\kappa = 100 \;\; k_B T$ and $S_t = 10^7$, this conversion would lead to $w \approx 10^{-4}\,\omega$.

2.5.1 Limiting behavior and the dependence on the binding strength of the ligand-receptor pair

Several important properties of ω are inherent from the allocation functions and are a result of the existence of the two sorts of equilibria (dominated by either by ligands or receptors) and their limits when $E_a \to \infty$. However, for both types of equilibria, ω vanishes as $E_a \rho_r N_t / S_t$ as $E_a \to 0$. In the receptor-dominated equilibria ($S_c < S_c^*$), a diverging linear regime (presented in the left panel of Figure 2.8) is found to dominate the behavior of ω:

$$\omega \propto \rho_r E_a + \rho_r \ln \frac{N_t}{2(S_t - N_t)}, \text{ for } \; E_a \to \infty . \tag{2.22}$$

In the ligand-dominated equilibria ($S_c > S_c^*$) inspection of the right panel in Figure 2.8 reveals a rapid increase of ω followed by convergence to a finite value:

$$\omega \approx \rho_r \ln \frac{\rho_r S_c}{\rho_r S_c - N_t}, \text{ for } \; E_a \to \infty . \tag{2.23}$$

After a certain binding strength, all of the ligands in the vesicle become bound. Hence, in this regime, further increasing the ligand-receptor binding strength does not influence the average adhesion strength.

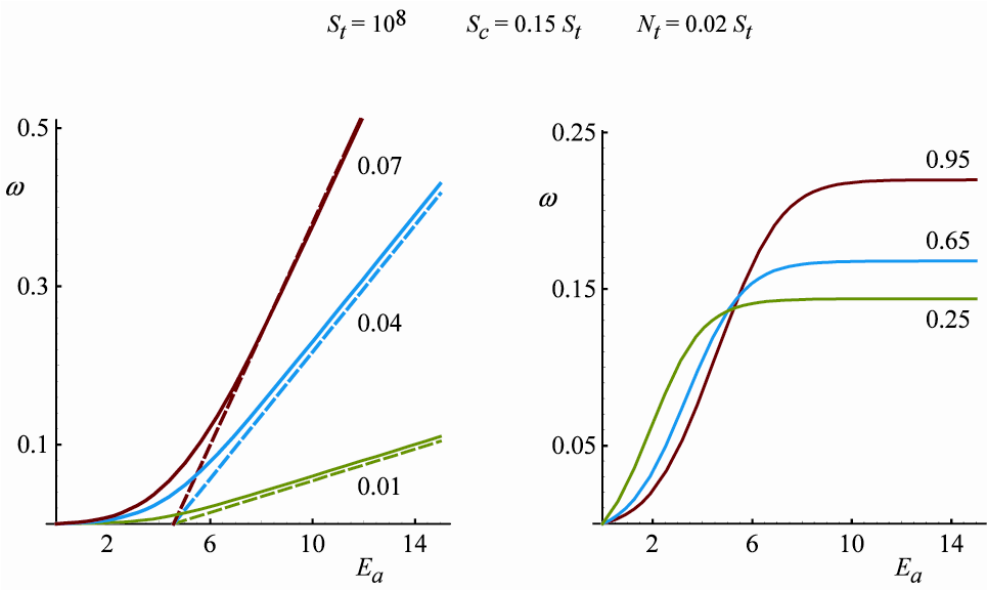

Figure 2.8: Effective adhesion strength as a function of the ligand-receptor binding strength for different coverage densities (numbers indicated next to curves). **Left:** Diverging of the effective adhesion strength characteristic for the receptor-dominated equilibria. The full solution (lines) and the asymptote from Eq. (2.22) (dashed lines) are shown. **Right:** The saturation of the average adhesion strength is characteristic for the ligand-dominated equilibria. The effective adhesion strength for this type of equilibrium converges to values given by Eq. (2.23).

2.5.1.1 Dependence on the size of the adhesion plate

Detaching the vesicle by means of local force application, flow, or the insertion of antibodies is usually associated with changes in the size of the contact zone. Hence, the work on the vesicle performed by any of these means can be evaluated from the change in the effective adhesion strength. Thus, it is particularly important to understand the dependence of the adhesion strength on the size of the contact zone.

It is easy to show that ω is a monotonically decreasing function of S_c independently of the choice of other parameters. This is a consequence of the fact that the density of bound ligands never increases in response to an increase in the size of the contact zone (at a given coverage, binding strength and total number of ligands in the vesicle). Instead, the large changes in ω are a consequence of the changes of the derivative of the density with respect to S_c. When the allocation function of bound ligands reaches its limiting values, imposed by the composition of the vesicle and the substrate, the density of bonds is

independent of the size of the contact zone. The maximum value in the effective adhesion strength (ω_0) is reached at S_c =0 and is calculated to be:

$$\omega_0 = \rho_r \ln\left[\left(e^{E_a} - 1\right)\frac{N_t}{S_t} + 1\right]. \qquad (2.24)$$

Interestingly, if Eq. (2.24) is plotted as a function of E_a, then excellent overlap is obtained with the curves presented in Figure 2.8 for small E_a for both types of equilibria (data not presented). Furthermore, for large E_a and in the receptor-dominated equilibria (left panel in Figure 2.8), ω_0 increases linearly with the same slope as predicted by the asymptote Eq. (2.22), but with a somewhat underestimated offset of ω_0. However, for a choice of parameters resulting in these receptor-dominated equilibria, at low coverage ω_0 provides a very good approximation to the full solution of ω over the entire range of E_a.

It is important to notice that, when the adhesion strength is presented as a function of the size of the contact zone (Figure 2.9), an inflection point occurs at $S_c^* = N_t / \rho_r$. In the region resulting in ligand-dominated equilibria, Eq. (2.23) (shown with a dotted line in Figure 2.9) can be used to approximate the real solution for ω. An analogous approximate relation is determined in the region producing receptor-dominated equilibria where $S_c < S_c^*$:

$$\omega \cong \omega_0 - \rho_r \ln\frac{N_t}{N_t - \rho_r S_c} \ . \qquad (2.25)$$

The comparison of Eq. (2.25) (short dotted lines) with the real solution is given in Figure 2.9. For large E_a, both Eq. (2.25) and Eq. (2.23) are found to be very useful, as shown on the left panel in Figure 2.9. In the intermediate range of binding strengths (middle panel of Figure 2.9), the region around the inflection point is badly reproduced by the approximate solutions. The width of this region depends entirely on the binding strength E_a. However, the position of the inflection point can be regulated by changing the density of ligands in the vesicle and the receptors on the surface. Both an increase of N_t and a decrease of ρ_r are capable of translating S_c^* to larger values. Therefore, for such intermediate values of E_a, Eq. (2.25) provides a good approximation for small sizes of the contact zone. Conversely, a decrease of N_t or an increase of ρ_r shifts S_c^* to smaller values. This permits the use of Eq. (2.22) at large sizes of the contact zone.

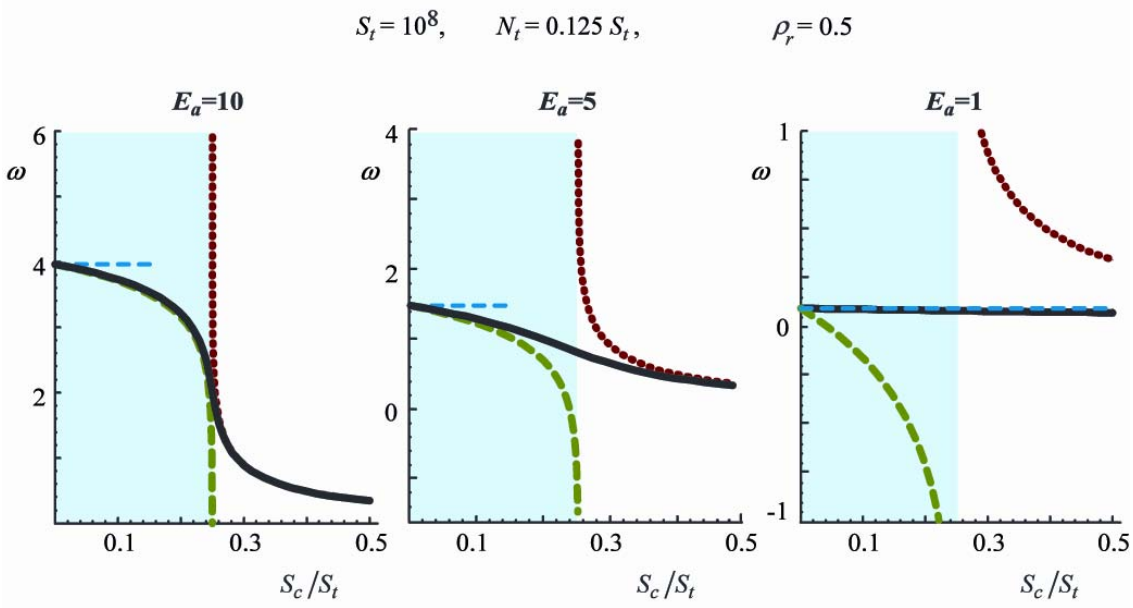

Figure 2.9: Effective adhesion strength as a function of the size of the contact zone. Due to geometrical constraints, the size of the contact zone is restricted to half of the total vesicle area. The shaded regions depicts the regions characteristic for receptor-dominated equilibria, whereas the region of parameters resulting in ligand-dominated equilibria is shown with a white background. **Left:** Nonlinear behavior with a crossover at S_c^* described with approximate solutions from Eq. (2.22) (dotted lines) and Eq. (2.25) (short dashed lines) characterize the ω for E_a. **Middle**: For intermediate binding strengths of the ligand-receptor pair, agreement with the approximate solutions is obtained only in some parts of the curves. These parts are imposed by the coverage density of the substrate. **Right:** For low binding strengths, the approximate solutions are not valid. The effective adhesion strength is a slowly varying function and its magnitude is given by Eq. (2.24), along the whole range of sizes of the contact zone.

For weak ligand-receptor pairs, the density of ligands in the contact zone is almost constant for any size of the contact zone and ω experiences only very small changes. Though neither Eq. (2.22) nor Eq. (2.25) is applicable in this range of E_a, the effective adhesion strength can be approximated with ω_0 as shown in the right panel of Figure 2.9.

As a final point, it is informative to compare the shapes of the curves shown in Figure 2.9 with the corresponding ones contained within Figure 2.6.

2.6 Consequences of the model

The calculation of the thermodynamic equilibrium for a vesicle containing ligands that are capable of specific binding to receptors on the substrate has been successfully performed. Although this work is, in spirit, based on the same physical ideas as those employed in the well known studies of Dembo, Bell and Torney [113,114], some important regimes in vesicle adhesion driven by specific binders have successfully been identified and characterized in an unencumbered manner.

The results of the calculations show that the choice of the statistical ensemble is an important issue. In particular, the experimental reality is such that the contact zone of the vesicle with the substrate is usually relatively large, so that the final number of receptors in the contact zone is at least comparable to the total number of ligands in the vesicle [106,115]. The large adhesion patches (of the order of μm^2) obtained in these experiments, indicate the formation of numerous ligand-receptor bonds. However, the ligands participating in these bonds have had to diffuse from the free part of the vesicle (hence the observation of diffusion limited adhesion). As the experiments are performed with a constant total number of ligands in the vesicle, the concentration of ligands in the upper part of the vesicle has therefore had to undergo considerable reduction upon adhesion. Under these circumstances, treating the adhesion in a grand canonical model where the ligands are coupled to a bath of constant chemical potential is not correct. Rather, a canonical statistical ensemble should be imposed on the vesicles. Regardless of the parameterization of the canonical ensemble, the condition of thermal equilibrium dictates that the chemical potential of the ligands in the contact zone and in the free part of the vesicle are equilibrated. The entropic cost for depletion in one region is balanced by the gain in the internal energy in the other region. Even if a given molecule is in the region of increased density, this molecule has on average, no incentive to penetrate the depleted region. Hence, differences in densities between the two regions cannot be directly interpreted as a lateral osmotic pressure. Such pressure would arise from unbalanced chemical potentials which would be contrary to the equilibrium condition.

A direct consequence of the canonical treatment of vesicle adhesion is the identification of two types of equilibria dominated by the contribution of ligands and receptors, respectively. When the number of receptors in the applicable contact zone is the same as the total number of ligands in the vesicle, the system undergoes a crossover between the

two types of equilibria. The existence of these two types of equilibria is a result of the finite reservoirs of ligands and receptors in the system and has implications not only on the allocation of bound and free ligands in the vesicle but also on the behavior of the effective adhesion strength.

The presented calculations suggest that the use of ligand-receptor pairs associated with a strong binding constant (as in the case of the biotin-streptavidin or RGD-integrin pairs), would lead the vesicle-substrate system into an equilibrium described by one of two limits of the allocation function of bound ligands for $E_a \to \infty$. Hence, there should be basically either no free ligands in the vesicle or no free receptors on the substrate.

The equilibrium of the system can be found either by finding the optimum number allocations (as in the case of the presented model) or by equilibration of chemical potentials. The result is independent of the procedure. However, in a possible experiment where one of the system parameters can be continuously tuned, the pathway will depend on whether each new state is associated with constant chemical potential or a constant number of particles. Changing the size of the contact zone by means of adjusting the osmotic conditions of the buffer solution, or influencing the binding strength by changing the content of the buffer are two possible ways that could be used for exploring the equilibrium adhesion of a single vesicle. As such processes are associated with a constant number of ligands in the vesicle, the number allocation functions should be employed to interpret the measured changes. Manipulating parameters of the system such as S_c or E_a would, according to the presented calculations, be equivalent to moving along one of the lines presented in Figure 2.5 or Figure 2.7, respectively.

An important fact emerging from the model is that the bending energy can be virtually omitted from the calculations. The bending energy is a function of the membrane elastic modulus κ and seldomly exceeds $10^{-5}\ k_BT$ per site on the vesicle. On the other hand, the contribution of each ligand in a vesicle is of the order of 1 k_BT. As the number of ligands is very large, it is clear that the bending is not of comparable magnitude. Hence, as long as the shape of the vesicle is not that of the spherical cap, deformations of the membrane are energetically inexpensive, provided that the ratio between the surface area of the contact zone and the free part of the vesicle remains unchanged. This explains the stability of strongly deformed membranes balanced by an agglomeration of ligand-receptor bonds at the edge of the contact zone, as often observed in experiments on weakly adhered vesicles. As the strength of adhesion (or the density of bonds) increases

and the spherical cap is approached, the tension in the vesicle becomes large and unusual deformations become energetically expensive and unobservable. Indeed, in experiments where the shape of a vesicle is a spherical cap, the contact zone is observed to be discoid with no pronounced deformations whatsoever [106].

Due to the divergence of the bending energy, a boundary minimum with respect to the size of the contact zone is identified. It leads to a thermodynamic equilibrium in which the contact zone is maximized and the vesicle always assumes the shape of a spherical cap, as seen in some experimental studies [107]. Depending on the coverage of the substrate and the density of ligands, the number of bound molecules can be determined by Eq. (2.7) or one of its approximate solutions ($N_b^{\ I}$, $N_b^{\ II}$ or $N_b^{\ LIN}$).

Despite the predicted existence of the boundary minimum, there are quite some experimental situations, where the vesicle appears to be in its equilibrium state without assuming the shape of the spherical cap [107,116]. The adhesion process associated with such a state is usually slow and stepwise, and should be expected when the probability for bond formation is reduced, due to either a low coverage or a low fraction of ligands in the vesicle. Technically, the slow equilibration leads to a relaxation of the free energy with respect to the number of ligands in the contact zone but not with respect to the size of the contact zone. In this constrained equilibrium, the allocation functions resulting from the minimization are still valid, but the size of the contact zone is not determined by the bending divergence but by factors such as the non-specific interaction potential, shape fluctuations and the probability for bond formation. The shape of the vesicle in this constrained equilibrium can be determined by the use of a continuum model [109] where the bending energy must be minimized for a chosen size of the adhesion zone. However, it is important to emphasize that the proposed allocations can be applied to both the thermodynamic and the constrained equilibria.

The densities of bound and free ligands in the contact zone are found to be responsible for the strength of the effective adhesive potential. This potential, in thermodynamic equilibrium, is equivalent to the spreading pressure obtained from the Young-Dupré law for liquid droplets. However, in the constrained equilibrium, the contact angle of the vesicle with the substrate is not well defined and so the Young-Dupré law is not valid. Under these circumstances, the effective adhesion strength and the shape of the vesicle can be calculated by minimizing the bending energy of a vesicle for a given size of the contact zone by the methods employed in the continuous models. The effective adhesion

strength of constrained equilibria is dominated by non-specific interactions. Hence, the ω originating from the current model should be interpreted as the bond contribution to the total effective adhesion strength.

The calculation of the effective adhesion strength provides a bridge between models based on a continuous potential and those based on discrete specific binding. As shown in [111, Appendix D], pulling on vesicles in constrained equilibria will result in continuous shape deformations, whereas pulling on vesicles in thermodynamic equilibrium results in tether formation [112, Appendix C]. Thus, the knowledge of the effective potential enables the determination of the vesicle shape (from continuous models) and the number of bonds in the contact zone (from the current discrete model) [117, Chapter 4]. In addition, the model outlined herein can be used for the identification of the main mechanisms in which a competitive binder (an antibody), injected into the surrounding buffer, acts on specifically adhered vesicles [118 or Chapter 3]. In conclusion, although the presented model is relatively simple, it produces practical results that are widely applicable to the interpretation of experimental data.

2.7 References

106. Guttenberg, Z., B. Lorz, E. Sackmann, and A. Boulbitch. 2001. *Europhys. Lett*. **54**:826-832.

107. Nardi, J., R. Bruinsma, and E. Sackmann. 1999. *Phys. Rev. E* **58**:6340-6354.

108. Landau L. D., and E. M. Lifshitz 1958. *Statistical Physics, vol 5*.

109. Seifert U., and R. Lipowsky. 1990. *Phys. Rev. A* **42**:4768-4771.

110. Kraus M., U. Seifert, and R. Lipowsky. 1995. *Europhys. Lett.* **32**:431-436.

111. Smith A.-S., E. Sackmann, and U. Seifert. 2003. *Europhys. Lett.* **64**:281-288.

112. Smith A.-S., E. Sackmann, and U. Seifert. 2004. *Phys. Rev. Lett.* **92**:208101.

113. Bell. G. I. 1978. *Science* **200**:618-627.

114. Bell G. I., M. Dembo, and P. Bongrad. 1984. *Biophys. J.* **45**:1051-1064.

115. Bruinsma R. F., A. Behrisch, and E. Sackmann. 2000. *Phys. Rev. E* **61**:4253-4267.

116. Lorz B. G., A.-S. Smith, C. Gege,and E. Sackmann. *In preparation.*

117. Smith A.-S., S. Goennenwein, U. Seifert, and E. Sackmann. *In preparation.*

118. Smith A.-S., B. Lorz, U. Seifert, and E. Sackmann. *Submitted for publication.*

CHAPTER 3

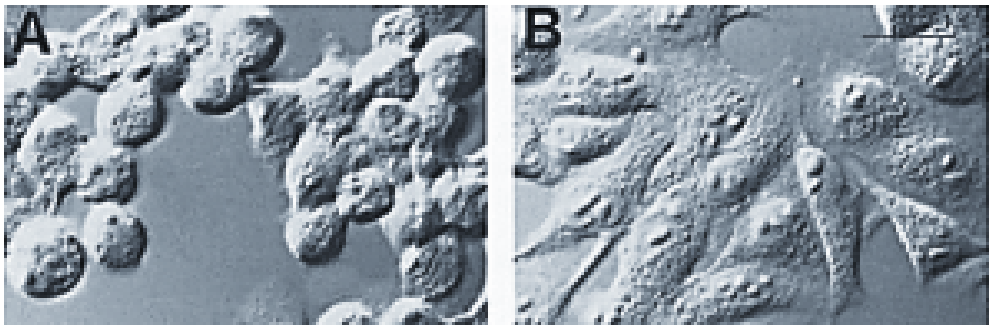

ANTAGONIST INDUCED UNBINDING 64

Above: Specific adhesion of Madia-Darby kidney cells is reduced when cells are treated with inhibiting antibodies (A) in comparison to the control sample (B). Picture from Zinkl *et al*. [3].

Chapter 3

ANTAGONIST-INDUCED UNBINDING

In the following chapter, a new type of control mechanism, inspired by the antibody-mediated competitive inhibition of proteins expressed on the cell surface, is investigated. Antibodies are types of protein made by white blood cells in response to foreign substances and are capable of binding to their specific complement (antigen). The strength of the receptor-antibody bond is a function of the specificity of the recognition [119]. Antibodies are a crucial component of the immune system, circulating in the blood and lymphatic fluid. Several mechanisms of antibody action can be identified in cell biology. For example, agglutination involves the conglomerate binding of multiple large particles with antigens on their surfaces (e.g., bacteria or red blood cells). The receptor-antibody binding can also create a molecular complex so large that it is rendered insoluble and precipitates (e.g., tetanus toxin). Neutralization occurs when the antibodies simply cover the toxic sites of the receptor.

The direct aggregation of antibodies on antigens is not usually sufficient to completely protect the body. The major protective efforts of antibodies take place through the amplifying effects of the "complement" system, a collection of about 20 different proteins. Many of these proteins are enzyme precursors that are normally inactive, but can be activated by the antigen-antibody reaction. When an antibody binds with its target, a specific reactive site on the antibody is activated. This site binds with a molecule of the complement system and sets a cascade of reactions into motion. A single antibody-receptor combination can thus activate many molecules, which in turn activate increasing amounts of enzymes. The multiple end products formed by this amplified process help to prevent damage by invaders.

Antibodies are also capable of influencing the cell morphology, polarity and behavior. For example, basal domains of epithelial cells polarize not only in response to cell-cell

contacts but also to contact with substratum-composed extacellular matrix proteins such as laminin, collagen IV, and heparin sulfate proteoglycans [120]. In the presence of the 12B12 monoclonal antibody, which binds specifically to the Forsmann glycosphyngo-lipid on Madia-Darby kidney cells, the polarization of basal proteins is disabled. This prevents the formation of focal adhesion points between the β1 integrin and the laminin network. Consequently, the adhesion of cells to the substratum is severely reduced [121].

Independently of the exact biological role that an antibody performs, it is intrinsic to its binding function to compete with one participant in a regularly occurring ligand-receptor interaction. It can be hypothesized that the underlying physical mechanism for such competition is provided by an osmotic pressure exerted by antibodies dissolved in solution. Such osmotic pressure would interfere with the chemical potential of the ligand-receptor pair in question.

In order to explore this hypothesis, an experimental model system has been developed. Receptors of the selectin family (E-selectin) are immobilized on a solid surface (acting as the target cell) while the conjugate ligands (lipid–coupled sialyl-Lewis^X) are incorporated in giant vesicles acting as test cells. As a source of competition, monoclonal antibodies against E-selectin are introduced following the establishment of the ligand-receptor-mediated adhesion equilibrium. Characterization of this model system has shown that antibodies indeed produce a large impact on the adhesive properties of the vesicles. By extending the theoretical considerations presented in the previous chapter, it is possible to identify and rationalize the experimental outcomes and provide a quantitative background for the observed unbinding mechanisms.

3.1 Observation of antibody inhibition in the model system

3.1.1 Adhesion of vesicles to the substrate

Prior to the formation of ligand-receptor bonds, the vesicle settles at a height governed by the effective potential acting between the membrane matrix and the substrate. Due to the passivity of the substrate and the repulsion exerted by the glycolipids reconstituted into the membrane, the minimum of this potential is sufficiently far from the substrate that a weakly bound vesicle still exhibits strong undulations [122]. After some time, ligand-receptor bonds begin to form. The adhesion process associated with this type of specific binding results in the aggregation of the ligand-receptor pairs, leading to two types of adhesion zones within the adhesion disc (see Figure 3.1 B). In the first type, the vesicle membrane is locally trapped in patches of strong adhesion generated by ligand-receptor bonds formed and the undulations are almost totally suppressed [123]. In the second type of contact, the membrane outside of the patch remains in the initial stage of weak adhesion and is subject to fluctuations (see Figure 3.1 B). When the formation of patches dominates the overall effective potential, they begin to grow beyond the initially established contact zone between vesicle and substrate, inducing a first order shape transition [124,125]. For the vesicles whose adhesion is mediated by the sLe^X-E-selectin pair, such transitions occur for high coverage of the substrate and a relatively large fraction of ligands in the vesicle [126]. When the equilibrium is attained, the contact zone is maximized and appears uniform within the resolution of the microscope (see Figure 3.1 C).

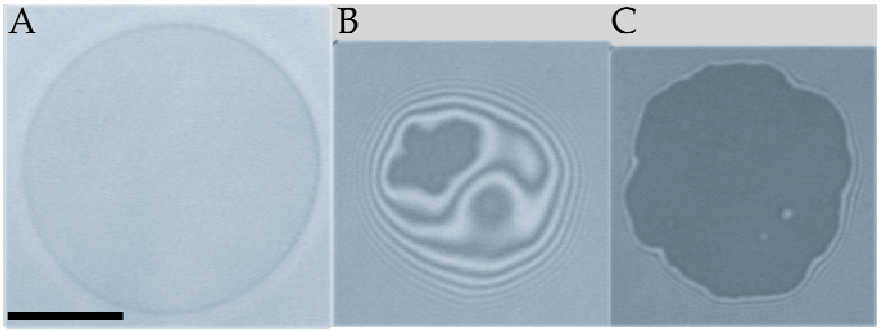

Figure 3.1: Different stages of the adhesion process of a single vesicle. The scale bar indicates the length of 10 μm. **A)** The bright field picture of the vesicle. **B)** Coexistence of a patch of strong adhesion (dark) and a region of contact of the weak adhesion (bright field exhibiting interference fringes). **C)** Adhesion following the shape transition induced by the growth of the patch to its maximum size, associated with the aggregation of the ligand-receptor bonds.

3.1.2 Antagonist-induced unbinding

Once a steady state of adhesion is reached, small amounts of antibodies are added to the buffer solution. The mouse anti-human E-selectin is capable of blocking the sLe^X binding site of E-selectin which may interfere with the receptor–ligand bonds. Indeed, upon insertion of antibodies into the solution, three phases of vesicle unbinding (denoted as Phases I to III) are observed.

3.1.2.1 Phase I – lateral pressure mechanism

Phase I is characterized by a decrease in the size of the contact zone. This is particularly apparent in the final row of Figure 3.2, where the edge of the vesicle contact zone prior to the antibody insertion is compared with the edge of the contact zone at the end of this phase. During this time, the contrast within the inner part of the contact zone is not altered. Instead, the entire adhesion plate still appears to be strongly bound, indicating the persistence of the ligand-receptor bonds inside this region (see the second row in Figure 3.2). As both the coverage of the substrate with E-selectin (about 3000 molecules/μm^2 as estimated by Lorz et al. [126]) and the concentration of ligands in the vesicle (10 mol%), are relatively high, the contact zone must be relatively densely packed with bonds. Diffusion of molecules the size of antibodies is thus strongly suppressed in comparison to the diffusion in the bulk solution, impeding their access to E-selectin buried within the contact zone. In this short initial stage (about 3 minutes), the action of the antibodies occurs merely at the rim of the adhesion plate, while the remaining part of the zone appears impermeable. Apparently, the binding of the antibodies to the substrate results in a lateral two-dimensional pressure on the rim of the contact zone, consequently reducing the excluded area of the adhesion plate. The final size of the zone is presumably determined by the balance between the antibody pressure and the spreading pressure of the vesicle.

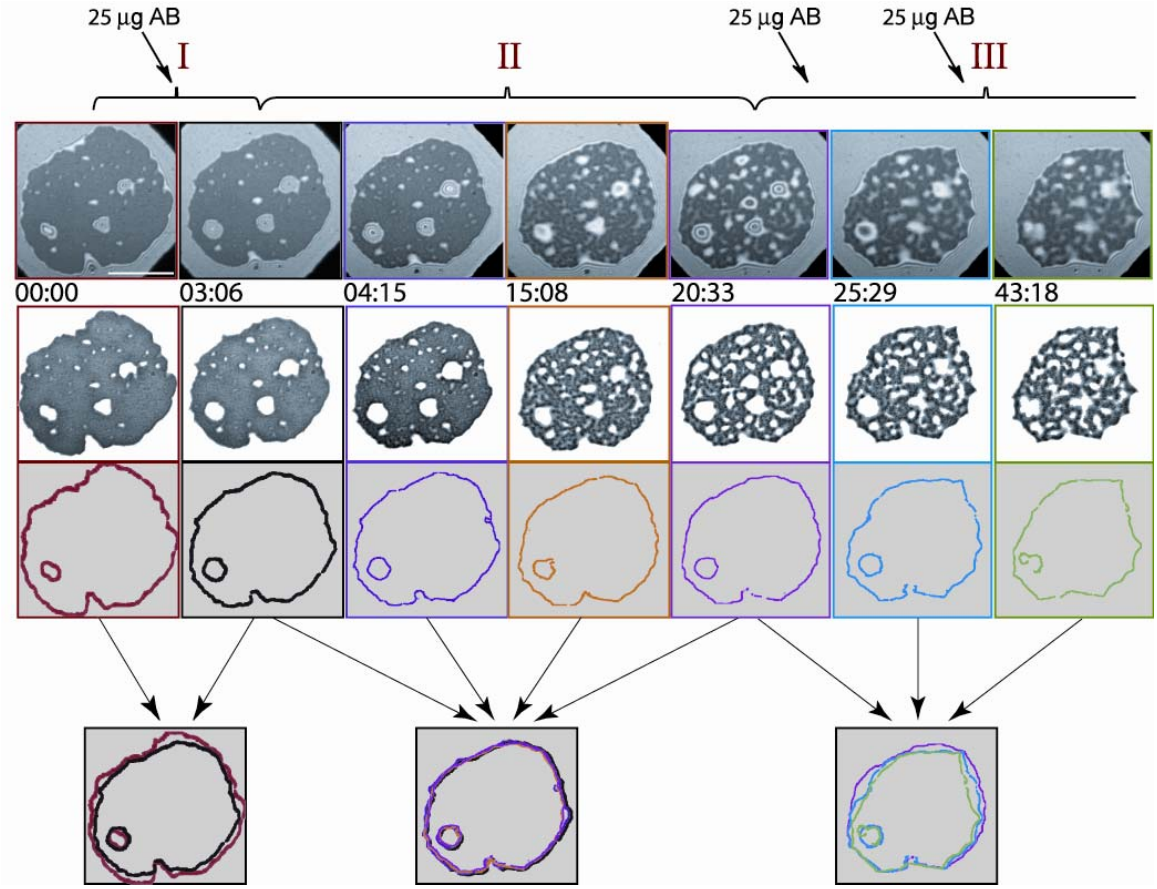

Figure 3.2: Unbinding of a vesicle by antibody titration. Injections of antibody solutions are marked with thick arrows in the top part of the figure. The scale bar in the top left frame indicates the length of 10 µm. The three phases of the unbinding process are indicated with red roman numerals. In the first row, the original RICM images, taken at the times (minutes and seconds) indicated at the bottom of each image, are presented. The strong adhesion zones are extracted in the second row while the rims of the contact zone are presented for the corresponding frames in the third row. The rims for each phase are superimposed in the last row, with the thin arrows indicating which frames are superimposed. **Phase I** is a short phase where the antibodies are acting on the rim of the contact zone merely as a lateral two-dimensional pressure. In **Phase II** the spreading pressure of the vesicle equilibrates with the lateral antibody pressure. In this slow phase, the antibodies are penetrating the adhesion patch, and the dewetting occurs as the competitive binding of antibodies to receptors takes place. **Phase III** occurs upon a further increase of antibody concentration. At this stage, both mechanisms (the receding of the rim and the penetration of antibodies into the whole adhesion zone) are in action.

3.1.2.2 Phase II – competitive binding mechanism and Phase III

Phase II is a much slower regime of the dewetting process and begins when the antibodies penetrate the contact zone. During this period (lasting about 20 min), the vesicle and the antibodies are seeking a new equilibrium and this process is driven by the chemical potential provided by the antibodies in the bulk solution. Although it is found that the size of the total contact zone remains almost unaltered (see the overlapping edges in the last row of Figure 3.2), the distribution of the bonds gradually changes from uniform to highly structured. The higher affinity of the antibodies for E-selectin causes the number of sLe^X-E-selectin bonds to decrease. After some time, the vesicle finds a new thermodynamic equilibrium and no further change in the structure of the contact zone is visible.

Further increasing the antibody concentration, after the thermodynamic equilibrium has been achieved in Phase II, induces a transition of the vesicle into Phase III of the dewetting process. At this point, the contact zone becomes highly permeable to antibodies, but the excluded area is still relatively large. Under these circumstances, both the lateral pressure mechanism that dominates Phase I, and the competitive binding mechanism prevailing during Phase II can act simultaneously. Considerable loss of both the size of the contact zone and the number of bound ligands can therefore be observed. The latter process can be identified by the change in contrast within the contact zone, and an increase of white area in the second row in Figure 3.2. The size changes are evident from the overlapping edges from this phase (final row of Figure 3.2).

The area of strong adhesion occupying the entire contact zone remains uniform during Phase I. In Phase II, however, it gradually decomposes into a very large number of domains reminiscent of focal adhesion complexes (FAC). After a certain time during Phase II the formation of FACs saturates and the number of newly formed FACs is negligible in comparison to those detaching from the substrate. This is demonstrated in Figure 3.3 where a highly structured contact zone from the beginning of Phase II is compared to the one from Phase III. Although the size of the patch has been considerably reduced over 30 minutes, all of the FACs persisting into Phase III can be traced in the earlier picture from Phase II. At the same time, only a few FACs (indicated in Figure 3.3 with yellow circles) were formed. Interestingly, the membrane retracts only by the loss of a whole FAC at once, which means that a FAC must have a critical minimum size. The

membrane released in the detachment of FACs is able to fluctuate, particularly where large holes appear in the patch. This is responsible for the light blue colors in Figure 3.3.

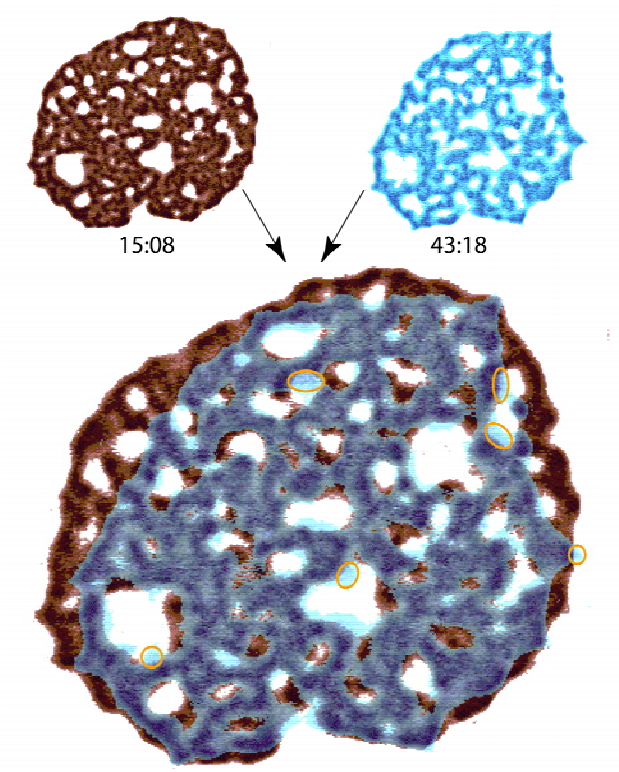

Figure 3.3: An overlay of two pictures of the contact zone dominated by ligand-receptor interactions. The two superimposed images are shown in the top left and top right corners together with the relative times at which the snapshots were taken. For better visualization, the gray color scale from the original pictures has been transformed into either a red or a blue scale. The pictures were then made transparent and overlaid. Where the two pictures overlap, the gray colors emerge. The intensity of the colors reflects the strength of binding.

If the experiment is repeated with half of the previous concentration of receptors on the substrate, somewhat different behavior is observed. In this case, as shown in Figure 3.4, prior to the insertion of antibodies one observes an assembly of strong adhesion patches with a total area smaller than that of the contact zone. When added, the antibodies penetrate into the patch almost immediately, thus circumventing Phase I. This is due to the smaller concentration of bonds within the patch resulting from the decreased coverage of the substrate by E-selectin. Furthermore, the appearance of FACs is observed very shortly after the insertion of antibodies, but the size of the contact zone remains virtually constant throughout the entire experiment. In the particular experiment presented, lateral displacement of the contact zone occurred upon the loss of a certain number of FACs, due to some drift in the chamber, but no patch-like formation developed upon the migration.

By subsequent addition of small aliquots of titre (1 μg of antibodies each time) and waiting until the new equilibrium was established on each occasion, the variation of the total area of the strong adhesion patches with the number of aliquots was constructed (Figure 3.4). As the area of the patch is proportional to the number of formed bonds, and the concentration of the antagonist is proportional to the weight of inserted antibodies, the sigmoidal curve in Figure 3.4 reflects the functional dependence of the number of bonds on the antibody concentration. Unfortunately, due to difficulties in determining the absolute concentration of active receptors on the substrate, it is only possible to roughly estimate the number of bonds present.

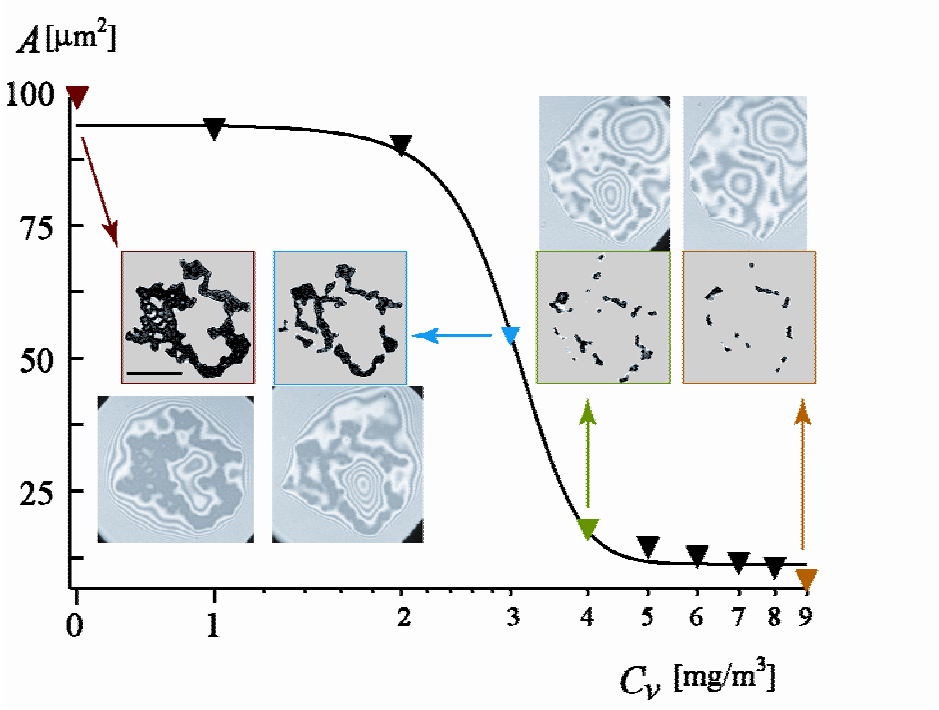

Figure 3.4: Area of the adhesion patch as a function of the concentration. The scale bar indicates the length of 10 μm. Data points are shown as inverted triangles. The line connecting the triangles is a sigmoid fitting function. Four original pictures are presented together with the pattern of strong adhesion patches that were extracted by image processing. Every data point was processed in exactly the same way and the error associated with each one is proportional to the ratio of the surface to the circumference of the patch. The arrows connect a given point with the original picture.

It can be seen from Figure 3.4 that most of the patch area is lost after the addition of the third and fourth aliquots. Upon insertion of the third milligram of antibodies, the area of the patch saturates to about 55% of its initial value, whereas after the fourth milligram the original area is reduced by 90%. Interestingly, five further aliquots are not sufficient to

completely destroy the patch resulting in unbinding of the vesicle. This is attributed to the fact that the concentration of free ligand in the vicinity of the patch (and in the vesicle) is much larger than the concentration of antibodies. Hence, the rebinding events occur much more frequently and are able to compensate for the lower binding affinity. In addition, the presence of 10 μg of antibodies begins to change the osmolality of the bulk solution and hence the reduced volume of the vesicle. At this stage, the experiment must be abandoned as it is not possible to maintain constant vesicle volume, and thus, the size of the contact zone changes not because of the binding of the antibodies to the surface but rather due to the increased osmotic pressure difference between the inner and outer buffer solutions.

3.2 Quantification of the observed unbinding

The experimental procedure described in the previous section has shown that it is virtually impossible to completely screen the non-specific interaction between the substrate and the vesicle. This interaction is responsible for the formation of the relatively small initial contact zone (see Figure 3.1 B). As discussed in Section 2.3.2, two scenarios for the final state of the vesicle can be anticipated from the adhesion model presented in Chapter 2. The vesicle can find the thermodynamic equilibrium governed by the diverging bending energy (as in the case of the vesicles in Figure 3.1 C and Figure 3.2 at t = 0.00), where bond formation completely dominates the non-specific interaction of the vesicle with the substrate. The adhesion process resulting in such adhesion plates is generally fast and uninterrupted. The final contact zone is usually uniform and densely packed with ligand-receptor pairs, and the shape of the vesicle is a spherical cap. The unbinding of such a vesicle by means of antagonists is determined by the mechanism that governs Phase I and only later can such a vesicle participate in the Phases II and III (as seen in Figure 3.2)

There are often cases, however, when the vesicle appears to be in its equilibrium state without assuming the shape of the spherical cap (see, for instance the vesicle in Figure 3.4). The adhesion process associated with such a state is usually slow and stepwise, and should be expected when the probability for bond formation is reduced, either due to the low coverage or a low fraction of ligands in the vesicle. Technically, the slow equilibration leads to a relaxation of the free energy with respect to ligand density variables but not with respect to the size of the contact zone. In this constrained equilibrium, the allocation resulting from the minimization of the free energy of an adhering vesicle given by Eqs. (2.7-2.8) is still valid, but the size of the contact zone is not determined by the bending divergence but by other factors such as the non-specific interaction potential, shape fluctuations and the probability for bond formation. Axially symmetric shapes of vesicles in this constrained equilibrium can be determined by the use of a continuum model [127] where the bending energy must be minimized for a chosen size of the contact zone.

The conditions for these two different equilibria have been experimentally explored in detail as a function of the composition of the substrate and vesicle but are discussed in Lorz et al. [126]. However, it is important to emphasize that the discussed adhesion

model can be applied to both the thermodynamic and the constrained equilibria, which is a prerequisite for the following considerations.

Within the same framework as was undertaken for describing simple adhesion, two similar models, which account for the dewetting mechanisms dominating Phase I and Phase II, are developed. In both cases, the vesicle is treated as a finite system whereas the antagonists (antibodies) are coupled to a bath of a constant chemical potential. The discrete particles corresponding to ligands and the antibodies retain their translational degrees of freedom, whereas receptors are taken to be immobile, and will not provide an entropic contribution to the free energy.

The vesicle surface is initially separated into a region parallel to the substrate, forming a contact zone, and a region consisting of the remaining part of the vesicle. The interactions of ligands with receptors can occur only within the contact zone. Nevertheless, the regions are able to exchange ligands and area. It is an assumption of the model that the contribution to the internal energy of the system from a single bond is realized whenever a ligand or an antibody is positioned over a receptor site. However, for the unbinding mechanism of Phase I, the size of the contact zone is determined by the equilibration of the spreading pressure of the vesicle and the lateral osmotic pressure of the antibodies. For the unbinding mechanism of Phase II, the size of the contact zone is taken to be constant and the number of formed ligand-receptor bonds is determined simultaneously with the number of antibody-receptor bonds.

3.2.1 The lateral-pressure mechanism - Phase I

Under the condition of an impermeable contact zone (high density of ligand-receptor bonds), the added antibodies exert lateral two-dimensional pressure on the edge of the contact zone (Π, see Figure 3.5), without penetrating the bulk of the zone. The vesicle, however, tries to maintain the size of the contact zone by the spreading pressure of the vesicle (ω, see Figure 3.5). Therefore, in the presence of antibodies, the system must find a new thermodynamic equilibrium, which is typically associated with a smaller size of the vesicle contact zone. In the case that the antibody pressure is very high, the vesicle will lose the entire contact zone and detach from the substrate.

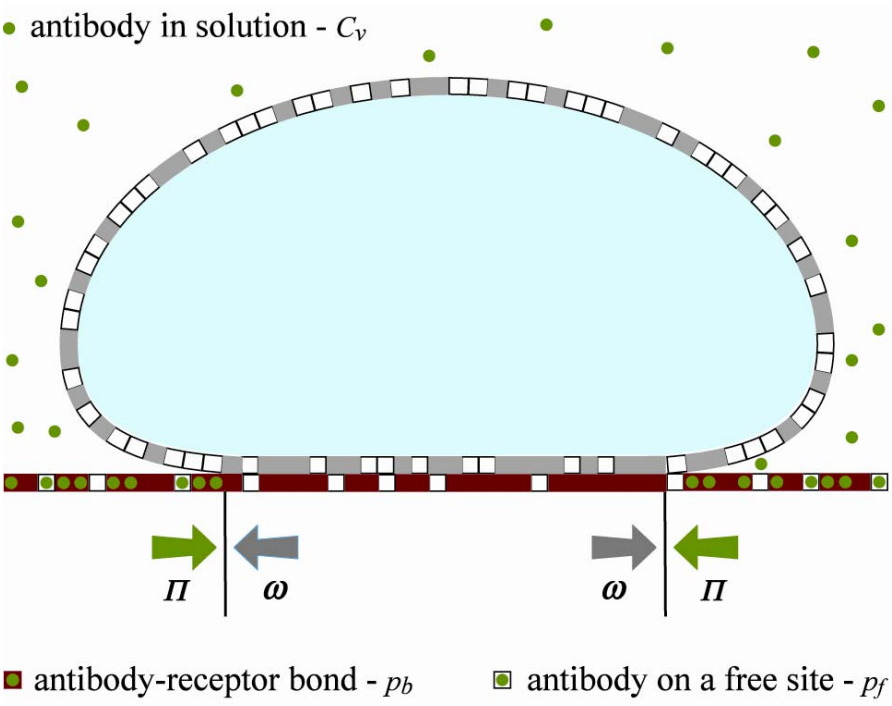

Figure 3.5: The balance between the spreading pressure of the vesicle (ω) and the lateral antibody pressure (Π). Antibodies are not penetrating the contact zone and are presented with circles. Gray sites in the vesicle indicate ligands and give rise to the fraction n_t. The red sites in the substrate can be associated with receptors that contribute to ρ_r. A circle within a red square represents an antibody-receptor bond, and contributes to p_b. A circle within a white square depicts an antibody on the surface but not bound to the receptor and gives rise to p_f. The contact zone s_c is depicted as the part of a vesicle at zero distance from the substrate. If, within this area, a gray site is on top of a black site, a bond is formed which contributes to n_b. A gray site over a white site indicates a free ligand in the contact zone and can be associated with n_f. The green and the gray arrows indicate the two balanced pressures at the edge of the contact zone.

In addition to the notation outlined in Chapter 2 (section 2.1.1), some additional quantities will be used in the course of this discussion:

- E_b – The antibody-receptor binding energy (in units of k_BT).
- p_b – The density of antibodies on the substrate bound to receptors.
- p_f – The density of antibodies on the substrate not bound to receptors.
- p_a – The total density of antibodies on the substrate.
- C_v – The concentration of antibodies in solution.

3.2.1.1 The lateral antibody pressure

a) Determination of the density of absorbed antibodies on the substrate

The calculation of the lateral antibody pressure is analogous to determining the Langmuir absorption isotherm of particles interacting with a substrate [128]. Accordingly, the free energy (in units of k_BT) of antibodies per unit surface area (area of a site) covered by receptors consists of the binding enthalpy and the mixing entropy terms:

$$F_a = -E_b p_b + p_b \ln p_b + (\rho_r - p_b)\ln(\rho_r - p_b) + p_f \ln p_f + (1-\rho_r - p_f)\ln(1-\rho_r - p_f) \tag{3.1}$$

Both p_b and p_f need to be in equilibrium with the antibodies in solution. Under the assumption of a very dilute antibody solution and a fixed chemical potential $\mu = \ln C_v$, minimizing the free energy and solving $\mathrm{d}F_a/\mathrm{d}p_b = = \mathrm{d}F_a/\mathrm{d}p_f = \mu$ results in the densities of absorbed antibodies to receptor-occupied and receptor-free sites on the substrate, respectively:

$$p_b = \rho_r \frac{e^{E_b} C_v}{e^{E_b} C_v + 1}, \qquad p_f = (1-\rho_r)\frac{C_v}{C_v + 1}. \tag{3.2}$$

The total density (p_a) of antibodies on the substrate is simply the sum of these two contributions:

$$p_a = p_b + p_f . \tag{3.3}$$

When E_b is small and $\rho_r < 0.5$, p_f is the dominant contribution. At large E_b, as well as at high coverage, p_f can be omitted from p_a as it is much smaller than p_b. However, it is important to note that, for fixed concentrations of both antibodies and receptors, p_a varies from zero to its maximum value in range of $0 < E_b < 20\ k_BT$. Further increases in binding strength do not significantly influence the number of bound antibodies on the substrate. For typical concentrations $C_v < 0.1$ and large antibody-receptor binding strengths, the density of antibodies on the substrate saturates ($p_a \rightarrow \rho_r$). In this regime, antibodies occupy all of the receptors on the surface.

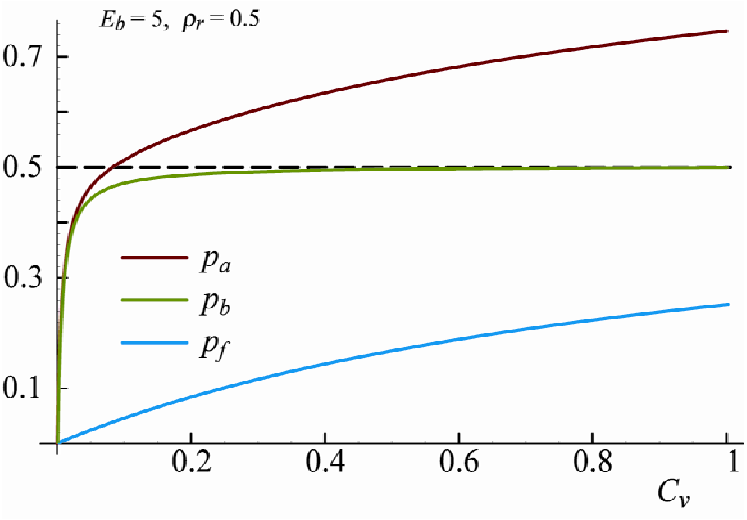

Figure 3.6: Coverage of the surface by antibodies as a function of the antibody concentration in the solution C_v. At low concentrations of antibodies in the solution p_f is considerably smaller than p_b. As the C_v increases, p_b saturates to ρ_r indicating that all the receptors on the surface are bound with antibodies.

An increase of C_v above concentrations of 0.1, leads to significant contributions of antibodies not bound to receptors but adsorbed on the surface p_f (Figure 3.6). However, such high densities of antibodies should be avoided in an experiment as they induce considerable changes in the reduced volume of the vesicle. In addition, in this limit, the description of absorption by Langmuir isotherms fails to provide accurate results.

b) Calculation of the lateral pressure

The lateral pressure of antibodies Π is, by definition, the gain in the free energy when the system increases its available size for a surface area of a unit site ($\Pi \equiv -\mathrm{d}F/\mathrm{d}a = -F_a(p_b, p_f)$). Substituting Eq. 3.2 and into Eq. 3.1, and reorganizing, results in the following expression for the antibody lateral pressure:

$$\Pi = \frac{\rho_r \ln C_v}{1 + C_v e^{E_b}} - \rho_r \ln \frac{\rho_r}{1 + C_v e^{E_b}} - \frac{(\rho_r + C_v)\ln C_v}{1 + C_v} - (1 - \rho_r)\ln \frac{1 - \rho_r}{1 + C_v}. \qquad (3.4)$$

As can be seen in Figure 3.7, when $E_b \to 0$, the lateral pressure from Eq. (3.4) becomes independent of the concentration:

$$\Pi_0 = -(1-\rho_r)\ln(1-\rho_r) - \rho_r \ln \rho_r \,. \tag{3.5}$$

In the case of a fixed concentration (left panel in Figure 3.7), the shape of the curve is determined by the first two terms on the right hand side of Eq. (3.4), whereas Eq. (3.5) determines the vertical offset. In the regime of large binding strengths (E_b>10), the antibody lateral pressure can be approximated by:

$$\Pi_a \approx E_b \rho_r + \Pi_0 \,. \tag{3.6}$$

Keeping in mind that the vesicle spreading pressure either diverges as $\rho_r E_a$ (see Eq. (2.22)) in a receptor-dominated equilibrium or saturates to a finite value given by Eq. (2.23) in a ligand-dominated equilibrium, it is immediately possible to estimate the antibody strength which is sufficient to influence the adhesion of a given vesicle-substrate system.

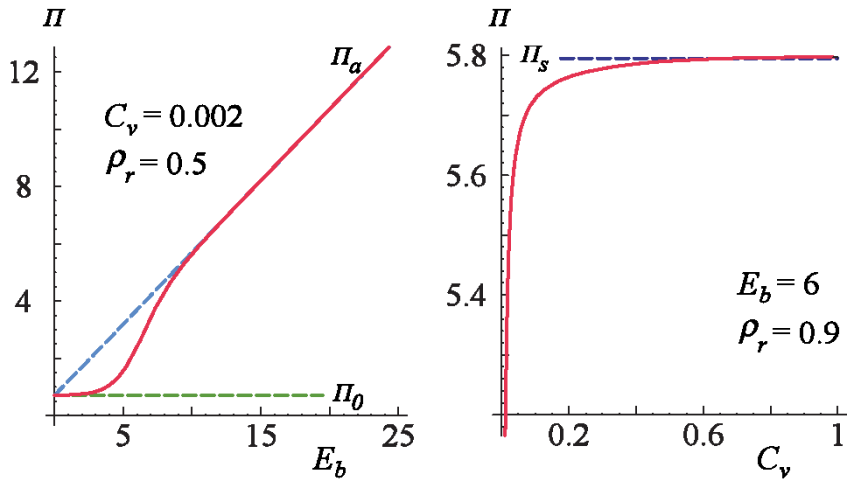

Figure 3.7: The lateral antibody pressure as a function of the antibody-receptor binding strength **(left)**, as a function of the concentration of antibodies in the solution **(right)**. Other parameters are kept constant and used as indicated. The onset value Π_0 from Eq. (3.5), the saturation value Π_s from Eq. (3.6) as well as the asymptotic solution Π_a given by Eq. (3.7) are indicated with green, purple and blue dashed lines, respectively.

For a fixed antibody binding strength, the lateral antibody pressure reaches saturation with increasing the concentration (right panel in Figure 3.7). In the case of large binding strengths this saturation value is:

$$\Pi_s \approx \Pi_a + (1-\rho_r)\ln 2\,. \tag{3.7}$$

Hence, in case of low antibody binding strength, it is possible that $\Pi_s < \omega_0$ (where ω_0 is given by Eq. (2.24)), and that increasing the antibody concentration does not result in the unbinding of the vesicle. However, in the regime of experimentally relevant concentrations of antibodies, the lateral pressure is changing rapidly and small changes in the concentrations can induce a large impact on the size of the contact zone.

3.2.1.2 The spreading pressure of the vesicle

The spreading pressure is the work required to increase the area of contact of a vesicle adhered to the substrate from S_c to $S_c + \mathrm{d}S_c$. However, this is exactly given by Eq. (2.20) and hence, a direct analogy between the average adhesion strength and the vesicle spreading pressure is found. The spreading pressure ω is thus given by Eq. (2.21) whereas the allocations of ligands are determined by Eq. (2.7-2.8). The behaviors of these quantities were analyzed thoroughly in Sections 2.4 and 2.5 and apply to this new situation as well.

3.2.1.3 Determining the size of the contact zone

The equilibrium size of the contact zone s_c^{eq} and the fraction of bound ligands n_b^{eq} in the presence of antibodies can be determined by solving the equilibrium condition for two-dimensional pressures:

$$\omega = \Pi\,. \tag{3.8}$$

A typical result of such a calculation is presented in Figure 3.8 where n_b^{eq} and s_c^{eq} are, shown as functions of the antibody concentration, for given total concentrations of ligands n_t and receptors ρ_r. The reduced volume of the vesicle determines the size of the contact zone prior to the insertion of antibodies. Thus in a real situation, s_c can not exceed the maximal value of 0.5 characteristic for completely deflated vesicles.

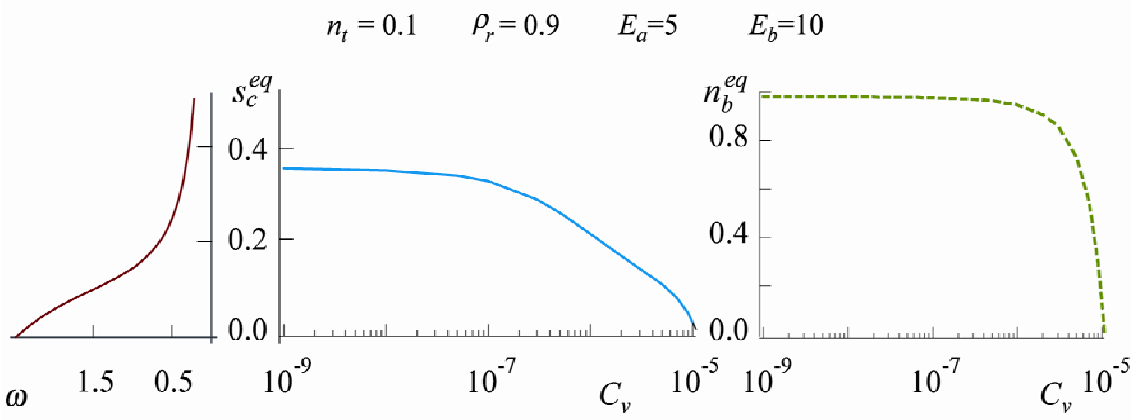

Figure 3.8: The equilibrium size of the contact zone (blue line-**middle**) and the equilibrium fraction of bound ligands (dashed green line-**right**) as a function of the antibody concentration, for the binding strengths and concentrations of other constituents as indicated in the header of the graph. The adjacent spreading pressure of a vesicle as a function of the size of the contact zone is shown with the red line (**left**).

For a given pair of binding strengths (for antibodies and ligands), there is a certain concentration (about 10^{-7} for the choice of parameters in Figure 3.8) at which the size of the contact zone is significantly influenced by the presence of the antibodies. The fraction of bound ligands, however, changes at somewhat larger concentrations ($C_v \approx 10^{-6}$), indicating an increase of the density of ligand-receptor bonds in the contact zone, accompanied by an increase of the average spreading pressure, even when the zone is reduced as shown in Figure 2.6.

a) Detachment concentration of antibodies

The critical concentration of antibodies C_v^* necessary for the detachment of the vesicle can be determined by solving $\omega_0 = \Pi$. This concentration depends on the ligand-receptor, and the antibody-receptor, binding strengths (as shown in Figure 3.9).

Importantly the logarithm of the critical concentration decreases linearly with the increasing antibody-receptor binding strength (see the left panel in Figure 3.9) at constant ligand-receptor binding strength. As can be seen from Figure 3.9, it is even possible to detach the vesicle with antibodies of lower binding strengths than that characterizing the ligand-receptor pair. However, this would require considerably higher antibody concentrations than that needed if the two binding strengths (E_a and E_b) were of comparable magnitude [129]. Nevertheless, at extreme antibody concentrations, there exists a minimum strength of antibodies capable of inducing vesicle detachment. When

the detachment concentration is explored as a function of the ligand-receptor binding strength (right panel in Figure 3.9), the critical concentration approaches zero very rapidly, for large differences between the two binding strengths. Following this divergence at low ligand binding strengths, the logarithm of the critical concentration enters a linear regime. This linear regime ends in another divergence, this time at ligand binding strengths somewhat larger than the antibody binding strength. This result demonstrates the insensitivity of the system to the presence of relatively weak antibodies.

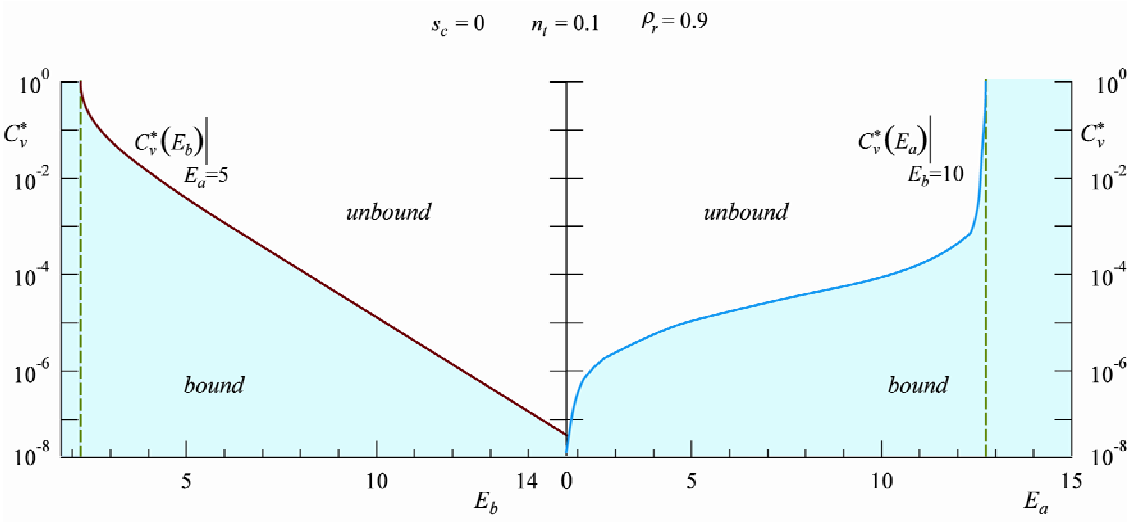

Figure 3.9: The logarithmic plot of the critical (detachment) concentration of antibodies as a function of the antibody-receptor binding strength (red line-**left**) and as a function of the ligand receptor binding strength (blue line-**right**). The minimum antibody-receptor binding strength for inducement of the detachment and the maximum ligand-receptor binding strength for which detachment can occur are shown with green dashed lines. The parts of the diagrams with shaded backgrounds indicate the regions of parameters where the vesicle is bound to the substrate, whereas the white background signifies free vesicles.

3.2.2 The competitive binding mechanism –Phase II

The penetration of antibodies into the contact zone may occur upon a spontaneous unbinding of the ligand-receptor pair, even after the spreading pressures are equilibrated. To account for this effect, the basic model for vesicle adhesion has been expanded to allow for competitive binding within the contact zone of a *constant size*. The ligands are still treated as a part of a finite system, while the antibodies are coupled to the solution by a constant chemical potential.

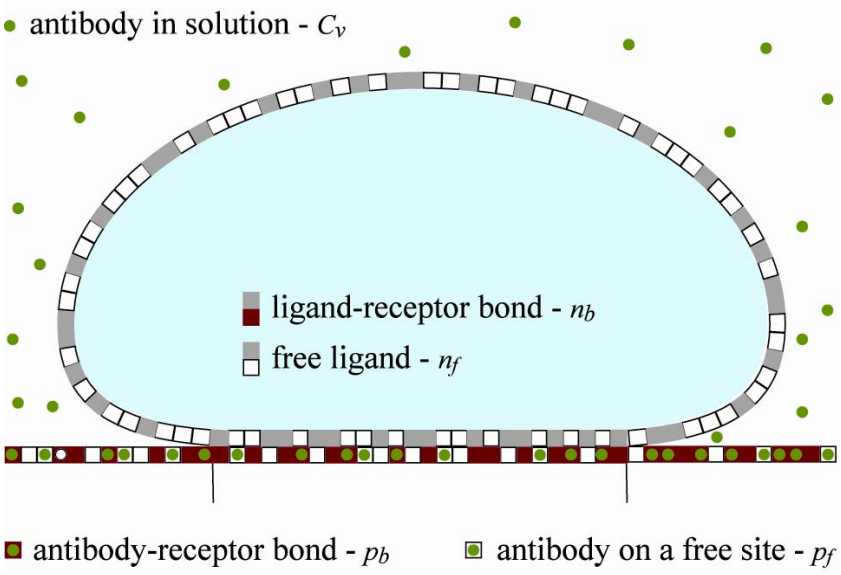

Figure 3.10: A schematic representation of the competitive binding mechanisms. The antibodies penetrate the contact zone and block the receptors from the ligands. Note that there are no gray squares indicating ligands above a site on the substrate occupied by a circle.

In a manner analogous to that used in the model for adhesion in the absence of antibodies (see Eq. (2.2)), the number of conformations of antibodies and ligands over sites occupied and unoccupied by receptor is found to be:

$$\Omega = \begin{pmatrix} (1-s_c)\cdot S_t \\ (1-n_f-n_b)\cdot n_t \cdot S_t \end{pmatrix} \begin{pmatrix} (1-\rho_r-p_f)\cdot s_c \cdot S_t \\ n_f n_t \cdot S_t \end{pmatrix} \begin{pmatrix} (\rho_r-p_b)\cdot s_c \cdot S_t \\ n_b n_t \cdot S_t \end{pmatrix} \begin{pmatrix} s_c\rho_r \cdot S_t \\ p_b s_c \cdot S_t \end{pmatrix} \begin{pmatrix} s_c(1-\rho_r)\cdot S_t \\ p_f s_c \cdot S_t \end{pmatrix} \tag{3.9}$$

The binding of both the antibodies and the ligands to the receptors contributes to the internal energy. This leads to a total free energy in units of k_BT for a finite vesicle with a constant size of the contact zone:

$$F = -\ln\Omega - E_b p_b \cdot s_c S_t - E_a n_b \cdot n_t S_t . \tag{3.10}$$

a) <u>Determining the densities of ligands and receptors in the contact zone</u>

To determine the fraction of bound ligands and the fraction of the area of the contact zone covered by antibodies (the density of antibodies in the contact zone), the free energy in

Eq. (3.10) must be minimized with respect to p_b, p_f, n_b, and n_f. The size of the contact zone (s_c) is maintained by the same mechanisms as discussed in the context of the original model (Section 2.3.2). The equations $\mathrm{d}F/\mathrm{d}p=\mathrm{d}F/\mathrm{d}p_f=\ln C_v$ need to be solved simultaneously with $\mathrm{d}F/\mathrm{d}n_b = \mathrm{d}F/\mathrm{d}n_f = 0$. The result for the fraction of area occupied by antibodies in the contact zone is:

$$p_b = (\rho_r - \frac{n_b n_t}{s_c})\frac{e^{E_b} C_v}{e^{E_b} C_v + 1}, \tag{3.11}$$

$$p_f = \left((1-\rho_r) - \frac{n_f n_t}{s_c}\right)\frac{C_v}{C_v + 1}. \tag{3.12}$$

These results are in the same form as those obtained for the non-permeable contact zone Eq. (3.2). The difference is that the coverage of the surface accessible to bound and free antibodies is reduced by the presence of bound and free ligands (n_b and n_f, respectively).

Determining n_b is a task beyond the analytical approach undertaken thus far. Rather than presenting the lengthy equations, numerical solutions are provided in Figure 3.11, where n_b is calculated for the case of titration with antibodies of different binding strengths, while all other parameters are kept constant.

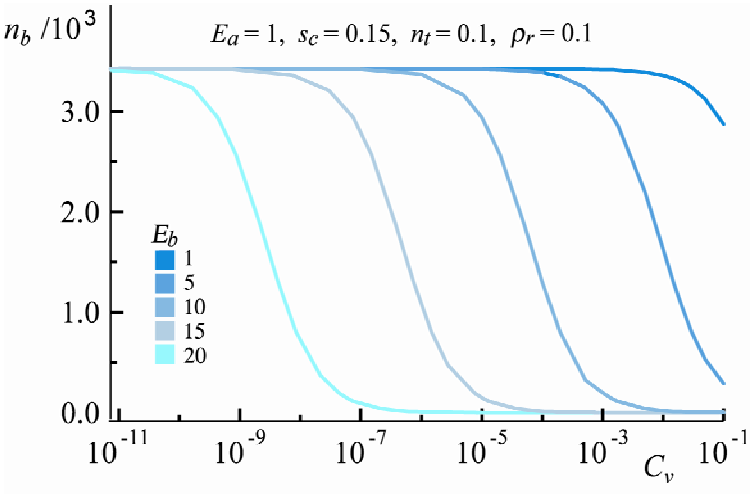

Figure 3.11: Fraction of bound ligands as a function of the antibody concentration for different antibody-receptor binding strengths. Other parameters are kept constant and are indicated in the header of the graph.

It is surprising that the increase of E_b provides only a shift of the decay function of bound ligands towards smaller concentrations. This shift is linear with respect to the antibody binding strength and is equal to $E_b \ln C_v + const.$ However, an increase of more than five orders of magnitude in the concentration of antibodies is needed for the complete unbinding of ligands. Nevertheless, most of the ligand bonds are lost in a relatively short window of two orders of magnitude in the antibody concentration. When $C_v \rightarrow 0$, the model for adhesion in the absence of antibodies, described in Chapter 2, applies.

Several important properties of the decay functions can be learned from the double logarithmic plot (Figure 3.12). It is easy to notice that the slope of the decay function therein remains almost constant, in this representation, despite the widely varying choice of parameters (presented for each curve in Table 3.1). This linear slope also suggests that it is not possible to completely block the receptors on the substrate from the ligands. However, this cannot be realistic as, at some stage, n_b will become small enough to give rise to less than one ligand bound to the substrate. Furthermore, in this limit, the thermodynamic laws on which this approach is based, are expected to fail due to insufficient statistics with small numbers. Taking into account the standard sizes of the ligands and the vesicle itself, the prediction should apply until $n_b=10^{-7}$, which corresponds to about 100 bound ligands.

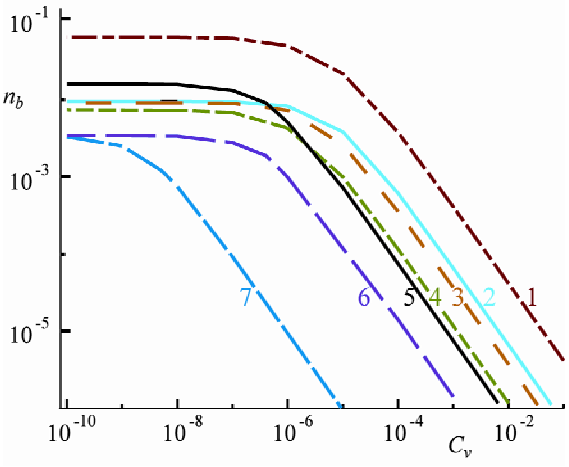

Figure 3.12: Double logarithmic plot of the fraction of bound ligands as a function of the antibody concentration for different sets of parameters. Although the parameters vary significantly, the decay slope seems to be insensitive to the change of the system conditions.

Curve	E_a	E_b	n_t	ρ_r	s_c
1	5	15	0.1	0.5	0.15
2	5	15	0.1	0.5	0.25
3	5	15	0.01	0.5	0.15
4	5	15	0.01	0.5	0.05
5	1	15	0.1	0.5	0.15
6	1	15	0.1	0.1	0.15
7	1	20	0.1	0.1	0.15

Table 3.1: Parameters of the curves given in Figure 3.12. The number in the first column corresponds to the number of the curve indicated in the graph.

From the analysis of the calculated data, two important laws for the number of bound ligands emerge:

$$\frac{n_b}{\rho_r} = const., \tag{3.13}$$

$$\frac{n_b}{n_t} = const.. \tag{3.14}$$

The law given by Eq. (3.13) is valid for the entire range of antibody concentrations and allows the prediction of the number of bound ligands if data for an analogous system are available. The scaling law with respect to the total fraction of ligands in the vesicle (Eq. (3.14)) is, however, correct only in the linear regime of Figure 3.12.

3.3 Implications of the unbinding mechanisms

As the two developed models are able to account for both dewetting mechanisms observed in experiments, we can be reasonably confident that the main physical aspects of the problems are well accounted for. Particularly striking is the agreement between the theoretical predictions (Figure 3.11) for the dependence of the number of ligand-receptor bonds on the concentration of the antibody solution, and the observed behavior of the vesicle (Figure 3.2). In the latter figure, the area of the patch is presented as a function of the mass concentration of antibodies. Due to difficulties in determining the surface coverage, it is hard to determine the exact number of bonds within the patch. However, as the coverage is uniform on the micrometer length scale, the number of bonds must be proportional to the patch area on the same scale. Furthermore, as mass concentration is evidently proportional to the volume concentration of the antibodies in the solution, the excellent qualitative agreement between the theoretical approach and the presented experiments is clearly visible. In both cases, as the concentration of antibodies is increased, an initial rapid loss of bonds is followed by a much slower regime for bond detachment.

The described experimental method of vesicle dewetting by antibody titration, supported by the two theoretical models, can be used as a powerful technique for determining important properties of the system. The adhesion model in the absence of antibodies should provide information concerning the ligand-receptor binding strength and the spreading pressure of the vesicle. Although it is not possible to exactly define the required quantities within the current experimental setup, the utility of the approach can nevertheless be demonstrated for the vesicle in Figure 3.2 by using a relatively large range for each quantity and assuming that every receptor in the adhesion patch is, prior to titration, bound to a ligand. That is, by using a radius of gyration of the ligand between 3.5 and 4.5 nm, and a receptor area between 2 x 10^{-4} and 8 x 10^{-4} μm^2 with 3000-4000 receptors on the unit of the substrate surface, Eq. (2.7) provides an estimate of the sLe^X-E-selectin binding strength of 4 to 6 k_BT. Interesting in this respect is the work by Evans [130] showing that the binding of selectin with its counter-partner in white blood cells has two pathways of dissociation, one of which is characterized by an unbinding force of 30 pN. If we assume that the characteristic length of the dissociation pathway is 1 nm, this would correspond to a binding energy of 6 k_BT, which is in good agreement with the data presented herein. Also in the work of Fritz [131] and co-workers, it has been noted

that a fast and a slow unbinding regime of E-selectin from its partner appears to occur. The fast off-rate has there been determined to be 0.002 s^{-1}, which again is in good agreement with the data obtained in the method presented herein. In a similar manner, Eq.(2.21) results in an estimate for the spreading pressure of 10^{-5} Nm^{-1}, which is in agreement with the state of strong adhesion observed in Figure 3.2.

The analysis of the experimental data obtained for the vesicle from Figure 3.2 by the use of an independent technique for the evaluation of the average adhesion strength (from the reconstruction of the vesicle height profile at the edge of the contact zone) suggests that the spreading pressure of the vesicle in equilibrium at the beginning of Phase I is less than the one evaluated from the equilibrium at the end of Phase I. The theoretical model proposed in this Chapter for Phase I, clearly shows that the average adhesion strength is always increasing with a decreasing size of the contact zone (see Section 2.5.1.1. and Figure 2.9). Hence, at least qualitative agreement between these two models and the experimental data is obtained.

The description of vesicle dewetting provides a method for determining several other important parameters of the system. In the case that the ligand-receptor binding strength is successfully determined, the binding strength of the inhibitor can be found. If the antibody-receptor binding strength is known, dewetting can also be used as an alternative approach for determining the ligand binding strength and the spreading pressure of the vesicle. By choosing both a ligand and an antibody with known binding strengths, the quality of the receptor coverage could also be probed. However, the ranges of the above estimates for the binding strengths and the coverage in the current experiments are too large to result in well-defined predictions. Though further elaboration would be clearly desirable, this work provides the foundation for systematic experimental measurements of the binding strengths of both antagonists and ligands.

The current approach is not only a valuable tool in the characterization of antagonist-induced unbinding of toy cells but it can also help to clarify the mechanisms of analogous processes in nature. For example, the integrin receptors of type $\alpha_V\beta_3$ in endothelial cell are known to bind selectively to fibronectin coupled to the inner wall of the blood vessels. An antagonist impeding this interaction would be fibrinogen, a soluble glycoprotein contained in the blood plasma that is able to compete with the receptors and influence the cell adhesion [132].

The competitive interaction of ligands anchored on cell surfaces and antagonists dissolved in the plasma with integrins could also play an essential role for the formation of immunological synapses [133]. These are transient tethers which form between immunological cells and endothelia cells and play an essential role during the initial state of the migration of white blood cells through the endothelial cell layers. The mechanisms for these interferences *in vivo* are expected to be closely related to these identified in the *in vitro* model systems as identified and characterized herein.

3.4 References

119 Guyton A. C. 1997. In *Human Physiology and Mechanisms of Disease, 6th edition*. 291-293.

120. Matlin K. S., and M. J. Caplan.1992. In *The Kidney: Physiology and Pathophysiology*. 447-473.

121. Zinkl G. M., A. Zuk, P. van der Bijl, G. van Meer, and S. Matlin. 1996. *J. Cell Biol*. **133**:695-708.

122. Bruinsma R., and E. Sackmann. 2001. *C. R. Acad. Sci. IV-Phys.* 2:803-815.

123. Bruinsma R., A. Behrisch, and E. Sackmann. 2000. *Phys Rev. E* **61**: 4253-426

124. Nardi J., R. Bruinsma, and E. Sackmann. 1999. *Phys. Rev. E* **58**:6340-6354.

125. Guttenberg Z., B. Lorz, E. Sackmann, and A. Boulbitch. 2001. *Europhys. Lett.* **54**:826-832.

126. Lorz B. G., A.-S. Smith, C. Gege, and E. Sackmann. *In preparation*.

127. Seifert U., and R. Lipowsky. 1990. *Phys. Rev. A* **42**: 4768-4771.

128. Hiemenz P. C., and R. Rajagopalan. 1997. *Principles of colloids and surface chemistry. 3rd edition*.

129. Equivalent experiments in which soluble sLe^X was as a source of competition required much larger concentrations for similar effects.

130. Evans E. A. 1994. In *Handbook of Physics and Biological System*s. 697-728.

131. Fritz J., A. G. Katopodis, F. Kolbinger, and D. Anselmetti. 1998. *Proc. Nat. Acad. Sci. U.S.A.* **95**:12283-12288.

132. Alon R., and S. Feigelson. 2002. *Semin. Immunol.* **14**:93-104.

133. Dustin M. L. and L. B. Dustin. 2001. *Nature Immunology* **2**:480-481.

CHAPTER 4

FORCE AS A CONTROL MECHANISM 91

Above: White blood cell adhering to the lining of the blood vessel from a model of human diabetes mellitus. Picture from http://www.anatomy.ubc.ca/Research_Areas/Todd.html. Taken by M. Todd.

Chapter 4

FORCE AS A CONTROL MECHANISM

Many of the processes accorded to cell function are known to utilize and/or generate external force. One of the most studied of such processes is the rolling of leukocytes (white blood cells) in the blood stream, essential for their transport throughout the body. Naturally, hydrodynamic force is an important ingredient in this process. In order for it to constitute part of feasible mechanism, however, a highly regulated sequence has had to be developed in order to selectively counteract the force and arrest the leukocyte at its target location.

White blood cells migrate from the bloodstream to specific sites of inflammation or injury in response to molecular changes which are displayed on the surface of the blood vessels at these sites. Several adhesion and signaling events are evoked by the inflammatory stimulus and determine which type of leukocyte will emigrate. At least four steps, with multiple molecular choices in each one, control leukocyte emigration and contribute to its selectivity. The attachment or tethering of circulating leukocytes to the vessel wall through labile adhesions permits leukocytes to roll in the direction of flow (step 1). The attachment process is mediated by calcium-dependent lectin receptors of the selectin family (P and E-selectin) [134], located on the endothelia cell wall. These receptors interact with glycoprotein counter-ligands containing a fucosylated and sialylated tetrasaccharide called sialyl-Lewis^X (sLe^X) [135]. The receptor-ligand pairs associate very quickly and with high affinity thus enabling them to tether cells over distances of up to 100 nm by their long chain-like structure. The selectin-ligand complexes are able to withstand high tensile forces and terminate their binding in a controlled manner that maintains rolling, without them being pulled out of the cell membrane.

Rolling is designed to bring the leukocyte into the proximity of a source of inflammation indicated by signals displayed on the endothelium. These signals (step 2) activate a second class of adhesion receptors, integrins [136], which firmly bind to immunoglobulin super-family members that are inducibly expressed on the inflamed blood vessel (step 3). This results in the arrest of the rolling leukocyte. The arrested leukocyte is then sensitized by chemo-attractant gradients originated in the nearby extravascular tissue enabling it to cross the endothelial lining of the blood vessel, using integrins, and migrates into the tissue (step 4). Every step in this process is intimately connected to different types of forces. To understand the nature of the formation of adhesion complexes in these circumstances, numerous studies on bond formation under force have been undertaken.

The formation of a bond between two molecules is a process of a statistical nature which is characterized by "on" and "off" rates describing the probability for the association and dissociation of the complex, respectively. Thus, even in the absence of an external force, every bond will experience spontaneous dissociation dependent on its average life-time. The action of force effectively induces a decrease in the energy barrier between the bound and unbound states. Furthermore, the presence of the force induces a global minimum in which the two bond contributors are infinitely separated. Such behavior can be described in terms of a modified Arrhenius law of chemical kinetics [137,138,139].

The enforced unbinding of a single complex, where the contributors are embedded into opposing surfaces is, by now, a well-understood problem [140,141]. An overall agreement has emerged from a manifold of different experimental approaches, such as atomic force microscopy [142], micropipette aspiration [139,143], surface force apparatus [144], optical tweezers [145] and shear flow experiments [146]. Thereby, the unperturbed binding affinity of a given pair of molecules, constrained to a two-dimensional surface, is reduced in comparison to the corresponding affinity in solution [147]. Somewhat more striking is the observed distribution of unbinding forces obtained as a function of the rate of the applied force load. Specifically, the bonds appear to be more resistant to higher force rates, so that rapid, force-induced unbinding is more difficult than the slower loading alternative [148,149].

In contrast to the single bond case, the understanding of the force resistance of ensembles of ligand-receptor bonds is still rudimentary. Depending on the manner in which the force is transduced, the bonds in the complex may respond as though they are either in series, where only molecules in the outer rim feel the load, or in parallel, where the load is

shared by all the bonds in the complex [150]. When the participants are restricted to surfaces, the complex maintains the surfaces in close proximity and thus allows for broken bonds to reform [151,137]. Lateral interactions between ligands or receptors have been found to produce additional collective phenomena. As demonstrated by Schwarz and his collaborators, this can result in a complex interplay of membrane-mediated elastic forces with segregational and specific ligand-receptor interactions, when a focal adhesion center is subjected to an external force [152,153].

In order to provide deeper insight into the understanding of membrane-mediated force on the bond complexes, the previously developed theoretical considerations are adapted to the new situation. At the same time, comparative experimental systems, where vesicles adhered through the action of the ligand-receptor pairs mentioned above (in the context of leukocyte rolling and arrest), were subjected to force by Lorz [154] and Gönnenwein [155]. Together, these works shed new light on vesicle response to external force and reveal how the force can, on short time scales, stabilize adhesion complexes.

4.1 Modeling the exertion of force

One of the most important outcomes of the adhesion model (Chapter 2) is that the equilibration with respect to the formation of bonds can be decoupled from the equilibration with respect to the size of the contact zone. In addition to allowing for the deduction of the effective potential, this result becomes a very powerful tool in exploring the influence of a force exerted on the vesicle. The force necessary for inducing a shape deformation is of the same order of magnitude as the bending energy. For this reason, the decoupling of the shape determination from the analysis of the binding equilibrium can continue to be used in the presence of an applied force. The force thus serves as a control mechanism for maintaining a particular size of the contact zone. It opposes the effective adhesion strength produced by the formation of bonds and other nonspecific contributions.

Two situations, connected to the two types of shape equilibrium discussed in previous chapters, must be distinguished. In the case that the vesicle has reached the thermodynamic equilibrium, the vesicle shape is that of a spherical cap and the effective adhesion strength from Eq. (2.21) can be directly interpreted as a contact potential acting on this shape. This situation will be referred to as strong adhesion. In case of a slow equilibration with respect to the size of the contact zone, the shape of a vesicle must be determined by the use of volume and area constraints, for a given size of the contact zone. The total effective potential is actually dominated by nonspecific contributions and the effective adhesion strength arising from Eq. (2.21) is then only a contribution. In this case (which will be called weak adhesion), the effective adhesion strength acting on a vesicle is an unknown parameter and must be determined self-consistently with the vesicle shape.

Application of a point force to the north pole of an adhered vesicle should induce shape deformations and, furthermore, cause a gradual decrease of the contact zone until the vesicle detaches from the substrate. In order to solve the shape aspects associated with the vesicle's response to the force, the continuum approach of Seifert and Lipowsky [156] for vesicle adhesion must be adapted to account for the vertical pulling. In this way, families of shapes for different strengths of effective contact potential and different reduced volumes can be obtained and mapped to the problem of discrete binding. Such

calculations are performed for the cases of both strong and weak adhesion, the results of which are presented in two publications contained in Appendices C and D, respectively.

Applying these results to the new situation where the vesicle is adhered by means of discrete receptor-ligand bonds, requires the development of a procedure for mapping the shapes calculated for a given contact potential w to those corresponding to the effective adhesion strength ω (resulting from the formation of bonds). As shown in Section 2.5, the link between these two quantities is given by:

$$w = \omega \cdot \frac{4\pi}{S_t} \frac{\kappa}{k_B T} . \tag{4.1}$$

Under standard laboratory conditions, a membrane with a bending rigidity of 100 $k_B T$ containing 10^7 ligand sites on the vesicle ($R_{vesicle}$~10μm, R_{ligand} ~1 nm), this conversion would lead to $w \cong 10^{-4} \omega$. Although the w and ω are clearly potentials of different magnitude scales, there is a range of parameters in which such mapping is sensible. This is due to the fact that vesicles can sustain relatively large adhesive potentials before undergoing lysis. Furthermore, the more the volume of a vesicle is reduced, the greater is the adhesive potential required to obtain strong adhesion. This leads to different orders of magnitude of potential strength required for vesicles with reduced volumes close to that of a sphere, in comparison to strongly deflated ones. Thus, the determination of the relation given in Eq. (4.1) permits the exploitation of the main results of the calculations on the continuous models (Appendices C and D) and the exploration of their consequences on the unbinding of specifically bound vesicles. This will be the subject of the discussion presented in following sections.

In light of the discrete adhesion model presented in Chapter 2, several specific aspects concerning the unbinding process can be anticipated. Firstly, the decoupling of the vesicle shape and the size of the contact zone from the relaxation of the number of bound molecules, allows for the possibility that the two relevant equilibration processes take place on different time scales. That is, if the equilibration of the size of the contact zone is slow relative to the time taken for the bonds to form, the bonds can follow the deformations, reaching equilibrium for each shape (and contact zone) given at a certain time. It is only once the relaxation of the contact zone has occurred that the system finds its true equilibrium.

Also in the context of the discrete adhesion model, it was shown that when the size of the contact zone is reduced, the equilibrium density of formed bonds (DN_b) increases until all available receptors are occupied and then it remains constant (or it continues increasing until all of the contact zone is lost, see Figure 2.6). This would mean that increased binding in the contact zone should be expected in response to an attempt to unbind the vesicle. If the equilibration of the bonds is faster than that of the contact zone, such increased binding should be expected even in the part of the contact zone that will be detached once the equilibration of the contact zone is achieved.

Even when the density within the contact zone has saturated to its maximum value, the effective adhesion strength (ω) is still expected to increase, in response to a contact-zone reduction (see Figure 2.9, note that this figure is produced for the same parameters as Figure 2.6). Hence, the discrete model implies that successful pulling should become progressively more difficult as the contact zone becomes smaller.

In addition to the aforementioned intuitive expectations, there are several more subtle features associated with the force-induced unbinding of adhered vesicles. In the following sections, the discrete adhesion model will be combined with the two continuous models, and measured experimental data, to shed some new light upon this phenomenon, particularly in the case of a weakly adhering vesicles

4.2 Strong adhesion

In a thermodynamic equilibrium, the vesicle is a spherical cap strongly adhered to the substrate with a well-defined number of ligand-receptor bonds. As a direct result of this shape, the entire excess area that resulted from the volume reduction is used for the formation of the contact zone that, as discussed in Section 2.2, corresponds to the size s_c^{max}. An attempt to detach such vesicles will encounter a strong resistance from the formed ligand-receptor bonds expressed in terms of either the spreading pressure or the effective adhesion strength.

Several experimental studies have shown that the application of a point-like force, to a membrane that provides a firm resistance mechanism, can result in the formation of tubular structures known as tethers. Rather than being subject to nonhomogenous elliptic deformations, it appears that it is energetically more convenient for the vesicle to undergo a transition to a shape consisting of a cylindrical tube (a tether) connected to the spherical cap (a vesicle) by a catenoidal neck. A catenoid is a minimal surface of zero total curvature and does not contribute to the bending energy. Therefore, the neck enters the free energy functional only within the total volume and area constraints. Due to the high tension induced by the strong adhesion and further increased by pulling on the vesicle membrane, the catenoidal neck should be very short, and can therefore be neglected in the development of the calculations presented in Appendix C. As the surface area of the tether has to arise from the material originally used for adhesion, the extraction of a tube is thus in direct competition with the maintenance of the contact zone, and therefore the spreading pressure of the vesicle.

To summarize the results presented in Appendix C, a critical onset force is identified where the tether spontaneously appears as part of a second order shape transition. This force is associated with the minimum effort that needs to be exerted to successfully overcome the spreading pressure of the vesicle in the thermodynamic equilibrium. Further growth of the tether initiates a detachment process which culminates in a continuous unbinding of the vesicle at a finite detachment force. Both critical forces, as well as all shape parameters, such as the height of the spherical cap and the size of the contact zone, can be calculated as functions of the reduced volume and the strength of the adhesive potential.

Choosing a vesicle with a specific reduced volume provides the equilibrium size of the contact zone s_c^{max} (see Table 2.1) and the height (h) of the vesicle. For given binding strength of the ligand-receptor pair E_a, and the concentrations of the system constituents ρ_r and n_t, s_c^{max} determines the equilibrium ω according to Eq. (2.21). In the next step w can be evaluated by the use of Eq. (4.1). Insertion of w and $A_o^* = s_c^{max}$ into Section C.1-Eq. (4), results in the onset force f_o.

In a similar manner, the system parameters ρ_r, n_t, and E_a determine the maximum value of the effective adhesion strength ω_0 in correspondence with Eq. (2.24). However, this value is achieved at exactly $S_c = 0$. Consequently, ω_0 is the effective adhesion strength which needs to be overcome in order to detach the vesicle. Introducing the equivalent w for the detachment, resulting from Eq. (4.1), into Section C.1-Eq. (5) provides the detachment force f_d. By the use of Section C.1-Eq. (6), this is sufficient to determine all remaining parameters, such as the detachment length and width of the tether as well as the tension in the vesicle.

The unbinding process that occurs between the onset and the detachment parameter values can be evaluated by calculating the force required to achieve a particular size of the contact zone associated with a particular value of the effective adhesion strength. The example of such a calculation is shown in Figure 4.1.

Due to the increase in the effective adhesion strength during the detachment process, more force needs to be applied (for a particular value of s_c) than would be required for a constant effective adhesion strength, in order to accomplish detachment. Depending on the value of s_c^*, the w behavior as a function of s_c (red points in Figure 4.1) mirrors that present in the force curve (blue points in Figure 4.1). That is, the pulling force under the conditions of variable ω, remains of the same order of magnitude as for the case of constant w, until the final stages of the detachment process. When the remaining contact zone becomes small (below 10% of the total vesicle area), the resistance to pulling is considerably increased. This effect is independent of the strength of the potential providing the resistance. However, as the detachment force is proportional to w_0, if the effective adhesion strength from onset to detachment changes for an order of magnitude, the detachment force will do so also. Thus, in this last stage, the two force curves can differ by up to several orders of magnitude.

Other parameters of the shape, such as the tether length or width are approximated to be simple functions of the force (Section C.1 Eqs. (2-3). Thus the behavior of the force can be directly projected onto these parameters.

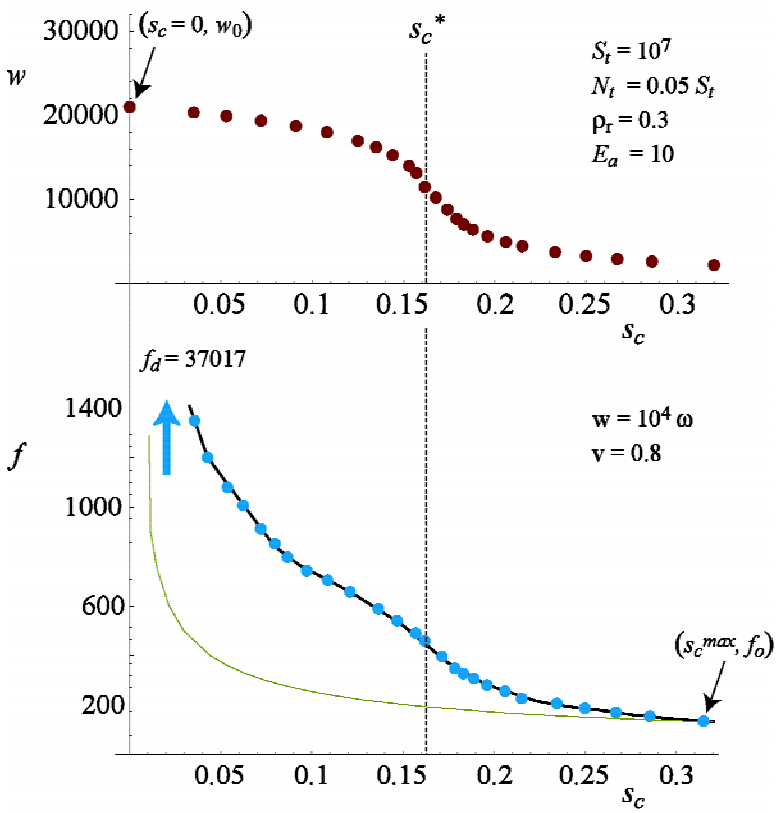

Figure 4.1: For a given composition of the vesicle and the substrate, the variation of the effective adhesion strength with a change in the size of the contact zone is shown (upper panel). For the same set of parameters, and the indicated reduced volume, the force associated with the thermodynamic equilibrium as a function of the size of the contact zone is calculated (blue points, lower panel). The results are compared with a curve which is calculated for a constant onset value of the effective adhesion strength (green curve).

The presented model is simple and well-defined enough to make it a good starting point for equivalent experimental studies. Although, some of the expressions that arose from the calculation (in particular Section C.1-Eq. (3)) are well known and commonly used in experiments with micropipettes [157], direct measurements where the remainder of this model could be tested have, due to technical difficulties, not yet been performed. In particular, the combination of obtaining information on the vesicle shape at the same time as the details of the contact zone is a laborious task. Further complications should be expected due to the small radius and considerable length of the tether that enhances the problems of the visualization and the vertical control of the pulling mechanism, which needs to be performed over relatively large vertical distances.

4.3 Weak adhesion

For a vesicle in a constrained equilibrium, the formation of bonds is dominated by nonspecific contributions to the overall potential. It has been shown that such a potential alone is not sufficiently strong to bind the vesicle to the substrate (see Figure 3.1) and induce the transition of the shape into a spherical cap. Therefore, excess free membrane remains in the vesicle following the establishment of the adhesive state. The existence of such surface area allows continuous deformations of the shape and leads to a rudimentarily different scenario for the detachment process, the details of which are presented in Appendix D. The results of these calculations show that, for relatively weak adhesive potential strengths, locally stable bound shapes, separated from the free shape by an energy barrier can be found for a range of applied forces. In this case, considerable continuous deformations of a vesicle can be observed prior to the onset of the detachment, indicating a competition between the applied force and the bending of the vesicle membrane. At a critical force, these shapes discontinuously unbind, since the vesicle disengages from the substrate while still in possession of a finite adhesion area.

As the nonspecific potential dominates, it should not be expected that the value of the effective adhesion strength changes considerably during the unbinding process. However, as the density of bonds is expected to increase during the detachment process (see the equilibrium density of bonds as a function of the size of the contact zone, Section 2.4.3.1c), it is possible that the bond formation dominates the nonspecific contribution for a particular critical size of the zone. Such a situation would be accompanied by a considerable increase in the effective adhesion strength. If the new adhesion strength is again not too high, continuous deformations of the shape should be expected to follow. On the other hand, if the resistance becomes very strong, continued pulling could induce shape instability towards either a tethered shape or lysis.

4.3.1 Experimental observations – shape decoupling

In order to provide evidence for the decoupling of the vesicle shape from the equilibration with respect to bond formation, measurements of the vesicle shape are performed with a laser scanning confocal microscope. The influence of the force could be explored by adopting a magnetic tweezers setup for use with the confocal technique [155]. Basic information on the technique and the preparation of the vesicle-substrate

system are described in Appendix B. Full details of the method can, however, be found in the works of Lorz [154] and Gönnenwein [155].

The vesicle is adhered to the substrate by the formation of bonds between the glycolsphingolipid sialyl-Lewis^X and the membrane protein E-selectin (as was the case for the experiments presented in Chapter 2). The low concentration of E-selectin on the substrate ensures a low value for the effective adhesion strength. The shapes of vesicles adhered under these conditions are distorted by placing an electro-magnet above the measuring chamber. A current through the coils of the magnet induces a magnetic field. This field produces a constant force on paramagnetic beads that are covalently attached to the vesicle. The beads move in the direction of the magnet and lift the vesicle membrane.

Once the initial equilibrium (in the absence of force) has been established, the shape of the vesicle is scanned. Following the application of the force and the re-establishment of equilibrium, the shape is scanned once again. Figure 4.2 presents an example of two sets of experimental data obtained in this way, overlaid with the appropriate theoretical reconstructions arising from the model presented in Appendix D.

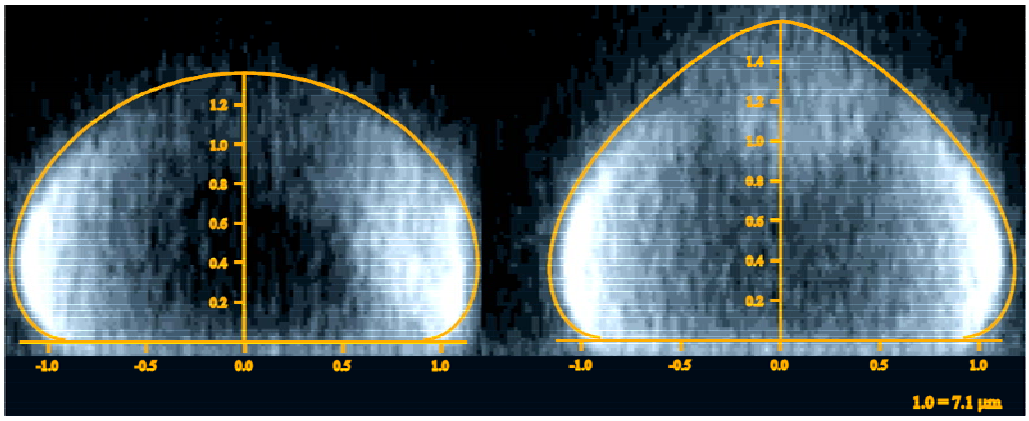

Figure 4.2: An overlay of a shapes originating from experiments and the continuous model. The same vesicle is presented in equilibrium with no force applied and pulled with a sub-piconewton force. Experimental data from Gönnenwein and Lorz [154,155]

The theoretical shape is first determined for the non-pulled state (left in Figure 4.2). This is achieved by calculating a family of shapes at zero force, with different reduced volumes, for a variety of adhesion strengths. Scaling these shapes to an appropriate size and choosing the best match provides a fitting estimate for the reduced volume (v) and the effective adhesion strength (w). The reduced volume (v) is constant as the osmotic conditions are not changed during the experiment. Due to low density of bonds in the

contact zone (RICM picture of a vesicle-substrate system with similar composition is given in Figure 4.3), the w is not expected to change during the pulling process (at least not before considerable loss of the contact zone is achieved), and can thus be used to calculate a set of shapes under force. After an identical scaling procedure, the best matching shape is then chosen, and the pulling force obtained (right Figure 4.2).

It is useful to compare the calculated adhesion strength (W) and the pulling force (F) with the measured data. For this preparation, $\kappa / 100\ k_BT$ [158]. The measured value of the reduced volume (0.8 ± 0.1 [159]) corresponds well to the calculated value of 0.89 ± 0.01. The theoretical model (Appendix D) provides a prediction for the effective adhesion strength of W = 0.12 ± 0.01 μNm^{-1} (in the units of Appendix D: w = 15 ± 1), which is in excellent agreement with the experimental average of W = 0.15 ± 0.05 μNm^{-1} *evaluated independently by the use of the Young-Dupré equation* for wetting droplets [160]). The applied force in the experiment is in the sub-piconewton range, but due to difficulties with calibration in this range it is not possible to determine its exact value. For the pulled vesicle in Figure 4.2, the matching shape is found for F = 0.73 ± 0.05 pN (in the units of Appendix D: f = 2.1 ± 0.1).

Such an agreement between the theoretically predicted and experimentally observed shapes provides important evidence that the vesicle-shape can indeed be determined independently from the number of formed bonds in the constrained equilibrium. That is, a description based on a simple contact potential is able to reproduce the experimental data, involving many discrete binding sites, remarkably well. Put another way, the major part of the system can be considered to be an unadhered membrane. Given an area and a volume, a good description of this membrane can be obtained merely by considering the free energy of curvature, subject to constraints concerning the application of the force and the contact with the surface. While these two constraints are interdependent, the contact of the membrane with the surface has only to obey the standard boundary condition. This condition holds, regardless of the exact mechanism of vesicle adhesion, as long as weak potentials are in action. The theoretical model should, however, be tested on different systems and for stronger forces, preferably close to the detachment. It would be important to change the composition of the system and thus vary the contribution of the bonds to the effective potential. Exploring the vesicle shapes around the critical size of the contact zone for bond-dominated equilibria would provide information on possible shape transitions, as discussed in previous sections.

4.3.2 Experimental observations – events in the contact zone

Combining the magnetic tweezers with the RICM technique allows for experiments in which the unbinding process can be followed in the contact zone. The first system explored is based on sLe^X binding to E-selectin, the results of which are presented in Figure 4.3. Due to the high concentration of sLe^X in the vesicle, a uniform contact zone is obtained. On the other hand, the low concentration of E-selectin on the surface and the relatively low binding constant of the pair suffice to maintain a low effective binding strength. As a result, the vesicle is still in the weak adhesion regime, with a shape similar to the one presented in Figure 4.2.

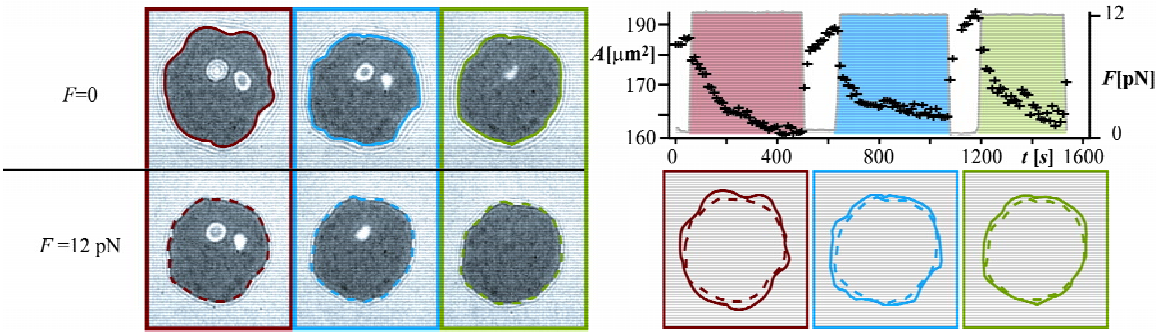

Figure 4.3: A Comparison of the equilibrium contact zone at zero force and F = 12pN is presented for a single vesicle adhered by the formation of sLe^X-E-selectin bonds. The vesicle was first allowed to adhere. The force was then applied and resulted in unbinding events (red frames). After a certain time, the vesicle was released and the force was applied again in two subsequent pulses (blue and green frames). The original data are shown on the left (pictures adopted from Lorz [154]) with the outline of the contact zone. The time evolution of the area of the zone is shown in the graph (upper right), and the comparison of outlines of the equilibrium contact zones in the un-pulled and pulled states are presented for each pulse (bottom-right).

The application of forces in this experiment, higher than those used above for shape reconstructions, induces a continuous detachment process resulting in a thermodynamic equilibrium with a contact zone smaller than at zero force (see the reconstructions of the zone edges for each pulse in Figure 4.3). If the membrane would serve only as a transducer of the force to the bonds at the edge of the contact zone, such equilibria should not be observed. That is, if this interpretation were correct, once the outermost bonds were broken, a critical force per bond must have been exceeded. Elementary reasoning would further suggest that, following the detachment of the outer-rim, the force per "remaining" bond is larger than this critical value, simply because the total force is

distributed over fewer bonds at a smaller circumference of the contact zone. Therefore, a constant pulling force would be manifested as an increasing force load in the contact zone. In this case, once the onset of bond failures occurs, there should be no "remaining" bonds able to withstand the unbinding process.

In contrast, the calculations presented in Appendix D, together with the adhesion model discussed in Chapter 2, show that a thermodynamic equilibrium with a finite contact zone is possible under force. This is a result of the response of the contact zone as a whole subsystem. Rather than perceiving the problem of the detachment as many bonds in series, the calculation presented herein shows that the contact zone responds by inducing a spreading pressure opposing the detachment. Furthermore, it was shown that such spreading pressure is always an increasing function of the decreasing size of the contact zone, even in a receptor dominated equilibrium where all of the receptors are occupied and no further bonds can be formed (Section 2.4). More importantly, these calculations show that an increased density of bonds should appear upon attempting to reduce the size contact zone (Section 2.4.3.1c). Indeed, closer inspection of the vesicle in Figure 4.3 shows that numerous binding events do occur in the contact zone following the application of the force. This can be visualized as a disappearance of the blisters in the middle of the contact zone. Releasing the vesicle, at the end of the pulse, results in the restoration of the initial contact zone. However, some memory effects can be seen as there is no reestablishment of the blister, leading to the conclusion that different bonds have been formed. The theory would suggest that the concentration of bonds for the vesicle in equilibrium arising before and after each pulse should be the same, but it is below the resolution of the microscope to really certify this result.

Similar experiments can be performed on a similar system. On this occasion, a vesicle containing lipid-anchored RGD groups (amino acid sequence Arg-Gly-Asp) is adhered to a solid supported membrane enriched with immobilized integrins. These receptors are capable of strongly binding the RGD ligand. For this reason, the concentrations of both the ligand and receptor are kept an order of magnitude lower than in the case of the sLe^X - E-selectin pair. Due to this fact, as well as the tendency of integrins to cluster during the preparation, the equilibrium adhesion of such vesicles appears quite different than that previously discussed (see Figure 4.4 at $t = 0$).

Prior to the application of the force, the vesicle saturates in a constrained equilibrium and experiences the formation of bonds in only several places in the contact zone (indicated

with arrows at $t = 0$ in Figure 4.4). The remaining part of the membrane fluctuates under the influence of the weak nonspecific potential. Imposition of the force results in unbinding of the weakly adhered parts of the contact zone. The resistance to pulling is provided only in several points, reminiscent of focal adhesion centers (FACs). Furthermore, an increased concentration of bonds is generated in the central region of the contact zone (indicated in second frame in Figure 4.4, at $t = 6.07$ s). Due to both the high affinity of the RGD-integrin pair and the fact that the diffusion constant of the RGD-lipid is much faster than the time-scale of seconds that characterizes the changes in the size of the contact zone, the increased density of bonds can be observed (see frames at. t=6.07, 7.906, 18.526) before the contact zone obtains its equilibrium size for a given force (t=18.998 and t=38.232). Although the FACs appear to be initially stabilized by the force, their failure happens at random instances (see $6.19 < t < 18.998$ s in Figure 4.4) until the equilibrium contact zone is obtained at $t = 18.998$, where no further changes in size of the contact zone occur. Further increase of the force leads to the detachment of the entire contact zone except for the last FAC that remains stable (last frame) even over an extended period of time, indicating that rebinding events must again take place.

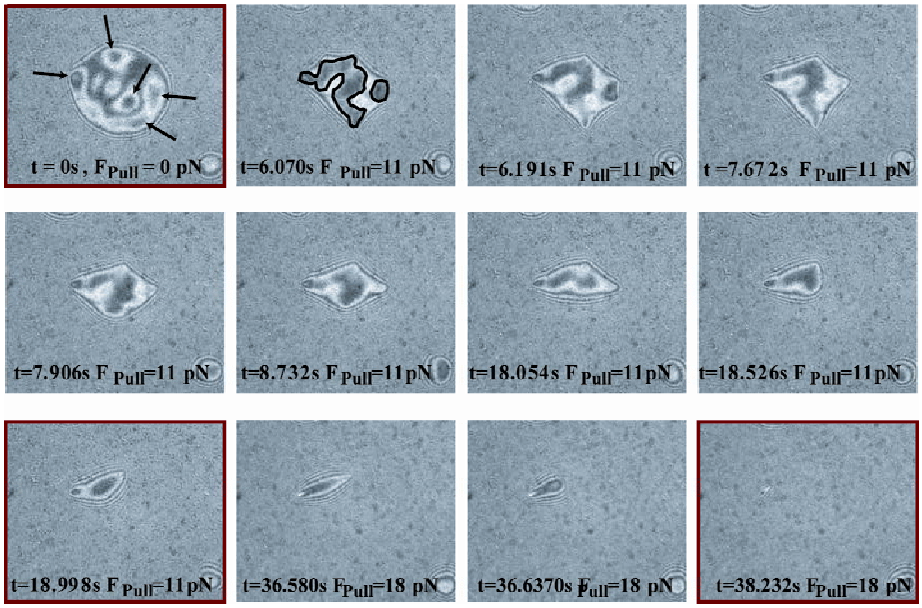

Figure 4.4: Time evolution of an unbinding process for a vesicle adhered by formation of RGD-integrin bonds. The equilibrium states are shown in pictures framed in red. The arrows in the first frame point to regions where tight contacts due to the bonds are formed between the vesicle and the substrate. The outlined area in the second picture is associated with a region where increased RGD – integrin binding occurs as a response to the application of force. Pictures adopted from Gönnenwein [155].

The faster equilibration of the RGD-integrin bonds (in comparison to sLe^X-E-Selectin), stabilizes the FACs by increased binding in their vicinity on short time scales. However, as a part of equilibration with respect to the size of the contact zone, FACs collapse at time scales of several seconds. In the thermodynamic equilibrium the contact zone is significantly reduced. However, the concentration of bonds in the contact zone is larger than it was prior to pulling.

Both systems show that the true response of a weakly adhered vesicle to the application of a pulling force involves a simultaneous increase of bond density and a reduced total number of bonds Unfortunately, in both cases it is difficult to determine the exact distribution of receptors on the substrate which precludes the complete quantitative comparison of the theoretical predictions with the real systems. Nevertheless, the qualitative behavior of the vesicle unbinding process can be understood by a combination of the models presented in this thesis.

4.4 References

134. McEver R. P., K. L. Moore, and R. D. Cummings. 1995. *J. Biol. Chem*. **270**:11025-11028.

135. Moore K. L., S. F. Eaton, D. E. Lyons, H. S. Lichenstein, R. D. Cummings, and R. P. McEver. 1994. *J. Biol. Chem*. **269**:23318-23327.

136. Springer T. A. 1994. *Cell* **76**:301-314.

137. Bell, G. I. 1978. Science **200**:618-627.

138. Dembo M., D. C. Torney, K. Saxman, and D. Hammer. 1988. *Proc. Roy. Soc. London B* **234**:55–83.

139. Evans E., and K. Ritchie. 1997. *Biophys. J.* **72**:1541–1555.

140. Merkel. R. 2001. *Phys. Rep.* **346**:344–385.

141. Leckband D., and J. Israelachvili. 2001. *Quarterly Reviews of Biophysics* **34**:105–267.

142. Florin E. L., V. T. Moy, and H. E. Gaub. 1994. *Science* **264**:415–417.

143. Simson D. A., M. Stringl, M. Hohenadl, and R. Merkel. 1999. *Phys.Rev. Lett.* **83**:652–655.

144. Leckband. D. 1995. *Nature* **376**:617–618.

145. Mehta A. D., M. Rief, J. A. Spudich, D. A. Smith, and R. M. Simmons. 1999. *Science* **283**:1689–1695.

146. Finger E. B., K. D. Puri, R. Alon, M. B. Lawrence, U. H. Von Andrian, and T. A. Springer. 1996. *Nature* **379**:266-269.

147. Nguyen-Duong M., K. W. Koch, and R. Merkel. 2003. *Europhys. Lett*. **61**:845-851.

148. Alon R., D. A. Hammer, and T. A. Springer. 1995. *Nature* **374**:539–542.

149. Merkel R., P. Nassoy, A. Leung, K. Ritchie and E. Evans. 1999. *Nature* **397**:50–53.

150. Seifert U. 2000. *Phys. Rev. Lett.* **84**:2750–2753.

151. Bell G. I., M. Dembo, and P. Bongrand. 1984. *Biophys. J.* **45**:1051–1064.

152. Schwarz U. S., N. Q. Balaban, D. Riveline, A. Bershadsky, B. Geiger, and S. A. Safran. 2002. *Biophys. J.* **83**:1380-1394.

153. Balaban N.Q., U. S. Schwarz, D. Riveline, P. Goichberg, G. Tzur, I. Sabanay, D. Mahalan, S. Safran, A. Bershadsky, L. Addadi, and B. Geiger. 2001. *Nature Cell Bio.* **3**:466-472.

154. Lorz B. G. 2003. *Etablierung enines Modellsystems der Zelladhäsion über spezifische Bindungen geringer Affinität – eine mikrointerferometrische Studie.*

155. Gönnenwein S. 2003. *Generic and specific cell adhesion: Investigations of model system by Micro-Interferometry*.

156. Seifert U., and R. Lipowsky. 1990. *Phys. Rev. A* **42**: 4768-4771.

157. Bukman D. J., J. H. Yao, and M. Wortis. 1996. *Phys. Rev. E* **54**, 5463-5468.

158. Sackmann E. 1994. *Handbook of Biological Physics*.

159. Guttenberg Z., A. Bausch, B. Hu, R. Bruinsma, L. Moroder, and E. Sackmann. 2000. *Langmuir* **16**:8984–8993.

160. Bruinsma R. *Proc.*1995. *NATO Advanced Institute of Physics and Biomaterials B*. 611-623.

SUMMARY AND CONCLUSIONS

The work presented in this thesis was undertaken with three main aims in mind. The first aim was to provide new insight into the establishment and control of the process of vesicle adhesion, as a model system for cell recognition. The second aim of this work was to provide an explanation for several particular experimental observations arising from the recent work of several groups on cell model systems. The third aim, somewhat related to the second, was to derive an easily applicable set of tools that could be used to directly interpret the results of general experiments involving vesicle adhesion. In order to achieve these goals, a ***thermodynamic model*** was developed for the ***equilibrium state of vesicle adhesion with a flat substrate***. The vesicle is treated therein by a canonical description with a fixed number of sites. A finite number of these sites are occupied by mobile ligands that are capable of interacting with a discrete number of receptors immobilized on the substrate. It was possible to show that this finiteness of the statistical ensemble has significant implications for vesicle adhesion and its control mechanisms.

Explicit consideration of the bending energy of the vesicle membrane has shown that the problem of the ***vesicle shape*** can be ***decoupled*** from the determination of the optimum ***allocation of ligands*** over the vesicle. This result is based on the fact that the contribution from the bending energy is much smaller than that of the arising from the mixing entropy and the enthalpy related to the formation of bonds. The only exception is the limit in which the vesicle shape is that of a spherical cap and the bending energy diverges. As a direct consequence of the divergence, the free energy has a boundary minimum with respect to the size contact zone. Hence, the vesicle in the thermodynamic equilibrium always assumes the shape of the spherical cap. If, for some reason, the equilibration with respect to the size of the contact zone is slow, the vesicle can find itself in a constrained equilibrium where the size of the contact zone is influenced by contributions to the interaction potential other than the one attributed to the formation of bonds. Nevertheless, as long as the reduced volume of the vesicle is known, the axially symmetric shape can still be calculated for a given contact zone. Even under such circumstances, the system is able to relax with respect to the interactions of the ligand-receptor pair.

The allocation of bound and free ligands in the vesicle could be determined as a function of the size of the contact zone, the ligand-receptor binding strength and the concentration of the system constituents. Several approximate solutions for different regions of system parameters were determined and, in particular, the ***distinction between receptor-dominated equilibria and ligand-dominated equilibria*** was found to be important. The crossover between these two types of solutions was identified to be associated with a critical size of the contact zone for which the total number of ligands in the vesicle overcomes the total number of receptors available in the contact zone.

The presented discrete approach enables the calculation of the ***effective adhesion strength*** of the vesicle. Most importantly, it was found that the effective adhesion strength is an explicit function of the size of the contact zone and, furthermore, that it is always increasing in response to a decrease in the size of the area of contact. The behavior of the effective adhesion strength was analyzed in detail and several approximate expressions for it were given. The knowledge of this variable can be put to effective use in several ways: (i) It permits meaningful comparisons with relevant experiments where the spreading pressure is a measurable quantity. (ii) It provides the link between the discrete treatment of the vesicle constituents and the proven successful continuum approach for modeling the shapes of adhering vesicles. (iii) It is a prerequisite for modeling of the control mechanisms for vesicle adhesion that rely on antagonist-induced unbinding or external force.

Regulation of adhesion by the presence of ***competitive binders*** is, to the field of physics of wetting, a novel problem. In order to simulate this situation, a series of experiments were performed in which giant vesicles, which were first adhered to a flat substrate by specific ligand-receptor bonds, were treated with monoclonal antibodies. The detailed analysis of the data arising from these investigations, undertaken within this thesis, has shown that the introduction of antibodies (which serve as ligand antagonists) into the surrounding solution in small concentrations, was able to induce unbinding of the vesicle through ***two distinct mechanisms***. The first of these is attributed to time scales shortly after the incubation of the antagonist. The main effect of this mechanism is apparent at the rim of the contact zone, which is seen to retreat and thereby cause a considerable reduction in the size of the contact zone. In the second mechanism, the antibodies induce unbinding by penetrating the contact zone without significantly affecting its size.

A theoretical framework, based on the basic adhesion model, was developed in order to understand these experimental observations. For the ***first mechanism***, the action of antagonists was attributed to the ***lateral pressure*** at the rim of the contact zone. This effect could be modeled by the use of the Langmuir formalism for the absorption of particles on a surface. The resulting lateral antibody pressure is ***balanced*** by the ***spreading pressure*** of the vesicle which is equivalent to the effective adhesion strength calculated in the basic adhesion model. For the ***second mechanism***, a variational procedure is used to simultaneously determine the density of bound antagonists and ligands within a ***contact zone of a fixed size***. Encouragingly, both experiment and theory show a ***sigmoidal decrease*** of the number of bound ligands as a function of the logarithm of the concentration.

A different control mechanism, in which the adhesion of vesicle is influenced by an ***external force***, has also been explored. The applied force is found to oppose the effective adhesion strength of the vesicle and thus serve as a control mechanism for maintaining a particular size of the contact zone. Making use of the fact that the force necessary to induce a shape deformation is of the same order of magnitude as the bending energy, the analysis of the ***binding*** equilibrium is ***decoupled*** from the problem of ***shape*** determination. The latter problem is then able to be solved within a continuum approach. The subsequent mapping of the obtained shape to the effective adhesion strength, originating from the discrete model, completes the treatment. Due to the existence of both thermodynamic and constrained equilibria, two different scenarios were distinguished.

In a ***thermodynamic equilibrium***, the vesicle is typically strongly adhered to the substrate and assumes the shape of a ***spherical cap***. Application of a force to the top of a vesicle is assumed to produce a transition toward a tethered shape. Within a continuous model, the investigation of the competition between adhesion and tether formation, in bound vesicles, resulted in several important conclusions. A critical onset force was identified where the ***tether*** spontaneously appears as part of a first order shape transition. Further growth of the tether initiates a detachment process that culminates in a ***continuous unbinding*** of the vesicle at a finite detachment force. Both critical forces, as well as all shape parameters, were calculated as a function of the reduced volume and the strength of adhesive potential. Mapping to a contact potential that depends on the size of the contact zone (obtained from the discrete adhesion model) allows for characterization of an unbinding process of a specifically adhered vesicle.

In a ***constrained equilibrium***, the vesicle is weakly adhered to the substrate. Application of a force to such vesicle produces ***continuous deformations*** which could be studied within the developed continuous model. It was shown that for a range of applied forces, locally stable bound shapes, separated from the free shape by an energy barrier, can be found. The phase diagram contains regions with either a unique bound shape or an additional meta-stable shape. Upon pulling, these shapes ***unbind discontinuously*** since the vesicles disengage from the substrate while still in possession of a finite adhesion area. The calculations of effective adhesion strength within the discrete adhesion model have shown that this quantity is basically independent of the size of the contact zone. Thus, a direct matching between the two models could be undertaken.

The hypothesis that the shape of the pulled vesicle can be decoupled from the determination of the equilibrium number of formed bonds was directly tested for the case of weak adhesion by comparison with real experimental data. Excellent ***agreement*** between the reconstruction of the ***experimental shapes*** and the shapes calculated by the use of the ***theoretical model*** was obtained. The analysis of different experiments that are concerned with changes in the contact zone during an unbinding process have confirmed the prediction of the theoretical calculations that indeed, application of constant force can result in an equilibrium with a finite adhesion area. The calculations ***predict*** that such equilibria can be achieved by an ***increased density of bonds*** in the diminished contact zone in response to pulling. Such an increase in density between the unperturbed and force-perturbed adhesive states could ***indeed be observed*** in the two experimental model systems.

The work presented in this thesis has resulted in several contributions to the understanding of vesicle adhesion and its control mechanisms as discussed above. However, several important refinements of these models can and should be performed in the future. For example, recently, more realistic experimental models for cell adhesion comprising a vesicle adhering to a substrate with mobile receptors have been developed. The basic adhesion model presented herein could be very easily adjusted to provide estimates for the allocation of ligands over the vesicle and the effective potential in this new situation.

Several approximations were undertaken in course of developing the basic model, of which the most important ones are the omission of the lateral interactions between

membrane constituents, as well as the indirect treatment of the distance dependence of the interaction potentials and the nonspecific contributions. Therefore, some better understanding of the constrained equilibria identified herein and observed in experiments, could potentially be achieved. In order to do so, one would need to be able to predict more accurately the nonspecific contributions to the total free energy. This can only be performed by calculating a self-consistent effective potential arising from the fluctuations of the vesicle shape, gravity, and the van der Waals potential between the membrane and the substrate. Such a calculation should result in both the average height of the vesicle above the substrate and the depth of the energy minimum in which the vesicle is resting. The understanding of the interplay between bond formation and the effective potential is a task associated with difficulties of both physical and mathematical nature. Nevertheless, it is a goal worth attaining. The results provided in this thesis are an important prerequisite for these more sophisticated calculations. In addition, they provide a limiting case with which any of these future theories would need to agree.

Finally, while it can not be claimed that the calculations presented in this thesis give a quantitatively accurate representation of the biological system, an acceptable level of trust in the results can be established. In particular, the work presented herein has been shown to constitute a useful and workable conceptual model of the process of cell adhesion. In addition, several insights into the nature of the control mechanisms, so well known but not yet understood, have been provided. Therefore, one can be reasonably confident that the physical approach to cell adhesion can provide valuable contributions to the understanding of the nature and purpose of important interactions in biological systems.

Appendix A

BENDING ENERGY OF A VESICLE SHAPE

The shape of an adhered vesicle should be determined for a fixed size of the contact zone. This can be achieved by the minimization of the free energy functional F, which takes the form [161]:

$$F = \frac{\kappa}{2}\oint\left(C_1 + C_2\right)^2 dA + P\int dV + \Sigma\oint dA - WA^* \qquad \text{(A.1)}$$

The first two terms constitute the Helfrich bending energy (E_{bend}) [162], which is a function of two principal curvatures (C_1 and C_2) and the bending rigidity κ. The next two terms emerge from constrains on the total volume and total area of the vesicle, respectively. The fifth term in Eq. (A.1) is the adhesion energy associated with the given size of the contact zone. For this definition of the problem, W is a Lagrange multiplier that adopts a magnitude equal to the strength of a contact potential necessary to form the contact zone of choice.

Minimization of Eq. (A.1) is performed for a set of reduced volumes, whereas the reduced area is set to unity. The results show a monotonic increase in the bending energy of a shape which deforms from a free shape to a spherical cap. Once the shape of a spherical cap (characterized by the size of the contact zone S_c^*) is achieved, the bending energy diverges.

A.1 Determination of the fitting function

In order to find an appropriate fitting function for the data obtained from the minimization of Eq. (A.1), a general polynomial basis can be used for the expansion of the bending energy (E_{bend}):

$$E_{bend} = \frac{K_1}{(S_c^* - S_c)^{K_2}} + \sum_{i=0}^{\infty} C_i (S_c^* - S_c)^i \ . \qquad \text{(A.2)}$$

The first term is added to account for the divergence of E_{bend} at $S_c = S_c$*. The second term in Eq. (A.2) should be the dominant contribution at small sizes of the contact zone.

To determine the coefficients associated with the divergence of the bending energy (K_1 and K_2), a fitting function of the form $y = K_1 /(x^{K_2} + C_0)$ is first applied to all the data in each set, as well as just those data relevant to the spherical limit (bottom-left and top-left in Figure A1, respectively).

As the obtained values for K_2 are very similar to unity for all reduced volumes, the data are re-fit with fixed K_2 (K_2 =1, bottom-right, top-right). In the spherical limit (top-left, and top-right), the standard deviations (V_{chisq}) resulting from these two fitting functions (K_2 = free, K_2 = 1), have comparable values for each reduced volume, implying that both fits are equally reliable. However, the standard deviations of the two fitting functions are considerably different when the entire data sets are used. In particular, the standard deviations of the fit with K_2 constrained are up to two orders of magnitude larger than those for the corresponding fit with variable K_2. This is an indication that, in the fit with the K_2 free, the parameters are able to adjust to obtain higher accuracy for small sizes of the adhesion plate (though large V_{chisq} is still obtained, particularly for small values of v).

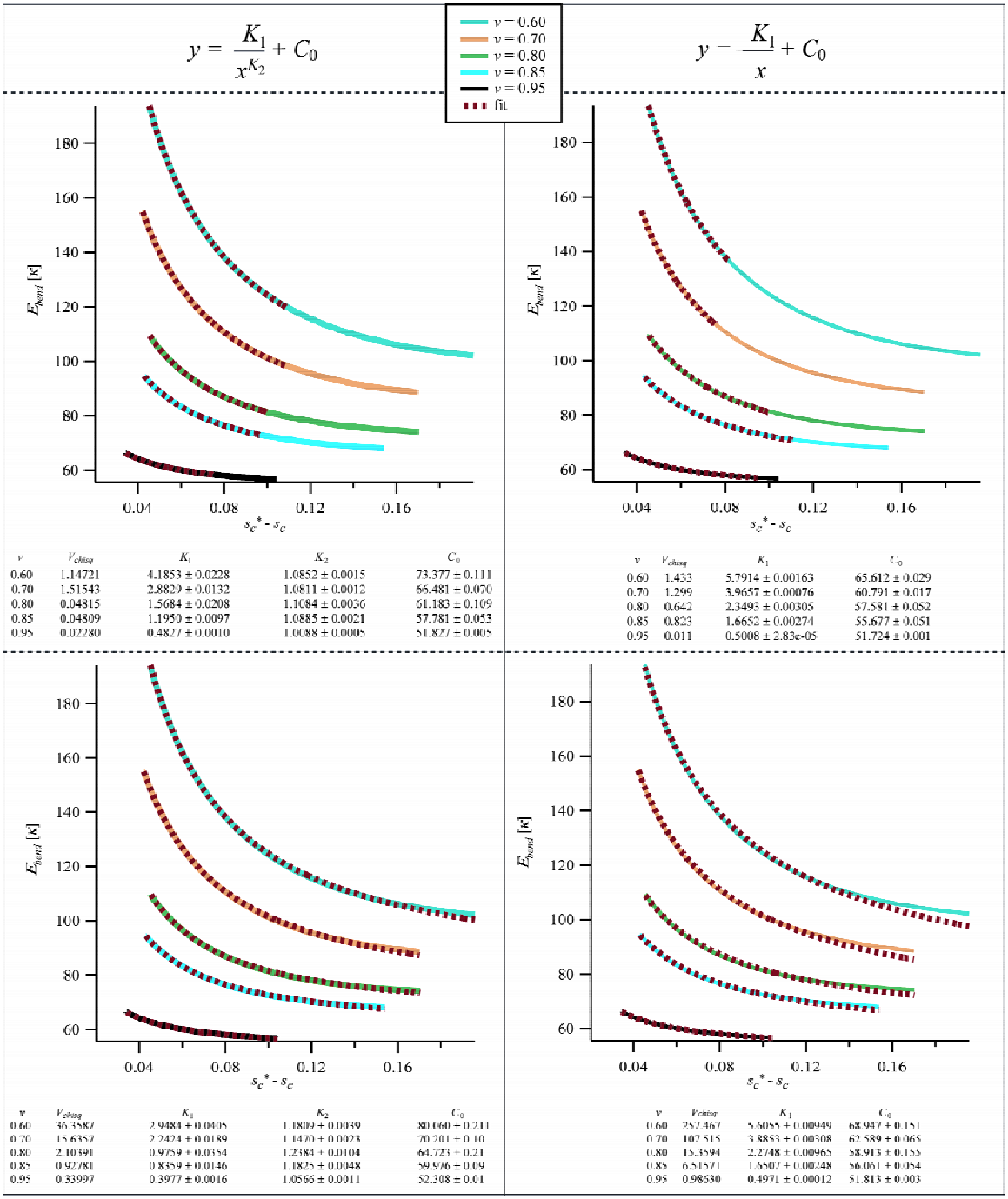

Figure A.1: Determination of the divergence term. Several fitting procedures and their parameters are presented for the spherical limit (top) and the entire data set (bottom).

When $K_2 = 1$, the number of coefficients in a simple fit is not sufficient to accurately fit the bending energy for small sizes of the adhesion plate. Rather, it appears that further terms of the sum from the Eq. (A2) would be necessary.

Figure A.2 shows the effect of including progressively more terms into the fitting function. It is obvious that the standard deviation decreases considerably with each additional step. With the inclusion of a second order term, the fitted curves can be seen to virtually reproduce the numerical data. However, a bending energy described by a second order polynomial (in s_c) could produce considerable numerical difficulties when minimizing the total free energy for vesicle adhesion. In addition, the parameters for such a fit (C_0, C_1 and C_2) are quite sensitive to the interval of a chosen data set, and therefore unsuitable for determining their dependence on the reduced volume. Nevertheless, for a particular choice of v, the K_1 parameter is almost independent of the fitting procedure. This at least assures that the divergence coefficient is correctly determined.

The conclusion that arises from the previous discussion is that the optimal balance between numerical accuracy and numerical difficulty seems to be associated with the fit which employs a fixed K_1 ($K_1 = 1$) and a first order polynomial:

$$E_{bend} = \frac{K_1}{(S_c^* - S_c)} + C_1(S_c^* - S_c) + C_0 . \qquad \text{(A.3)}$$

From the standard deviation V_{chisq}, it can be seen that the expansion is more reliable for less reduced volumes. However, very good results are obtained, even for $v = 0.60$, which is the limit for experimentally relevant reduced volumes.

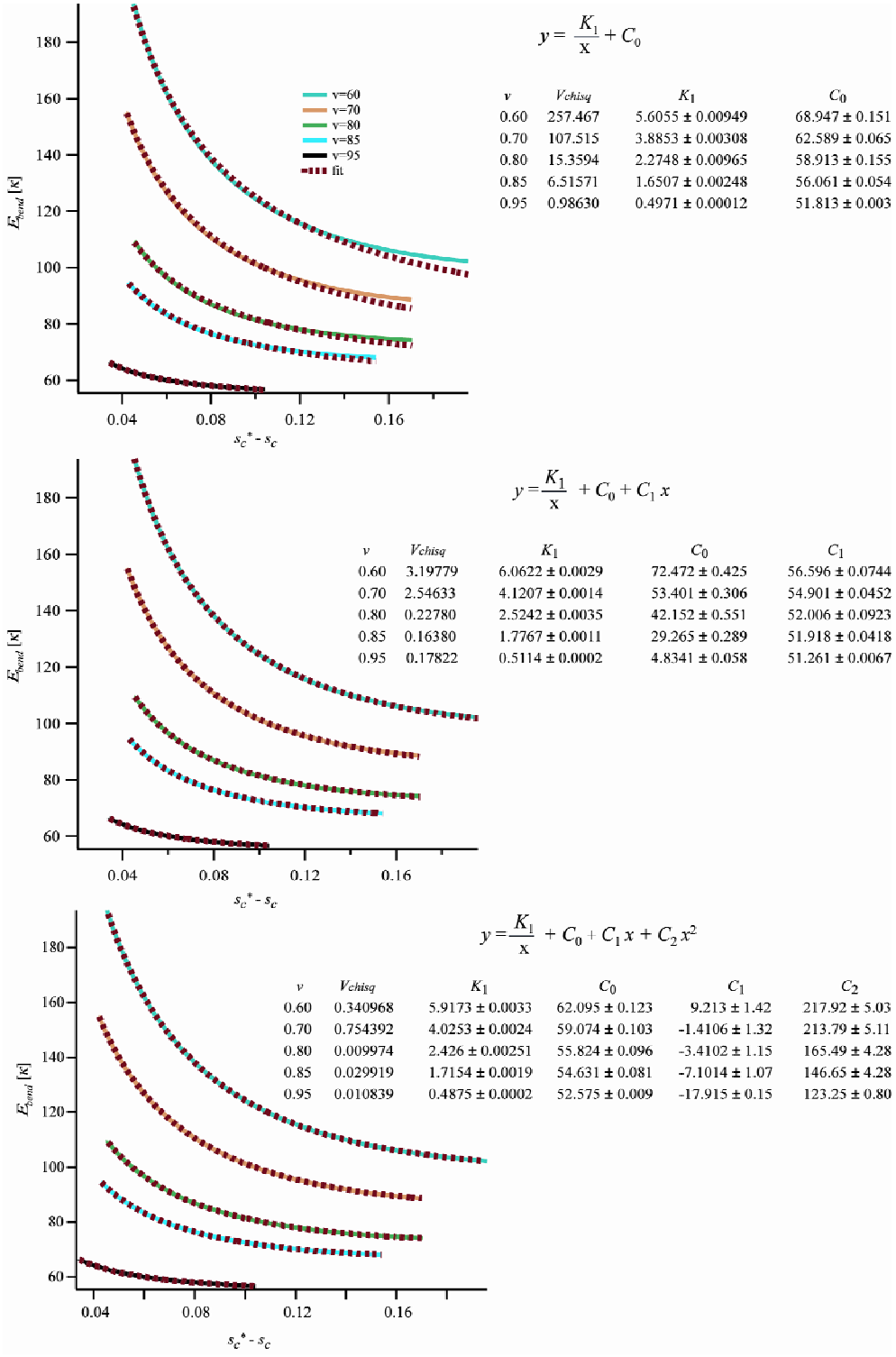

v	Vchisq	K_1	C_0
0.60	257.467	5.6055 ± 0.00949	68.947 ± 0.151
0.70	107.515	3.8853 ± 0.00308	62.589 ± 0.065
0.80	15.3594	2.2748 ± 0.00965	58.913 ± 0.155
0.85	6.51571	1.6507 ± 0.00248	56.061 ± 0.054
0.95	0.98630	0.4971 ± 0.00012	51.813 ± 0.003

v	Vchisq	K_1	C_0	C_1
0.60	3.19779	6.0622 ± 0.0029	72.472 ± 0.425	56.596 ± 0.0744
0.70	2.54633	4.1207 ± 0.0014	53.401 ± 0.306	54.901 ± 0.0452
0.80	0.22780	2.5242 ± 0.0035	42.152 ± 0.551	52.006 ± 0.0923
0.85	0.16380	1.7767 ± 0.0011	29.265 ± 0.289	51.918 ± 0.0418
0.95	0.17822	0.5114 ± 0.0002	4.8341 ± 0.058	51.261 ± 0.0067

v	Vchisq	K_1	C_0	C_1	C_2
0.60	0.340968	5.9173 ± 0.0033	62.095 ± 0.123	9.213 ± 1.42	217.92 ± 5.03
0.70	0.754392	4.0253 ± 0.0024	59.074 ± 0.103	-1.4106 ± 1.32	213.79 ± 5.11
0.80	0.009974	2.426 ± 0.00251	55.824 ± 0.096	-3.4102 ± 1.15	165.49 ± 4.28
0.85	0.029919	1.7154 ± 0.0019	54.631 ± 0.081	-7.1014 ± 1.07	146.65 ± 4.28
0.95	0.010839	0.4875 ± 0.0002	52.575 ± 0.009	-17.915 ± 0.15	123.25 ± 0.80

Figure A.2: Determination of the coefficients and the order of the polynomial expansion. The order of the polynomial used as a fitting function is increasing from top to bottom.

A.2 Dependence of the coefficients on the reduced volume

For numerical purposes it is convenient to obtain a functional form for the coefficients. As shown in Figure A.3, a parabolic fit is relatively good, for C_1, but some important deviations (V_{chisq} = 0.67) are still present. For K_1, it is possible to use a linear fit (indicated with the orange line). However, a parabolic fit results in a significantly smaller standard deviation (V_{chisq} = 0.001) and should hence be used to determine intermediate values of the K_1 coefficient.

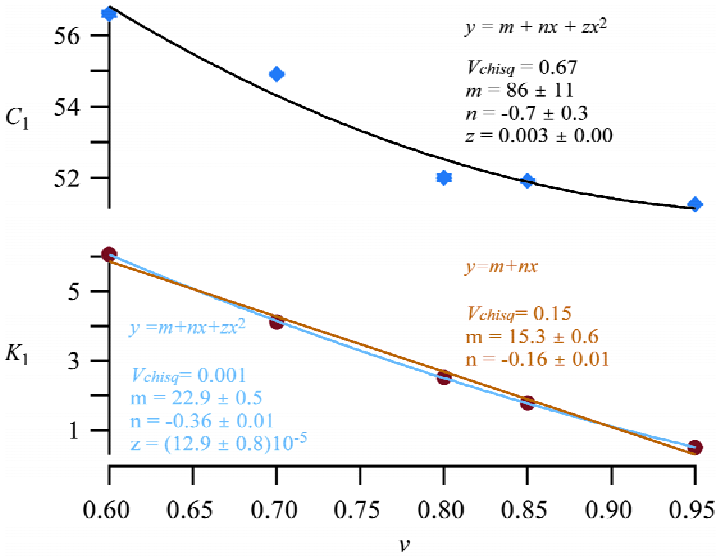

Figure A.3: Fitting coefficients as functions of reduced volume. The lines indicate various fitting options.

A.3 References

161. Seifert. U and R. Lipowsky. 1990. *Phys. Rev. A* **44**:1182-1202.

162. W. Helfrich. 1973. *Naturforsch*. **28C:**693-703.

Appendix B

SPECIFICATIONS OF THE EXPERIMENTS

B.1 Materials

B.1.1 Preparation of vesicles and substrates for the sLe^X-E-selectin binding pair

- Vesicles

Giant vesicles were prepared from an equimolar mixture of DMPC (1,2-dimyristoyl-sn-glycero-3-phosphocholine) and cholesterol. To screen the nonspecific Van der Waals attraction by the glass substrate, the vesicles were doped with DMPE-PEG2000 (1,2-dimyristoyl-sn-glycero-3 phosphoethanolamine-N-polyethylene-glycol) by adding this lipid at a concentration of 1% with respect to DMPC. In addition, to allow for specific ligand-receptor based binding of vesicles to the substrate, 8% of sialyl-Lewis^X-glycosphingolipids [163] were reconstituted into the bilayers. The vesicles were prepared by electro-swelling [164,165] in a 170mOsm sucrose solution. To prevent suppression of adhesion due to osmotic tension, the vesicles were placed in a 210 mOsm salt buffer (100mM NaCl, 1mM $CaCl_2$, 1mM NaN_3, 10 mM HEPES at pH of 7.2). This was sufficient to deflate the vesicles and enable the formation of a contact zone parallel to the substrate. The vesicles were deposited on the substrate from the suspension by sedimentation under gravity.

- Substrates

The substrate was a clean glass cover slide which was hydrophobized by emersion into a 1% toluene solution of aminosilanes (3-aminopropyltriethoxysilane) for 4 minutes at 60^{o}C which was followed by rinsing with pure toluene and drying under N_2 [166]. Finally a recombinant form of the extracellular domain of human E-selectin was physabsorbed on the substrate exposing the silane layer [167]. This was achieved by incubating the protein solution (maximum 5 μg/ml in the salt buffer) for two hours at room temperature, while the whole chamber was gently mixed on a shaking platform. After rinsing with buffer, the substrate was incubated at room temperature for one more

hour with a buffer solution containing 3% of Blotting Grade Blocker Non-Fat Dry Milk in order to prevent any direct contact of glass with the vesicle. Final careful rinsing of the slide with buffer completed the preparation. Additional details of this procedure as well as the characterization of both the vesicles and the substrates are published in references [168] and [169].

- Preparation for antibody experiments and the confocal microscopy

For the competitive binding experiments, mouse anti-human E-selectin was diluted in the salt buffer at concentrations of 10 to 25 μg/ml and inserted into the measuring chamber with a Hamilton pipette.

For confocal experiments 0.2 mol% of the fluorophore bodipy was added into the DMPC-cholesterol matrix.

B.1.2 Preparation of vesicles and substrates for RGD-integrin binding pair

- Vesicles

The same procedure as that employed for sLe^X containing vesicles was undertaken here, except that the mixture contained 1mol% of DMPE lipid with a cyclic RGD peptide headgroup. For details see Guttenberg *et al.* [170].

- Substrates

Small DMPC: DMPG (equimolar mixture) vesicle with incorporated integrin receptors of type $\alpha_{IIb}\beta_3$ are self assembled in a buffer solution (159 mM NaCl, 20 mM TRIS, 1mM NaN_3, 1 mM $MgCl_2$ at pH = 7.3) with a final ratio of integrin to lipid of about 1:650 molecules. In order to spread the vesicles and form a bilayer, 150 μl of vesicle solution is pipetted onto a clean glass substrate. After 2.5 hours of incubation at 40 ^oC, the osmolality of the buffer is increased for 25 mOsm by adding 100 μl of the same buffer but with 200 mM NaCl. A further 1 hour of incubation is followed by extensive rinsing with buffer to remove free lipids and vesicles. Incubation of the substrate with 3 wt.% solution of BSA in buffer (100 mM NaCl, 10 mM HEPES, 1 mM NaN_3 and 1 mM $CaCl_2$, pH = 7.3, 205 mOsm) renders the substrate passive. Careful rinsing with the last buffer finalizes the preparation. Additional details for this preparation can be found in reference [171].

B.1.3 Preparation for magnetic tweezers experiments

For experiments with magnetic tweezers 1 mol% of amine-PEG2000 lipid is incorporated into the vesicle matrix in order to covalently attach the vesicles to the surface of paramagnetic beads.

Tosylcoated monodisperse paramagnetic beads (diameter 4.5 ± 0.2 μm) are diluted in the concentration of 4×10^6 beads per ml. This solution is added to the buffer used for the suspension of vesicles. After gentle rotation for 1 hour at room temperature, covalent bonds between amine groups on lipid anchored PEGs are formed with the tosyl groups on the beads. Such a preparation results in the attachment of 1 bead to 25% of vesicles.

B.1.4 Sources of chemicals

All of the lipids and the cholesterol were purchased from Avanti Polar Lipids, Inc., AL, USA. The aminosilanes and toluene were obtained from Fluka, Switzerland, while the cover glasses originated from Merck, Germany. E-selectin was made by Calbiochem, San Diego, CA, USA, whereas the antibodies were manufactured by Chemicon, Temecula, USA. The Millipore water used for rinsing and the buffers was prepared with a system from Millipore, France. The fat free milk was purchased from BioRad, Hercules, CA, USA. Paramagnetic beads are obtained from Dynal, Inc., Norway.

B.2 Methods

B.2.1 Reflection Interference Contrast Microscopy

Reflection interference contrast microscopy (RICM) is a micro-interferometric technique that generates an interference pattern by the interference of light waves reflected at the interfaces between the substrate and the buffer, and the buffer and the membrane. It allows for the reconstruction of the surface profiles of adhering bodies with ~10 nm out-of-plane and ~0.3μm in-plane spatial resolution. Relative membrane displacements in the vertical direction can be measured with resolutions of up to 5 nm. The spatial variations of the substrate–membrane distances can be directly visualized through the variations of gray scales which can be represented in terms of 255 gray scale colors. Strongly bound parts of the membrane appear as dark regions of the interference pattern while weakly adhering regions separated from the substrates by ~100 nm appear as grey areas. In

combination with fast image processing, thermally excited membrane fluctuations can be analyzed quantitatively to evaluate the control of adhesion by the undulation forces.

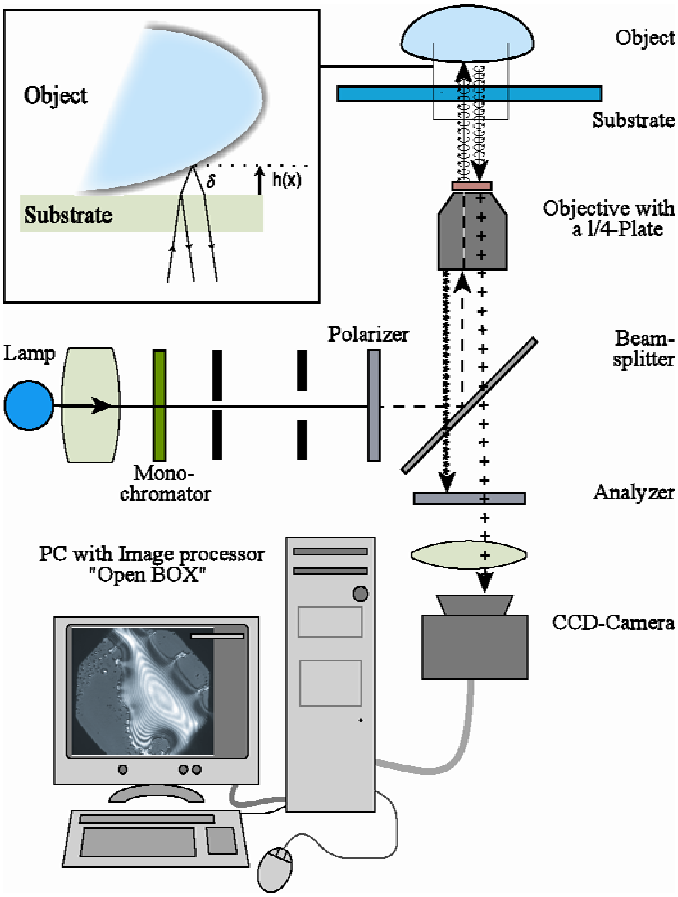

Figure B.1: Schematic presentation of an RICM. Monochromatic light is used to obtain an interference pattern resulting from the reflections on the glass-buffer and buffer-membrane interfaces. Due to the very low refractive index of the buffer-membrane interface $r = 6.5\times10^{-4}$ [172], light reflected by any component within the microscope is much more intense. Thus, to extract the signal, an anliflex technique consisting of two polarizers and a $\lambda/4$ plate, has been developed [173]. Thus, only the light that passes through the quarter-wave plate twice is registered on the CCD-camera. Picture adapted from [7].

The bottom of the 900 µl measuring chamber is formed by a cover glass pressed onto the Teflon frame by a metal ring. The chamber is mounted on an inverted Axiomate 100 microscope (Zeiss, Germany), equipped with an antiflex objective (Plan Neofluar, 63× /1.25 Oil, Zeiss, Germany). The interferograms are observed with a Peltier-cooled 10 bit CCD camera (C4880-80, Hamamatsu, Japan) and the digitized images are stored directly using real-time imaging software [174].

B.2.2 Magnetic tweezers

Magnetic tweezers is a setup that manipulates magnetic beads. In this case it is realized is such a way that the pulling force exerted by the magnet is normal to the plane of observation (see Figure B.2). The construction allows for observation of samples with bright field illumination on an inverted microscope. It can also be combined with a confocal microscope or an RICM.

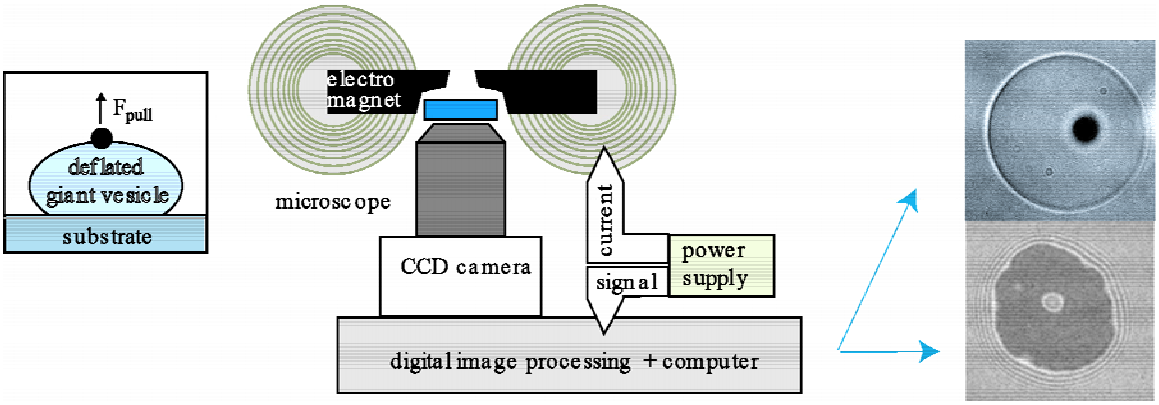

Figure B.2: Schematic view of the vertical magnetic tweezers mounted on an inverted microscope. In the vicinity of the measuring chamber are magnetic poles that generate the field. The current through the coils of the magnet is controlled by the power supply that produces a pulse-like signal. The digital unit stores the signal that is either a bright field picture or an RICM interferogram. Picture adopted from [175].

The vertical distance between the measuring chamber and the poles can be varied between 1-10 mm. Together with the variation of the current (0 - 5 A), the pulling force can be tuned in range of 0 – 100 pN. Details of this setup can be found in reference[175].

B.2.3 Laser Confocal Scanning Microscopy

The Laser scanning microscope uses a focused laser beam to illuminate a particular spot in the sample and fluorescently excite a target. By scanning an object, layer by layer, a three-dimensional reconstruction can be obtained. The microscope used is Odyssey XL (Noran, WI, U.S.A.) adopted for a Ar-Kr-Laser (wavelengths 488, 567 and 647 nm)

B.3 References

163. Gege C., S. Oscarson and R. R. Schmidt. 2001. *Tetrahedron Lett*. **105**:5178-5185.

164. Dimitrov, D. S. and M. I. Angelova. 1988. *J. Electroanal. Chem*. **253**:323-336.

165. Albersdörfer, A., T. Feder and E. Sackmann. 1997. *Biophys. J*. **73**:245-257.

166. Petri, D. S. F., G. Wenz, P. Schunk and T. Schimmel. 1999. *Langmuir* **15**:4520-4523.

167. Greenberg, A. W., D. K. Brunk and D. A. Hammer. 2000. *Biophys. J*. **79**:2391-2402.

168. Lorz B. G., A.-S. Smith, C. Gege and E. Sackmann. *In preparation*.

169. Lorz B. G. 2003. *Etablierung enines Modellsystems der Zelladhäsion über spezifische Bindungen geringer Affinität – eine mikrointerferometrische Studie.*

170. Guttenberg. Z., B., A. Bausch, B. Hu, R. Bruinsma, L. Moroder and E. Sackmann. 2000. *Langmuir* **16**:8984-8993.

171. Gönnenwein S., M. Tanaka, B. Hu, L. Moroder and E. Sackmann. 2003. *Biophys. J*. **85**:646-655.

172. Born M. And E. Wolff. 1999. *Principles of Optics, 7th edition.*

173. Ploem J. 1975. *Mononuclear Phagocytes in Immunity, Infelction and Pathology.*

174. Schilling J. 1999. *Entwicklung einer Echtzeit-Bildverarbeitungssoftware undi digitaler Videoaufnehmetechnik zur quantitativen Mikrorheonetie von Aktin_Netzwerken*.

175. Gönnenwein S. 2003. *Generic and specific cell adhesion: Investigations of a model system by Micro-Interferometry*.

Appendix C

CONTINUOUS MODEL FOR UNBINDING: STRONG ADHESION

VOLUME 92, NUMBER 20 PHYSICAL REVIEW LETTERS week ending 21 MAY 2004

C.1 Pulling Tethers from Adhered Vesicles

Ana-Sunčana Smith,[1] Erich Sackmann,[1] and Udo Seifert[2]
[1]*E 22 Institut für Biophysik, Technische Universität München, D-85748 Garching, Germany*
[2]*II. Institut für Theoretische Physik, Universität Stuttgart, D-70550 Stuttgart, Germany*
(Received 8 September 2003; published 21 May 2004)

The competition between adhesion and tether formation in bound vesicles is investigated. A theoretical model is developed in which tethers are induced by the application of a pulling force to the top of a strongly adhered vesicle. A critical onset force is identified where the tether spontaneously appears as part of a first order shape transition. Further growth of the tether initiates a detachment process that culminates in a continuous unbinding of the vesicle at a finite detachment force. Both critical forces, as well as all shape parameters, are calculated as a function of the reduced volume and the strength of adhesive potential.

DOI: 10.1103/PhysRevLett.92.208101 PACS numbers: 87.17.–d, 87.16.Dg, 87.80.Fe

Fluid membranes are unique among all two-dimensional elastic sheets due to their vanishing shear modulus. This property allows for spectacular deformations of these slender layers such as the formation of thin tubular structures, known as tethers. Their extraction can be realized by the application of a highly localized force, balanced against an appropriate resistance mechanism. The paradigmatic case for tether formation involves pulling on beads [1] or micropipettes irreversibly bound to a vesicle. These may serve as a means to exert axial tension [2] or as anchor points in the case of flow experiments [3].

The manipulation of tethers has been used as an investigative tool to elucidate the properties of membrane materials. In this manner, the bending modulus of bilayers [1] and the nature of the dynamic interaction of monolayers within a single bilayer [4] have been determined. Tether extraction from cells has enabled the quantification of the coupling of the cell membrane to the supporting cytoskeleton [5]. Recently, molecular motors have been employed to induce tubulation in giant vesicles [6].

Several theoretical models relevant to tether formation have appeared. The initial interest was focused on the stability of free tubes [7] and cylindrical vesicles under axial tension [8,9]. More recently, asymmetric tethered shapes have been found to result from the application of a force to the opposing poles of a vesicle [2]. In flat membranes, tether induction has been shown to rely on appropriate boundary conditions imposed at the rim of the tether [10,11], as has been verified experimentally [12].

A problem of significant biological and technological relevance is that in which the resistance mechanism to tether formation is provided by a finite adhesion potential acting on another part of the vesicle. For example, such counteraction has been used for the construction of complex networks from tethered fluid vesicles [13]. Nevertheless, a theoretical work that provides an understanding of the external adhesive counteraction to tether formation has not yet been provided. The present investigation deals with this problem and reveals a rich competition between the attractive potential and shape deformations.

Simple intuition suggests that the response of an adhered vesicle to pulling would depend strongly on the type of the adhesion achieved by the vesicle [14]. When the vesicle is bound in a *weak* potential, only part of the excess free area (resulting from the volume reduction during vesicle preparation) is used to form the adhesion plate. Pulling on such a shape causes continuous deformations, made possible by the unused excess area [15]. A *strongly* adhered vesicle should clearly undergo a different scenario. In these circumstances, the excess free area is entirely consumed by the adhesion plate so that the vesicle assumes the shape of a tense spherical cap [14]. Because of constraints on the area and volume, no deformations can be induced while maintaining a constant adhesion area. However, should sufficient force be applied to overcome the adhesive potential, a tether will be pulled out of the vesicle, initiating a detachment process. The tether can be expected to grow until the adhesion plate is spent and the detachment process is complete. In the current work, we quantitatively investigate this regime of strong adhesion. As it is safe to assume a cylindrical tether geometry [2], we consider shapes consisting of a spherical cap (a vesicle) connected to a thin tube (a tether). Variational methods are thus used to minimize the following free energy functional:

$$\mathcal{F} = \frac{\pi\kappa L}{R} - F(h + L) - WA^* + \Sigma A_{\text{tot}} + PV_{\text{tot}}. \quad (1)$$

The first term is the bending energy of a cylinder with radius R and length L, and is proportional to the bending rigidity κ. The variation of the bending energy of a spherical cap is an order of magnitude smaller than that of the other terms and may therefore be omitted. The second term is the energy arising from the application of a point force to the north pole of the vesicle. This energy is a function of the strength of the force ($F > 0$), and the total height (sum of the heights of the spherical cap h and the tether). The next term is the adhesion energy associated

VOLUME 92, NUMBER 20 PHYSICAL REVIEW LETTERS week ending 21 MAY 2004

with a given contact potential, of strength $W > 0$, and is proportional to the area of the adhered surface A^*. The last two terms in Eq. (1) emerge from constraints imposed to maintain constant total area (A_{tot}) and volume (V_{tot}), by adjusting the Lagrange multipliers for the tension (Σ) and pressure (P), respectively.

The results are presented in reduced units, scaled by the area of a unit sphere $A_s = 4\pi R_s^2$, and $R_s = 1$. Hence p, σ, w, v, and f become dimensionless parameters, and are defined as $p = PR_s^3/\kappa$, $\sigma = \Sigma R_s^2/\kappa$, $w = WR_s^2/\kappa$, $v = 3V_{\text{tot}}/(4R_s^3\pi)$, and $f = FR_s/(\pi\kappa)$. In addition, $A_{\text{tot}} = A_s$. For a vesicle of radius of $R = 10\ \mu\text{m}$ and bending modulus $\kappa = 10^{-19}$ J, one unit of force f is equal to 0.3 pN, and one unit of adhesion strength w is $10^{-7}\ \text{J m}^{-2}$.

To find stationary solutions of the free energy functional, the first variation with respect to all shape parameters (A^*, h, L, and R) is performed. The obtained relations are then solved simultaneously with the constraints on the total volume and area, for a given set of v, w, and f. Physically relevant solutions are those that are real and have values of all shape parameters greater than zero (in addition, the tether radius must be smaller than the radius of the spherical cap). Generally, there exist two solutions that satisfy these requirements for a given set of parameters. The shape associated with the lower total energy is considered to be locally stable and is thus the relevant one in the following discussion. Examples of the calculated shapes are presented in Fig. 1.

Phase diagram.—The phase diagram can be presented for either constant v (left panel of Fig. 2) or constant w (right panel). In both cases, three regions can be observed. Most prominent is the region shaded in gray, where stable solutions are tethered vesicles. This region is open in the $f - w$ diagram as there is no theoretical upper limit to the strength of the adhesion potential. As the reduced volume of the vesicle must be in the range $0 < v \leq 1$, the entire phase space (for fixed w) is presented in the $f - v$ diagram. The lower boundary of the gray regions is congruous with the onset of tether formation (denoted as f_o) and is a line of a first order shape transition. For forces below this line, the shape of a tetherless spherical cap is a stable solution. The upper boundary of the regions where tethers are stable (denoted as f_d) corresponds to forces at which the tethered vesicle detaches from the surface with the adhesion area $A^* \to 0$ when $f \to f_d$. As detachment is a continuous process, this boundary is a line of a second order shape transition. Above this line, the stable solution corresponds to a free vesicle far away from the substrate.

Tethered shapes.—The calculation of shapes, by minimizing Eq. (1) subject to constraints, results in algebraic expressions for all variables. Because of the complexity of these equations, they will not be presented here in their full form. However, it is possible, by assuming that the volume of the tether is much smaller than the volume of the vesicle, to obtain an expression for the tether length as a function of force:

$$L \simeq (1 - v^{2/3})f. \tag{2}$$

This approximate relationship assumes the role of an asymptote at large forces and adhesion strengths (see Fig. 3). For small w, the exact solution is nonlinear in the whole range of applicable forces and the approximate solution defined by Eq. (2) is reached only at the detachment point. For larger adhesion strengths, the linear dependency of the tether length on the applied force is in good agreement with the exact solution, for the majority of feasible forces. This result predicts that, for smaller values of v, the tether length grows faster with the force. Nevertheless, for a fixed volume, very similar solutions for the tether length are obtained for very different w. As an application of Eq. (2) the linear regime of tether retraction from Fig. 5 of Ref. [13] has been fitted and resulted in a reduced vesicle volume of $v = 0.93 \pm 0.02$.

Extracting the leading terms from the exact solutions (not presented) leads to well known results for the tether

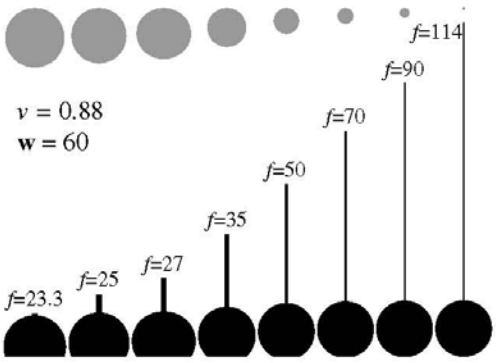

FIG. 1. An adiabatic force load initiates a detachment process. Finite forces are found for both the tether onset ($f_o \simeq 23.3$) and the vesicle detachment ($f_d \simeq 114$). Shapes of tethered vesicles are presented for different forces in black. Gradual but total loss of the adhesion area (top, gray circles) can be observed as the tether length increases.

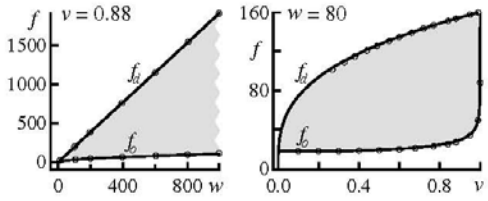

FIG. 2. Examples of $f - w$ (left) and $f - v$ (right) phase diagrams. Regions of locally stable tethered shapes are indicated in gray. The line associated with f_o is the boundary between regions of stable tethered shapes and stable shapes consisting of a bound spherical cap. The f_d line belongs to continuous unbinding transitions from bound tethered shapes to free vesicles. Approximate solutions (lines) from Eqs. (4) and (5) and the exact solutions (circles) are shown.

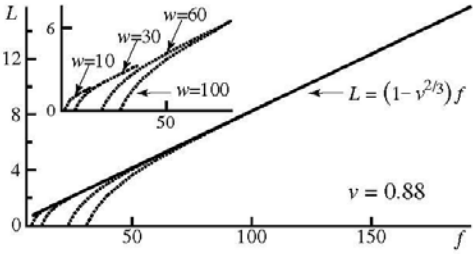

FIG. 3. The length of a tether as a function of force for different adhesion strengths. The approximate solution (thick line) is overlaid with exact solutions (dotted lines).

radius and tension:

$$R \approx \frac{2}{f}, \qquad \sigma \approx \frac{f^2}{8}. \tag{3}$$

These relationships have already been derived and verified experimentally [1,8], for the special case of a tether extracted from a vesicle partially drawn into a pipette. Now, however, these results are obtained as part of a more general model, which includes a finite adhesion strength. As was the case for the tether length, these expressions will become exact in the limit of large f and w (and $f/w = \text{const}$). Inspection of Fig. 4, where the approximate result is compared to the exact solution, clearly demonstrates this limit.

Within the current model, shapes with arbitrarily high tensions can be calculated, but their existence is limited by the lysis tension of the membrane ($\Sigma_l \approx 10^{-3}\,\mathrm{N\,m^{-1}}$). Once such tension is exceeded, the tether will rupture. Using Eq. (3), it is easy to estimate the lysis point force to be $F_l \approx 90$ pN for a membrane with $\kappa = 25kT$. Interestingly, the approximate solutions obtained for R and σ, are not sensitive to the adhesion strength or the reduced volume. Consequently, for any value of the applied force ($f_o < f < f_d$), almost identical solutions can be found for quite different values of v and w. This can be seen in Fig. 4, where the intervals of stable solutions

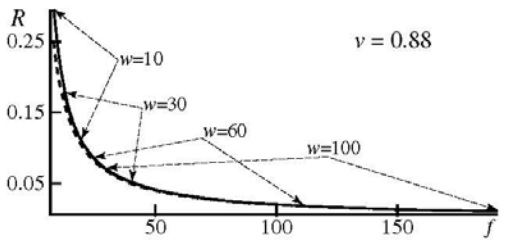

FIG. 4. The tether radius as a function of force for different adhesion strengths. The exact solution (thick line) is rapidly approached by the approximate one (dotted line). The broken arrows indicate the regions where stable solutions are found for a particular adhesion strength.

belonging to different w overlap. It is therefore important to define the boundaries of the interval where tethered shapes exist as a function of state variables (v and w). This will be discussed in the following sections.

Onset of tether formation.—The conditions for tether appearance can be determined by setting R and L to zero. In this case, the constraints on the area and volume of the vesicle with no tether are sufficient to determine the characteristics of the spherical cap (h and A^*). The shape obtained in this way is identical to the one arising from the variation of the free energy at $f = 0$. It is the spherical cap of minimum height h_o (see Fig. 5) and maximum adhesion area ($A_o^* = 2 - h_o^2/2$). Because of strong adhesion, this shape is a function of only the reduced volume and is not dependent on the adhesion strength. At the onset of tether formation, the tension must approach that given in Eq. (3). This may be used to derive the approximate onset force [$f_o = f_o(v, w)$] and pressure [$p_o = p_o(v, w)$]:

$$f_o \simeq \frac{-h_o + \sqrt{h_o^2 + A_o^{*2} + A_o^* h_o^2 w}}{0.5 A_o^*}, \qquad p_o \simeq \frac{4w - f_o^2}{2h_o}. \tag{4}$$

The comparison of this force with the exact solution is presented in the phase diagram (see Fig. 2, both panels). Excellent agreement is obtained for the whole range of adhesion strengths and reduced volumes. As the height of the vesicle (h_o) and the size of the adhesion plate (A_o^*) are independent of the adhesion strength, the onset line (f_o) in the left panel of Fig. 2 is proportional to $\sqrt{w}$. This analysis infers that for all $f < f_o$, the spherical cap parametrized with h_o and A_o^* is a stationary stable solution. A force load will merely adjust the tension and the pressure until the tether emerges at $f = f_o$.

In the *limit* of strong adhesion ($w \to \infty$) this scenario is exact. However, in the *regime* of strong adhesion ($w \gg 1$), the very small amounts of excess area that remain free upon adhesion could allow for continuous (but slight)

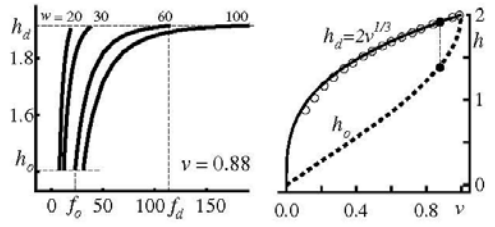

FIG. 5. Left: The exact results for the height of the vesicle as a function of force for different adhesion strengths (thick lines). Approximate onset and detachment heights (all w) and forces ($w = 60$) are indicated. Right: The exact onset heights (dotted line) and a comparison of approximate (thin line) and exact (empty circles) solutions for the detachment height as a function of reduced volume. Exact solutions are calculated with $w = 80$. The filled circles indicate solutions for $v = 0.88$.

vesicle deformations at forces close to the zero force. Within the current model, these shapes are mapped onto the spherical cap at $f = 0$ and should not affect the discontinuous nature of the shape transition. The appearance of such a transition is a consequence of both the applied constraints and the adhesion strength. Hence, it is not surprising that models for tether formation [10,11], which lack an equivalent of adhesion to provide a counteractive contribution to the free energy (and are in a different geometry), find a continuous transition.

Detachment.—A critical detachment force (f_d), corresponding to zero adhesion area ($A_d^* = 0$), can be calculated by assuming that the volume of the tether is much smaller than the volume of the vesicle. In this case $h \to 2v^{1/3}$ when $A^* \to 0$. The validity of this assumption can be confirmed by the inspection of Fig. 5. For constant reduced volume (left panel), the asymptotic detachment height ($h_d \approx 2v^{1/3}$) is reached independently of the adhesion strength. For a constant adhesive potential (right panel), very good agreement between the asymptotic and the exact solutions is obtained. However, discrepancies emerge for small values of v, implying that the chosen w ($w = 80$) acts as a strongly adhesive potential for large values of the reduced volume, but is relatively weak for very deflated vesicles ($v < 0.35$). Indeed, as w increases, the agreement between the approximate and exact solution improves for small v. Minimizing the free energy using the expression for h_d leads to an approximate relationship for the detachment force:

$$f_d \approx 2v^{1/3}w. \tag{5}$$

This equation is plotted in the aforementioned phase diagrams (Fig. 2). For constant volume (left panel), the linear dependence of f_d on the adhesion strength is confirmed. In the diagram for constant w (right panel), f_d obeys the inverse cubic dependence on the reduced volume. The discrepancies for small volume between the full algebraic solution and the approximate one share the same origin as those discussed above for the detachment height. When the expression for f_d is combined with Eqs. (2) and (3), the remaining detachment variables emerge as functions of only the state parameters v and w:

$$\begin{aligned} R_d &\approx v^{-1/3}w^{-1}, \qquad L_d \approx 2(v^{1/3} - v)w, \\ \sigma_d &\approx \tfrac{1}{2}v^{2/3}w^2, \qquad p_d \approx -v^{1/3}w^2. \end{aligned} \tag{6}$$

Closer inspection reveals that the obtained detachment pressure and tension satisfy the Laplace equation.

Summarizing perspective.—Applying a pointlike force to a strongly bound vesicle leads to tether formation for a range of forces intermediate between the onset and detachment values. These two critical forces are uniquely determined by the experimentally relevant variables, w and v. Together with good estimates of the tether length and radius, this model should provide an experimentally useful tool to quantitatively probe the adhesion strength by monitoring the geometrical properties of the tether.

An important future ramification of this model will allow for discrete binding sites. In this case, the effective strength of adhesion may vary during a force load, due to the exchange of mobile receptors between the bound and free parts of the membrane. Therefore, during the detachment process, the plain applicability of the current results is not obvious. However, at the very least, average adhesion strengths, for both the onset and detachment points, should be obtainable from the presented model.

The conclusions outlined herein arise because of the competition between adhesion and tether formation. As such, a similar treatment should be applicable to arbitrary tether positions. In this way, the stability of lipid nanotube-vesicle networks [13] could well be understood following the reasoning presented in this Letter.

This work has been supported by Deutsche Forschungsgesellschaft through SFB 563. A.- S. S. gratefully acknowledges the Department of Applied Mathematics at the ANU, Canberra, Australia, for hospitality.

[1] L. Bo and R. E. Waugh, Biophys. J. **55**, 509 (1989); R. E. Waugh and R. M. Hochmuth, Biophys. J. **52**, 391 (1987); V. Heinrich and R. E. Waugh, Ann. Biomed. Eng. **24**, 595 (1996).
[2] V. Heinrich *et al.*, Biophys. J. **76**, 2056 (1999).
[3] O. Rossier *et al.*, Langmuir **19**, 575 (2003).
[4] E. Evans and A. Yeung, Chem. Phys. Lipids **73**, 39 (1994).
[5] D.V. Zhelev and R. M. Hochmuth, Biophys. J. **68**, 2004 (1995); R. M. Hochmuth and W. D. Marcus, Biophys. J. **82**, 2964 (2002).
[6] A. Roux *et al.*, Proc. Natl. Acad. Sci. U.S.A. **99**, 5394 (2002).
[7] H. J. Deuling and W. Helfrich, Blood Cells **3**, 713 (1977); Z.-C. Ou-Yang and W. Helfrich, Phys. Rev. A **39**, 5280 (1989).
[8] D. J. Bukman, J. H. Yao, and M. Wortis, Phys. Rev. E **54**, 5463 (1996).
[9] B. Božič *et al.*, Biophys. J. **61**, 963 (1992); B. Božič, S. Svetina, and B. Žekš, Phys. Rev. E **55**, 5834 (1997).
[10] T. R. Powers, G. Huber, and R. E. Goldstein, Phys. Rev. E **65**, 041901 (2002).
[11] I. Derényi , F. Jülicher, and J. Prost, Phys. Rev. Lett. **88**, 238101 (2002).
[12] N. Maeda, T. J. Senden, and J.-M. di Meglio, Biochim. Biophys. Acta **1564**, 165 (2002).
[13] M. Karlsson *et al.*, Proc. Natl. Acad. Sci. U.S.A. **99**, 11573 (2002).
[14] U. Seifert and R. Lipowsky, Phys. Rev. A **42**, 4768 (1990).
[15] A.-S. Smith, E. Sackmann, and U. Seifert, Europhys. Lett. **64**, 281 (2003).

C.2 Methodology

The letter style of the publication presented in the previous section produced a very short description of the calculations presented therein. For this reason and for the sake of anybody trying to reproduce the results, several further steps in the methodology shall be presented.

In Figure C.1 the parameterization of the vesicle used for the construction of the free energy (Eq. (1)) of the publication is shown. In addition, the pressure and the tension in the vesicle (not shown in Figure C.1) are denoted as p and σ, respectively.

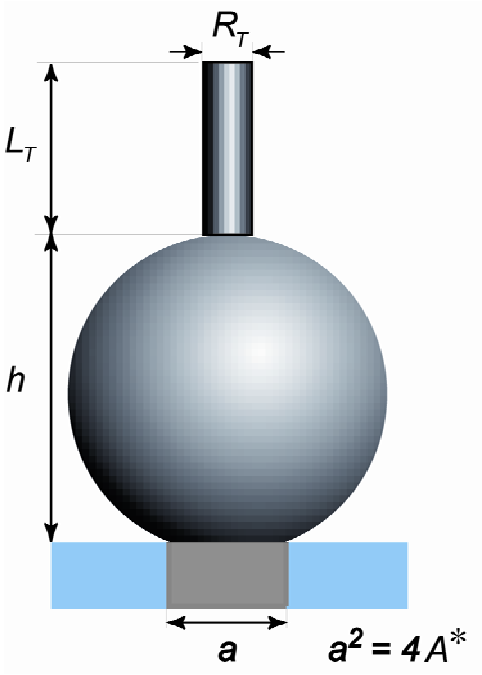

Fig. C.1: The parameterization of the tethered vesicle as used in the presented publication.

The presented variables are scaled by the radius of a sphere with the equivalent area. The free energy is given in the reduced units of $\pi\kappa$. The units for other parameters are given in the paper.

C.2.1 The detachment process

The free energy presented in Eq. (1) of the publication, in reduced units, can be written as:

$$F = \frac{L}{R} - f\left(L+h\right) - wA^* + p\left(\frac{A^*h}{2} + \frac{h^3}{6} + LR^2\right) + \sigma\left(2A^* + h^2 + LR\right). \qquad \text{(C.1)}$$

Minimization of the free energy C.1 results in a set of Euler Lagrange equations:

$$\frac{\partial F}{\partial A^*} = 0 \rightarrow \frac{hp}{2} + 2\sigma = w, \qquad \text{(C.2)}$$

$$\frac{\partial F}{\partial h} = 0 \rightarrow A^*p + h\left(hp + 4\sigma\right) = 2f, \qquad \text{(C.3)}$$

$$\frac{\partial F}{\partial L} = 0 \rightarrow \frac{1}{R} + 2\sigma R + pR^2 = f, \qquad \text{(C.4)}$$

$$\frac{\partial F}{\partial R} = 0 \rightarrow -\frac{1}{R} + 2\sigma R + 2pR^2 = 0. \qquad \text{(C.5)}$$

Equations (C.1-C.5) have to be solved together with the constraints on the area and volume:

$$\textit{area}: \qquad \frac{A^*}{2} + \frac{h^2}{4} + \frac{LR}{2} = 1 \qquad \text{(C.6)}$$

$$\textit{volume}: \quad \frac{1}{8}\left(3A^*h + h^3 + 6LR^2\right) = v, \qquad \text{(C.7)}$$

It is relatively simple to obtain solutions of the set of equations given by Eqs. (C.1-C.6), and write them as a function of the force and the tether radius:

$$p = \frac{fR - 2}{R^3}, \qquad \text{(C.8)}$$

$$\sigma = \frac{2fR - 3}{2R^2}, \tag{C.9}$$

$$h = \frac{2R\left(3 - 2fR + R^2 w\right)}{fR - 2}, \tag{C.10}$$

$$A^* = \frac{2R^3\left[f^2 R + 2Rw\left(3 + R^2 w\right) - 2f\left(1 + 2R^2 w\right)\right]}{\left(fR - 2\right)^2}, \tag{C.11}$$

$$L = \frac{2}{R}\frac{4 - 9R^2 + 2fR\left(5R^2 - 2\right) + f^2\left(R^2 - 3R^4\right) + w^2 R^6}{\left(fR - 2\right)^2}. \tag{C.12}$$

Substitution of Eqs. (C.8-C.12) into Eq. (C.7) produces the final equation that should be solved in order to find a relation between R and f. However, in this manner a double entangled cubic equation is obtained. By the use of an appropriate mathematical software package (such as Mathematica 4), three analytic solutions for $f(R)$ are obtained. Only one is physically relevant, but, due to its length will not be presented here. The leading term of this solution can be extracted:

$$R \approx \frac{2}{f}. \tag{C.13}$$

Incorporation of Eq. (C.13) into Eq. (C.9) produces Eq. (3) from the publication:

$$\sigma \approx \frac{f^2}{8}. \tag{C.14}$$

In order to obtain $R(f)$, which was the principle objective, this solution must be inverted. This can only be done *a posteriori*. However, solutions for the set of equations (Eqs. C.2-C.7) can be obtained numerically for a choice of f, w, and v. Such a procedure will give rise to a number of solutions, out of which only physically relevant ones should be extracted. Usually two such solutions, characterized by a thin tether and wide tether, respectively, are found. The solution with the thin tether has the lower free energy and is associated with the thermodynamic equilibrium.

The development of the approximate solution for the tether length given by Eq.(2) in the publication and again by Eq. (C.29) will be shown in Section C.2.3.

C.2.2 Determination of the onset shape

The task of this section is to calculate the critical force necessary to overcome the adhesive potential and induce the onset of the tether. In this case R=L=0 which simplifies the free energy from Eq. (C.1) to the following form:

$$F = -fh_o - A_o^* w + p_o\left(\frac{A_o^* h_o}{2} + \frac{h_o^3}{6}\right) + \left(2A_o^* + h_o^2\right), \tag{C.15}$$

whereas the constraints can be written as:

$$\textit{area}: \qquad \frac{A_o^*}{2} + \frac{h_o^2}{4} = 1, \tag{C.16}$$

$$\textit{volume}: \qquad \frac{3A_o^* h_o}{8} + \frac{h_o^3}{8} = v. \tag{C.17}$$

The subscript o indicates the onset values of the parameters.

The constraints from Eqs. (C.16-C.17) are, as a matter of fact, a system of two equations with two unknown parameters: h_o and A_o*:

$$h_o = \frac{1 - \mathrm{i}\sqrt{3}}{\left(\sqrt{v^2 - 1} - v\right)^{\frac{1}{3}}} - \left(1 + \mathrm{i}\sqrt{3}\right)\left(\sqrt{v^2 - 1} - v\right)^{\frac{1}{3}}, \tag{C.18}$$

$$A_o^* = 2 - \frac{h_o^2}{2}. \tag{C.19}$$

The solution given by Eq. (C.18) belongs to the set of real numbers and is displayed on the right panel of Figure 5 in the publication with the short-dashed line.

The calculated height (Eq. (C.18)) and area (Eq. (C.19)) define the shape of the vesicle and are independent of the force. The obtained shape is a property of the reduced volume

and is the same as the shape in the absence of force. The signature of this effect is in the expressions for the area and volume constraints that are independent of the tension and the pressure in the vesicle.

Minimization of Eq. (C.15) with respect to the area and the height of the spherical cap results in analogies of Eqs. (C.2-C.3) for the onset. Keeping in mind that Eq. (C.14) provides an approximate solution for the tension, the onset analogies of Eqs. (C.2-C.3) can be solved exactly for the onset force and pressure:

$$f_o = \frac{2}{A_o^*}\left(\sqrt{h_o^2 + \left(A_o^{*2} + A_o^* h_o^2\right)w} - h_o\right), \tag{C.20}$$

$$p_o = \frac{4w - f_o^2}{2h_o}. \tag{C.21}$$

Substitution of Eq. (C.20) into Eq. (C.14) provides the approximate form for the onset tension in the vesicle.

$$\sigma_o \approx \frac{f_o^2}{8}. \tag{C.22}$$

Equations (C.18-C.22) are a complete set defining the vesicle shape and the conditions necessary for the onset of tether formation.

C.2.3 Determination of detachment conditions

In the following section the parameters and the conditions for the vesicle detachment will be derived. Parameters describing this situation will be indexed with *d*. The detachment shape of the spherical cap is associated with a vanishing contact zone. Henceforth:

$$A_d^* = 0. \tag{C.23}$$

Because the tether is typically very thin, the assumption that the volume of the vesicle is much larger than the volume of the tether can be made. As the detachment shape is

approached, the vesicle becomes a sphere of volume v, and h becomes the diameter of such a sphere. Therefore:

$$h_d \to 2v^{\frac{1}{3}} \tag{C.24}$$

The solution from Eq. (C.23) can be set equal to the one obtained for the detachment process Eq. (C.10). Similarly Eq. (C.24) is equal to Eq. (C.11). In this way, two equations are obtained from which the detachment force and radius of the tether can be extracted:

$$f_d \approx 2v^{\frac{1}{3}} w . \tag{C.25}$$

The solution for the tether radius is rather lengthy and is not presented. Moreover, at this stage, the radius of the tether is in excellent agreement with its approximate solution from Eq. (C.13), and thus one can confidently assume:

$$R_d \approx \frac{2}{f_d} = \frac{1}{v^{\frac{1}{3}} w} . \tag{C.26}$$

If Eqs.(C.23-C.24) are incorporated into the area constraints, one obtains a new expression that is valid at the detachment point:

$$area: \qquad \frac{h_d^2}{4} + \frac{L_d R_d}{2} = 1 . \tag{C.27}$$

Incorporating Eq. (C.24) and Eq. (C.26) into Eq.(C.27), results in the detachment value for the tether length:

$$L_d \approx 2\left(v^{\frac{1}{3}} - v \right) w . \tag{C.28}$$

It is now that an approximate relationship for the detachment process can be obtained:

$$L \approx L_d \frac{R_d}{R} \approx L_d R_d f \approx \left(1 - v^{\frac{2}{3}} \right) f . \tag{C.29}$$

The calculation for the detachment pressure is somewhat more delicate and requires setting the Eq. (C.23) equal to Eq. (C.10). After reorganizing and solving for f, an expression where f is a function of R is obtained. Expanding that solution around R=0, up to the linear term, results in:

$$f \approx \frac{2}{R} + Rw + O\left(R^2\right). \tag{C.30}$$

After combining Eq. (C.30) and Eq. (C.25), with Eq. (C.8), the detachment pressure emerges:

$$p_d \approx -v^{\frac{1}{3}} w^2 . \tag{C.31}$$

In case of the detachment Eqs. (C.23-C.26, C.28, C.31) provide a complete set of solutions which are only functions of the reduced volume and the adhesion strength. This set, together with the set of solutions for the onset of detachment were extensively probed for various system parameters are in excellent agreement with solutions from Eqs. (C.8-C.12).

281-287

Appendix D

7850 2003-9-12

EUROPHYSICS LETTERS 15 October 2003

Europhys. Lett., **64** (2), pp. 281(2003)

CONTINUOUS MODEL FOR UNBINDING: WEAK ADHESION

D.1 Effects of a pulling force on the shape of a bound vesicle

A.-S. SMITH[1], E. SACKMANN[1] and U. SEIFERT[2]

[1] *Technische Universität München, E22 Institut für Biophysik D-85748 Garching, Germany*

[2] *Universität Stuttgart, II. Institut für Theoretische Physik D-70550 Stuttgart, Germany*

(received 20 May 2003; accepted in final form 4 August 2003)

PACS. 87.16.Dg – Membranes, bilayers, and vesicles.

Abstract. – We develop a theoretical model to describe the vertical pulling of vesicles adhered in a contact potential. For a range of applied forces, locally stable bound shapes, separated from the free shape by an energy barrier, can be found. The phase diagram contains regions with either a unique bound shape or an additional meta-stable shape. Upon pulling, these shapes unbind discontinuously since the vesicles disengage from the substrate while still possessing a finite adhesion area.

Cell adhesion is regulated by a complex interplay of specific forces between receptor-ligand pairs, generic interfacial interactions and elastic stresses in the cell envelope [1,2]. In terms of elastic forces, the control of the adhesion strength is mediated by the coupling of the actin based cytoskeleton to the intracellular domains of the cell surface receptors, by means of specific coupling proteins [3]. Giant vesicles adhering to flat (functionalized) substrates are a proven simplified model for the systematic study of the effects of forces on adhesive properties. For example, the influence of shear forces on the shapes and behavior of weakly adhered vesicles has been investigated both experimentally [4,5], and theoretically [6,7]. Local forces inducing formation of tethers have been used to study the adherence of the cell membrane to the underlying cytoskeleton [8]. From the theoretical point of view, the stability of cylindrical vesicles under axial tension [9], the shapes of strained axially symmetric free vesicles [10,11] and force induced tether formation from a flat membrane, have been investigated [12,13].

In this paper, motivated by recent experiments in which the vesicle is initially adhered to a flat substrate and then pulled with vertical magnetic tweezers [14], we study the interplay between an externally exerted force and adhesion, applying weak to moderate adhesive potential strengths. The case of strong adhesion where tether formation can be expected will be discussed else where [15]. In our minimal model, vesicles adhered in contact potential are pulled, with a vertical point force, away from the surface. Equilibrium shapes of vesicles under force are therefore calculated by minimization of the free energy functional:

$$\mathcal{F} = \frac{\kappa}{2} \cdot \oint (C_1 + C_2)^2 \cdot dA + P \int dV + \Sigma \oint dA - WA^* - F \cdot [Z^0 - Z_0^0]. \qquad (1)$$

The first term is the local bending energy [16], which is a function of two principal curvatures (C_1 and C_2) and the bending rigidity κ. The next two terms in eq. (1) emerge from

constraints imposed in order to keep the total volume and total area of the vesicle constant. The fourth term in eq. (1) is the adhesion energy associated with a given contact potential of strength W, where $W > 0$, and is proportional to the area of the adhered surface A^* [17]. The last term represents the energy arising from the application of a point force to the north pole (Z^0) of the vesicle. This energy is a function of the displacement of the north pole from its position at zero force (Z_0^0), and the strength of the applied force ($F > 0$). In this mechanistic model entropic contributions from thermal fluctuations are not included.

For simplicity, we consider only those shapes $X(Z)$ with axial symmetry about the Z-axis. It is convenient to parameterize such shapes by the angle of the contour $\psi(s)$, where s is the arclength along the contour. In this case, eq. (1) can be rewritten as

$$\frac{\mathcal{F}}{2\pi} = \int_0^{s^*} \mathrm{d}s \cdot \left\{ \frac{X}{2}\left(\dot{\psi} + \frac{\sin\psi}{X}\right)^2 + \gamma \cdot \left(\dot{X} - \cos\psi\right) + \chi \cdot \left(\dot{Z} + \sin\psi\right) + \right.$$
$$\left. + p \cdot \frac{X^2}{2} \cdot \sin\psi + \sigma \cdot X \right\} + (\sigma - w) \cdot \frac{{X^*}^2}{2} - f \cdot \left[Z^0 - Z_0^0\right]. \qquad (2)$$

The integration runs from the north pole of the vesicle ($s = 0$), to the point of contact between the vesicle and the substrate ($s = s^*$). The two terms involving the Lagrange multipliers $\gamma(s)$ and $\chi(s)$ are introduced to account for the geometrical dependence of ψ on X and Z, respectively. The reduced variables, v, p, s, w, and f are defined as $v = 3V/(4\pi R^3)$, $p = PR^3/\kappa$, $\sigma = \Sigma R^2/\kappa$, $w = WR^2/\kappa$, and $f = FR/(2\pi\kappa)$, with $A = 4\pi R^2$ and $R = 1$.

The "*Euler-Lagrange*" equations (and the appropriate boundary conditions) corresponding to eq. (2) are derived in a manner analogous to that in ref. [18]. In order to solve the resulting set of differential equations, the behavior of the contour in the vicinity of the symmetry axis requires attention. In a manner similar to that previously employed [10], the general shape equation is calculated [19] and solved in the limit of $s \to 0$ and $X \to 0$. The solution for the contour angle, in this limit, can then be written as

$$\psi = -f \cdot X \cdot \ln X + U^0 \cdot X + \frac{\sigma}{3} \cdot X^2. \qquad (3)$$

Here U^0 denotes the value of the principal curvature ($U = \dot{\psi}$) at the north pole in the absence of applied force. From eq. (3), it is apparent that the contour of the vesicle is smooth at the pole ($\psi(0) = 0$), but that the principal curvature is singular for $s = 0$. An asymptotic solution is therefore required in this region.

Computations are generally performed in the "f ensemble" by increasing the force from $f = 0$. The shape can alternatively be obtained from calculations in the "Z ensemble". In this case, the displacement $[Z^0 - Z_0^0]$ is imposed and the force is calculated as a Lagrange multiplier to meet this deformation. Regardless of whether the calculation is performed in the "f" or the "Z ensemble", the same free energy functional has to be solved. A unique solution (shape) is associated with a particular set of v, w, and f (or Z^0), and has a certain total energy. However, the definition of the total energy belonging to a particular shape depends on the design of the problem (or experiment). In the "f" ensemble, the total energy ($E(f)$) is comprised of the adhesion energy, the bending energy and the energy due to the imposition of the force. Alternatively, in the "Z" ensemble, the total energy ($E(Z^0)$) is composed of only the bending and adhesion energies. As the force is generally the control parameter under experimental conditions, we choose to present our data as a function of this variable.

The solutions of the previously described procedure are first found in the absence of an applied force. Evidently, solutions for vesicle adhesion in three dimensions [17] are reproduced,

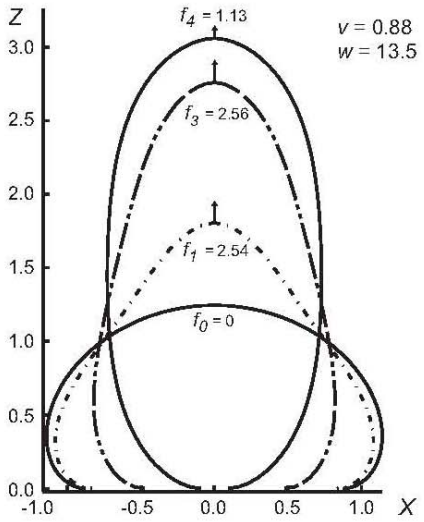

Fig. 1 – The shapes of the vesicle with reduced volume $v = 0.88$, adhered in the potential of a strength $w = 13.5$. The full contour (f_0) denotes the shape in the absence of force. The short-dashed contour is calculated at $f = f_1$ where the unbinding transition occurs. The long-dashed shape (f_3) is an example of a meta-stable solution. The shape f_4 is the unstable solution at the saddle point corresponding to the barrier for the detachment process at f_4.

and an example of such a shape is presented in fig. 1 (at $f_0 = 0$). Generally, for a given v, there exists a range of w where stationary solutions corresponding to adhered vesicles are the global minima in the free-energy landscape. At zero force, the free vesicle is also a locally stable solution. However, at any non-zero force in the "f ensemble", the free shape (infinitely distant from the substrate) is the global minimum, so that any bound shape is only locally stable. The application of an external force to the bound vesicle should eventually remove it from the bound state and bring it to the free shape through a detachment process. Indeed, we have found that for every v and w investigated, there exists a range of forces larger than zero where stationary stable solutions of a deformed bound vesicle can be found. These shapes are separated from the corresponding free shape by an energy barrier. Surprisingly, for very weak forces, the adhering part of the vesicle is found to be slightly larger than the adhesion plate in the absence of the applied force. This remains true up until a particular value of the force is reached ($f_{\rm on}$, *vide infra*). Further increase of the force is followed by a reduction of the adhesion plate. Nevertheless, there is a maximum force (generally denoted as f_1) that can be applied to the vesicle before the bound shape loses its local stability and detaches from the surface (*e.g.*, short dashed curve in fig. 1). Interestingly, for this value of the force the vesicle is still in possession of a finite adhesion area. In this sense, the force-induced unbinding is a discontinuous transition since the adhesion area switches from a finite value to zero at $f = f_1$.

The total energy of the stationary bound states is shown in fig. 2 for several reduced volumes and adhesion strengths. Two regimes can be observed with respect to the reduced volume of the vesicle. In the case of a reduced volume close to that of a sphere ($v = 0.99$), starting from the adhered vesicle (with $f = 0$), the total energy increases slowly in response to the increasing force until the detachment force $f = f_1$ is achieved. For this value of the force, the curves exhibit a perpendicular tangent, corresponding to the loss of the locally stable

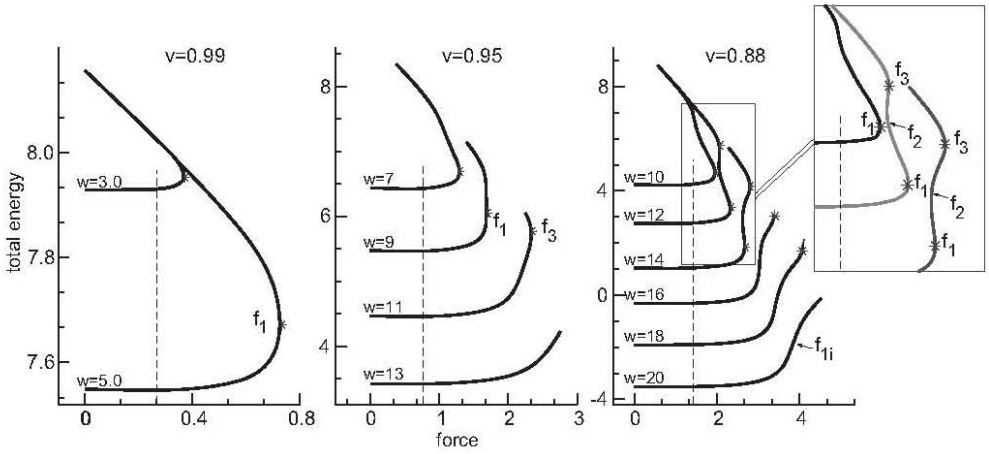

Fig. 2 – The total energy (in units of $2\pi\kappa$) of vesicles as a function of force (in units of $2\pi \cdot R/\kappa$) for $v = 0.99$ on the left, $v = 0.95$ in the middle, and $v = 0.88$ on the right, for different adhesion strengths. The stars indicate the detachment point(s) on each curve. The short-dashed line indicates the position of $f = f_{\rm on}$.

solution and concomitant detachment of the vesicle from the surface.

For forces smaller than f_1, two solutions in the total energy plot can be observed for a single force. Since the solutions of the above variational procedure correspond either to a minimum or a saddle point of the free energy functional ($\mathcal{F}$), the solution of the lower energy should be associated with the locally stable shape. The solution of higher energy then belongs to an unstable saddle point of the phase space. The difference in these energies, at a given force, thus represents the height of the aforementioned barrier between the distorted adhered shape and the free vesicle. Locally stable points form a branch (denoted as stable) that ends at $f = f_1$. Here the height of a barrier is equal to zero and a first-order unbinding transition occurs. The unstable branch originating from this point constitutes of the set of saddle solutions, and smoothly extends the stable branch. For volumes close to the sphere, this branch is monotonic until its end is reached in a shape with a single pinning point (*e.g.*, the shape calculated for $f = f_4$ in fig. 1).

For more deflated vesicles (*e.g.*, $v = 0.88$ in fig. 2), the energy diagram has more structure. In this regime of reduced volumes, three critical values of adhesion strength arise (w_1, w_2 and w_3). While $w < w_1$ (*e.g.*, $w = 10$ in the inset of fig. 2) the situation resembles the almost spherical case discussed above. That is, for $f < f_1$, there are two solutions for every force and a single unbinding transition at $f = f_1$. At $w = w_1$, two additional perpendicular tangents f_2 and f_3 appear in the $E(f)$ plot (as in, *e.g.*, $w = 12$). This is summarized in the phase diagram fig. 3, where characteristic forces (f_1, f_2 and f_3) are plotted as a function of adhesion strength.

In the region $w_1 \leq w < w_2$, $f_2 < f_3 < f_1$ holds true. While $f < f_2$, there are still only two stationary solutions and the barrier height is given by the difference in their energies. In the interval $f_2 < f < f_3$, however, there are four stationary solutions of the free energy functional for a given force. The solution of the lowest energy belongs to the previously defined locally stable branch. The second lowest-energy solution is unstable, and the barrier height for the detachment to the free vesicle is given by the difference in energies between these two solutions. The third solution is again locally stable, but of higher energy and therefore denoted as locally meta-stable. The barrier to the free shape for this minimum is given by the difference in energies between the meta-stable solution and the solution belonging to the

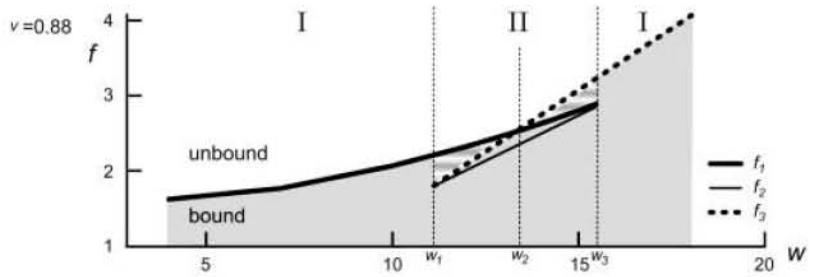

Fig. 3 – Phase diagram with unbinding transitions for $v = 0.88$. For this volume $w_1 \approx 11.5$, $w_2 \approx 13$ and $w_3 \approx 15.5$. The detachment force increases as a linear function of the adhesion strength, with the exception of small w. Roman numerals indicate the number of unbinding transitions in a particular region. The regions shaded in grey contain bound states whereas in the white region no bound states can occur. For a vesicle of radius 10 μm and bending modulus $\kappa = 10^{-19}$ J, one unit of a dimensionless force f corresponds to 0.25 pN, and one unit of the adhesion strength w equals 10^{-7} Jm^{-2}.

higher-energy unstable branch (the fourth and highest-energy stationary solution). As both the locally stable and locally meta-stable branches end in a perpendicular tangent (at f_1 and f_3, respectively), there are two first-order unbinding transitions for a single adhesion strength under these conditions. It should be possible to traverse both the locally stable and locally meta-stable branches through an adiabatic process, such as a force load. However, the locally meta-stable branch should only be observable if a vesicle were to be submitted to excitations such as a step force, since it cannot be reached continuously starting at $f = 0$. For forces $f_3 < f < f_1$, there are once again only two extrema in the energy diagram. These are the stable minimum and the saddle point toward the free shape.

In the region $w_2 < w < w_3$, $f_2 < f_1 < f_3$ (as, *e.g.*, $w = 14$ in the inset of fig. 2). While $f \leq f_1$, the above phase space description continues to apply. However, beyond f_1, additional locally stable solutions arise from the meta-stable branch. That is, the initial locally stable branch ends at f_1, with detachment of the vesicle. This detachment should be the only one observable in adiabatic processes. However, for forces beyond f_1 part of the locally meta-stable branch becomes the lowest energy (and only locally stable) solution for a bound vesicle. This second locally stable branch ends in a perpendicular tangent at f_3 implying the existence of an additional first-order unbinding transition. As discussed above, this transition should only be accessible through excitation processes of the vesicle.

At $w = w_3$, f_2 and f_1 merge so that f_3 becomes the only point in the energy plot associated with a perpendicular tangent and an unbinding from the surface (as, *e.g.*, $w = 16$). For adhesion strengths $w \geq w_3$, the stable branch is continuous and for forces $f < f_3$ there are only two solutions, a minimum and the saddle point to the free shape. In this region of adhesion strengths f_1 becomes an inflection point in the stable branch and is denoted as f_{1i} in fig. 2.

The two regimes of reduced volume (almost spherical or deflated) are separated by a critical volume ($v_c \approx 0.95$, see fig. 2). For reduced volumes slightly lower than v_c, the three critical values of adhesion strength (w_1, w_2 and w_3) start to appear, but the separation between them is initially very small. As the reduced volume continues to decrease (to $v = 0.88$ and beyond), the separation of the critical adhesion strengths increases. This implies that for low values of the reduced volume, the region of adhesion strengths in which there are multiple solutions ($w_1 \leq w \leq w_3$), and hence two first-order unbinding transitions, becomes quite sizeable.

There are several further aspects associated with the vesicle shapes that warrant further discussion. Most significant is the behavior of the adhesion area which is presented as a

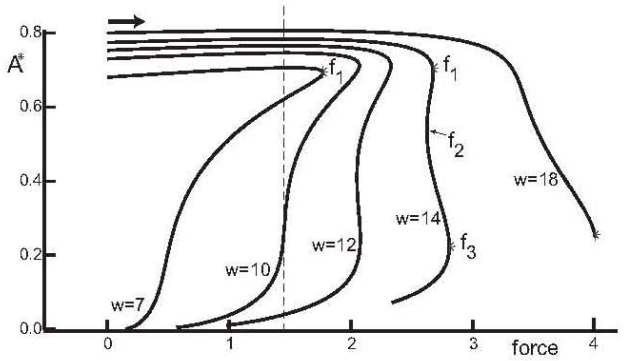

Fig. 4 – The adhesion area of the vesicle with reduced volume $v = 0.88$, as a function of the force for different adhesion strengths. The short-dashed line denotes $f = f_{\rm on}$.

function of force in fig. 4. The adhesion area changes only slightly until the first perpendicular tangent (associated with f_1) is reached. Closer inspection reveals a very broad maximum at $f = f_{\rm on}$ ($0 < f_{\rm on} < f_1$), which, from the point of view of the adhesion area, marks the onset of the detachment of the vesicle. Interestingly, for a given volume, the position of this maximum, which also corresponds to the minimum in the adhesion energy, is independent of w. For forces smaller than $f_{\rm on}$, the equilibrium shape at low force actually has an adhesion area larger than it does at $f = 0$. Indications of such growth have recently also been experimentally observed [20]. When $f = f_{\rm on}$, the adhesion plate reaches its maximum size $A^*_{\rm on}$. For $f > f_{\rm on}$, partial loss of the adhesion plate ($A^* < A^*_{\rm on}$) can be observed until the force reaches its critical "detachment" value. Considerable loss of the adhesion area appears after passing through f_1 or f_{1i}, as appropriate for the particular adhesion strength. For $w < w_3$, the loss of adhesion plate arises mainly in the locally stable branch of higher energy and the unstable branches. For these w, locally stable shapes with less than 30% of the original adhesion area can be found such as the contour f_3 in fig. 1. However, when $w > w_3$, adiabatically accessible locally stable bound shapes with widely varying adhesion areas can be found beyond $f = f_{1i}$.

The height of the vesicle shows a force dependence similar to that of the adhesion area. Figure 5 shows the force as a function of the absolute height ($f(Z^0)$) of the vesicle (for $v = 0.88$). There is one point in fig. 5 where all of the curves intersect (within numerical accuracy). Consequently, there is a single force, which happens to be $f_{\rm on}$, where all vesicles have identical height (denoted as $Z^0_{\rm on}$), irrespective of the value w.

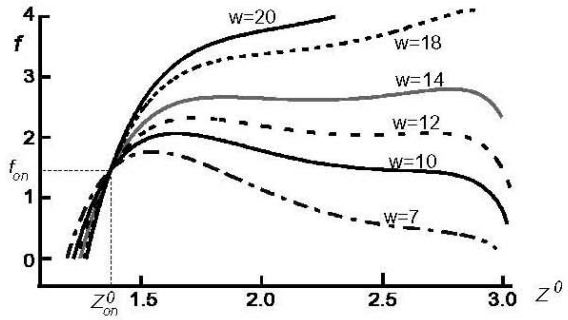

Fig. 5 – The typical dependency of the force on the absolute height of the vesicle. Data presented are for the reduced volume $v = 0.88$. The height of $Z^0_{\rm on} = 1.37$ is obtained with the force of $f_{\rm on} = 1.42$.

In conclusion, we have implemented a simple model for the pulling of adhered vesicles that leads to variety of scenarios for the detachment process. Naturally, these scenarios depend on the particular values of the reduced volume. However, for most volumes relevant to studies of adhesion, four distinct regimes of the detachment process are found as a function of the adhesion strength. For very small adhesion strengths, one detachment force is determined. At this force, the vesicle detaches (in an adiabatic process) with adhesion area very similar to the area in the absence of force. Increasing adhesion strength leads to a regime where an additional meta-stable detachment force appears. In contrast to the locally stable shapes, which should be observable in any pulling experiment, the meta-stable shapes should only be accessible following excitation of the vesicle (possibly by relaxation of the vesicle after the application of a step force). However, it is only for the meta-stable solutions that considerable loss of the adhesion plate occurs. Further strengthening of the adhesion potential is followed by the return to the regime of a single unbinding transition at the end of the locally stable branch. Detachment continues to occur with a finite adhesion area. Moreover, shapes with considerably reduced adhesion plates should be, in this regime, observable independently of the experimental design. In the limit of very strong adhesion ($w > \kappa^2/R$), the shape of a non-pulled vesicle is a spherical cap with height larger than $Z_{\rm on}^0$. For such w, tether formation should be expected to precede the detachment process, which will be studied in future work.

* * *

This work has been supported by Deutsche Forschungsgesellschaft through SFB 563.

REFERENCES

[1] BELL G. I., *Science*, **200** (1978) 618.
[2] EVANS E. A., *Biophys. J.*, **48** (1985) 175; **48** (1985) 185.
[3] SIMSON R., WALRAFF E., GERISCH G. and SACKMANN E., *Biophys. J.*, **74** (1998) 514; SACKMANN E. and BRUINSMA R., *Chem. Phys. Chem.*, **3** (2002) 509.
[4] LORZ B. *et al.*, *Europhys. Lett.*, **51** (2000) 468.
[5] ABKARIAN M., LARTIGUE C. and VIALLAT A., *Phys. Rev. Lett.*, **88** (2002) 068103.
[6] CANTAT I. and MISBAH C., *Phys. Rev. Lett.*, **83** (1999) 880.
[7] SUKUMARAN S. and SEIFERT U., *Phys. Rev. E*, **64** (2001) 011916.
[8] HOCHMUTH R. M. and MARCUS W. D., *Biophys. J.*, **82** (2002) 2964.
[9] BUKMAN D. J., YAO J. H. and WORTIS M., *Phys. Rev. E*, **54** (1996) 5463.
[10] BOŽIČ B., SVETINA S. and ŽEKŠ B., *Phys. Rev. E*, **55** (1997) 5834.
[11] HEINRCH V., BOŽIČ B., SVETINA S. and ŽEKŠ B., *Biophys. J.*, **76** (1999) 2056.
[12] POWERS T. R., HUBER G. and GOLDSTEIN R. E., *Phys. Rev. E*, **65** (2002) 041901.
[13] DERÉNYI I., JÜLICHER F. and PROST J., *Phys. Rev. Lett.*, **88** (2002) 238101.
[14] GUTTENBERG Z. *et al.*, *Langmuir*, **16** (2000) 8984.
[15] SMITH A.-S., SACKMANN E. and SEIFERT U., in preparation.
[16] HELFRICH W., *Z. Naturforsch. C*, **28** (1973) 693.
[17] SEIFERT U. and LIPOWSKY R., *Phys. Rev. A*, **42** (1990) 4768.
[18] SEIFERT U., BERNDL K. and LIPOWSKY R., *Phys. Rev. A*, **44** (1991) 1182.
[19] JÜLICHER F. and SEIFERT U., *Phys. Rev. E*, **49** (1994) 4728.
[20] GOENNENWEINE S. (private comunication).

D.2 Methodology

The object of this section is to present the development of the model in more detail than that shown in the publication presented in the previous section. The task is the development of a simple model for the pulling of adhered vesicles, with a point force, away from the adhesion surface. The shape of the vesicle is expressed as a function of the arclength s (along the contour), the azimuthal angle ϕ, and the tilt angle $\psi(s)$ (see Figure D.1).

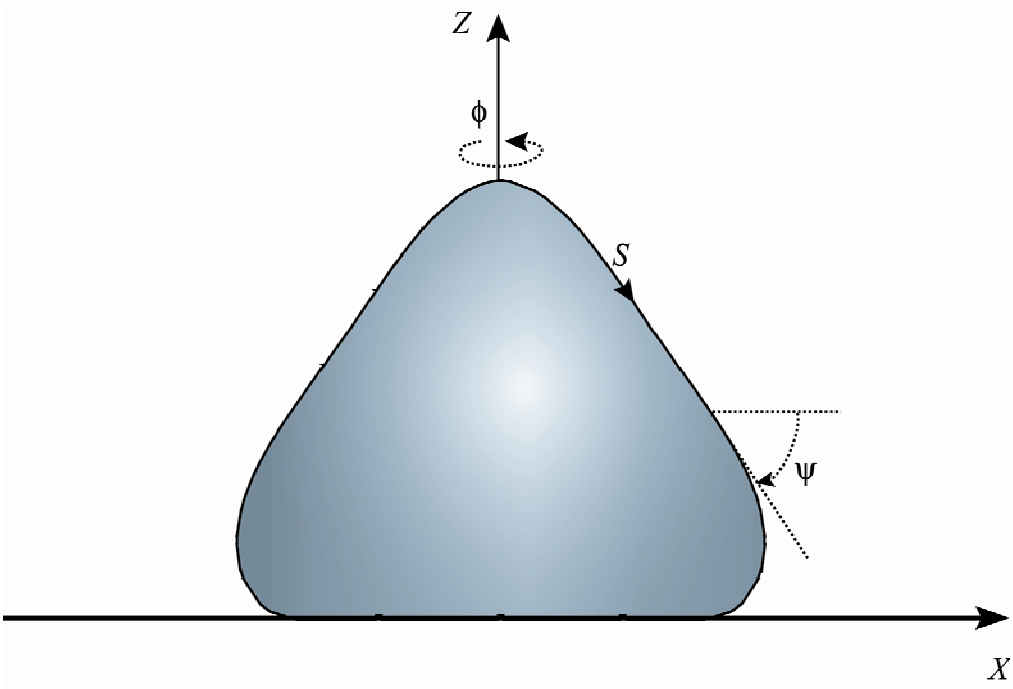

Figure D.1: The coordinate system

This parameterization is used to avoid singularities in the alternative $Z(X)$ representation. Furthermore, the coordinates Z and X which are parallel and perpendicular to the axis of symmetry, respectively, are geometrically related to s and ψ through:

$$\dot{X} = \cos\psi \,, \tag{D.1}$$

$$\dot{Z} = -\sin\psi \,. \tag{D.2}$$

The dot here denotes a derivative with respect to s. If the principal curvatures are written as:

$$C_1 = \dot{\psi}, \tag{D.3}$$

$$C_2 = \frac{\sin\psi}{X}, \tag{D.4}$$

the free energy from Eq. (2) in the publication is obtained. The energy is given in units of ($2\pi\kappa/R$), where R is the radius of a sphere of equivalent area:

$$F = \int_0^{s^*} ds \left[\frac{X}{2}\left(\dot{\psi} + \frac{\sin\psi}{X}\right)^2 + p\frac{X^2}{2}\sin\psi + \sigma\left(X + \frac{X^{*2}}{2}\right) \right.$$
$$\left. - w\frac{X^{*2}}{2} - f\left(Z^0 - Z(0)\right) + \gamma(\dot{X} - \cos\psi) + \chi(\dot{Z} + \sin\psi) \right] \tag{D.5}$$

The integration runs from the north pole (s = 0), to the contact point (s = s*). In Eq. (D.5), two additional Lagrange multipliers ($\gamma(s)$ and $\chi(s)$) are required to account for the fact that X and Z are not independent coordinates, but are subject to the restrictions outlined in Eq. (D.1) and Eq.(D.2), respectively.

Due to the fact that F contains terms which are functions at the boundaries, it may be written in the form:

$$F = \int_{x=d}^{x=u} dx \left[f\left(y_1,....,y_n,\dot{y}_1,...,\dot{y}_n\right) + \sum_{i=1,n} g\left(y_i(u)\right) + \sum_{i=1,n} h\left(y_i(d)\right) \right]. \tag{D.6}$$

without loss of generality. Here u and d denote the upper and lower boundaries of integration, respectively. Comparing Eq. (D.5) and Eq. (D.6), it is obvious that:

$$g\left(X(s^*)\right) = (\sigma - w)\frac{X^{*2}}{2}, \tag{D.7}$$

$$h\left(Z(0)\right) = -f\left(Z(0) - Z_0\right), \tag{D.8}$$

The first variation of Eq. (D.6) leads to a set of Euler-Lagrange equations (*L.E.*) which, with additional contributions, reaches the form:

$$V_1 = \sum_i \left(\left[\frac{\partial f}{\partial \dot{y}_i} \right]_{x=u} \partial y_i(u) - \left[\frac{\partial f}{\partial \dot{y}_i} \right]_{x=d} \partial y_i(d) + \left[\frac{\partial g_i(y_i)}{\partial y_i} \right]_{x=u} \partial y_i(u) + \right.$$

$$\left. + \left[\frac{\partial h_i(y_i)}{\partial y_i} \right]_{x=d} \partial y_i(d) \right) + \int_d^u L.E.dx \qquad \text{(D.9)}$$

Application of this variation to Eq. (D.5) gives:

$$V_1 = \left[X^* \left(\dot{\psi}^* \right) \partial \psi^* - X^0 \left(\dot{\psi}^0 \right) \partial \psi^0 \right] + \left[\gamma^* \partial X^* - \gamma^0 \partial X^0 \right] + \left[\chi^* \partial Z^* - \chi^0 \partial Z^0 \right] +$$

$$(\sigma - w) X^* \partial X^* - f \partial Z^0 + \int_0^{s^*} L.E.ds \qquad \text{(D.10)}$$

The Euler-Lagrange equations, together with Eq. (D.1) and Eq. (D.2), form a set of nonlinear ordinary differential equations:

$$\dot{\psi} = U \,, \qquad \text{(D.10)}$$

$$\dot{U} = -U \frac{\cos\psi}{X} + \frac{pX}{2} \cos\psi + \frac{\gamma}{X} \sin\psi + \frac{\chi}{X} \cos\psi + \frac{\sin\psi \cos\psi}{X^2} \,, \qquad \text{(D.11)}$$

$$\dot{\gamma} = \frac{U^2}{2} - \frac{\sin^2\psi}{2X^2} + \sigma + pX \sin\psi \,, \qquad \text{(D.12)}$$

$$\dot{\chi} = 0 \,, \qquad \text{(D.13)}$$

$$\dot{X} = \cos\psi \,, \qquad \text{(D.14)}$$

$$\dot{Z} = -\sin\psi \,, \qquad \text{(D.15)}$$

It is this set of equations that has to be solved to determine the shape of the vesicle.

The natural boundary conditions that arise from the model are:

$$X^0 = 0\,, \tag{D.15}$$

$$\psi^0 = 0\,, \tag{D.16}$$

$$\psi^* = \pi\,, \tag{D.17}$$

$$Z^* = 0\,. \tag{D.18}$$

The contact angle (ψ^*) obeys Eq. (D.17), since any other angle would imply an infinite curvature.

To obtain the total variation of F, the second variation (variation of the boundaries):

$$V_2 = \sum_i \left\{ \left([f]_{x=u} + \left[\frac{\partial g_i(y_i)}{\partial y_i} \right]_{x=u} \dot{y_i}(u) \right) \partial x(u) + \left([f]_{x=d} + \left[\frac{\partial h_i(y_i)}{\partial y_i} \right]_{x=d} \dot{y_i}(d) \right) \partial x(d) \right\} \tag{D.19}$$

has to be considered. In terms of the current model, after taking into account Eqs. (D.15-D.18), the variation of the boundaries gives:

$$V_2 = \left[\frac{X^*}{2} \left(\dot{\psi}^* \right)^2 - \sigma X^* + (\sigma - w) X^* (\dot{X}^*) \right] \partial s^* - f(\dot{Z}^0) \partial s^0\,. \tag{D.20}$$

The necessary condition for an extremum requires the total variation to be zero:

$$V_T = V_1 + V_2\,. \tag{D.21}$$

The natural boundary conditions given in Eqs. (D.15-D.18) act as the constraints of the first variation for the second variation. In general, if $y_i(b)$=constant, where b denotes the upper or lower boundary, then:

$$\partial y_i(b) = -\dot{y_i}(b)\, \partial x(b)\,. \tag{D.22}$$

Specifically:

$$\partial X^0 = -\partial s^0, \tag{D.23}$$

$$\partial \psi^0 = -\dot{\psi}^0 \partial s^0, \tag{D.24}$$

$$\partial \psi^* = -\dot{\psi}^* \partial s^*, \tag{D.25}$$

$$\partial Z^* = 0. \tag{D.26}$$

Equation (D.23) is a consequence of the auxiliary condition:

$$\dot{X}^0 = \cos 0 = 1. \tag{D.27}$$

Similarly, Eq. (D.26) follows from:

$$\dot{Z}^* = -\sin \pi = 0. \tag{D.28}$$

Substituting Eqs. (D.23-D.26) into the result of the first variation Eq. (D.10), and ensuring that the total variation Eq. (D.20) is zero, one finally obtains:

$$V_T = \left(\frac{\left(\dot{\psi}^*\right)^2}{2} + w - \left(\dot{\psi}^*\right)^2 \right) X^* \cdot \partial s^* + \left(\gamma^* + (\sigma - w) X^* \right) \cdot \partial X^* + \gamma^0 \cdot \partial s^0 + \left(\chi^0 + f \right) \cdot \partial Z^0. \tag{D.29}$$

By inspection, the new boundary conditions can be written:

$$\dot{\psi}^* = U^* = \sqrt{2w}, \tag{D.30}$$

$$\gamma^* = -(\sigma - w) X^*, \tag{D.31}$$

$$\gamma^0 = 0, \tag{D.32}$$

$$\chi^0 = -f\,. \tag{D.33}$$

With the condition from Eq. (D.33), it is trivial to integrate directly the Euler-Lagrange equation Eq.(D.13) for the Lagrange multiplier $\chi(s)$. This can be then used in Eq. (D.11).

It is important to note that, since F does not explicitly depend on s, the "Hamilton function":

$$h = -f + \sum_i \frac{\partial f}{\partial \dot{y}_i}\dot{y}_i$$

$$= \frac{X}{2}\left[\left(\dot{\psi}\right)^2 - \left(\frac{\sin\psi}{X}\right)^2\right] - p\frac{X^2}{2}\sin\psi - \sigma X + \gamma\sin\psi - \chi\cos\psi\,, \tag{D.34}$$

is conserved. Particularly:

$$h^0 = h^*\,. \tag{D.35}$$

Combining Eq. (D.34) and Eq. (D.35) with Eq. (D.30) and the natural boundary conditions given by Eqs. (D.15-D.18), one obtains:

$$\gamma^0 = \gamma^* + (\sigma - w)X^*\,. \tag{D.36}$$

This leads to the conclusion that the boundary conditions Eq. (D.31) and Eq. (D.32) are equivalent, and therefore only one of them must be used to solve the set of differential equations. The other boundary condition is thus a conserved quantity, and does not have to be imposed but will be calculated automatically.

It is often convenient to work directly in the V and A ensembles. In these circumstances, two equations, constraining the total area and volume should be added to the set of Euler-Lagrange equations. In units of $2\pi R$, the constraints are:

$$\textit{volume}:\ \dot{v} = \frac{X^2}{2}\sin\psi\,, \tag{D.37}$$

$$area: \ \dot{a} = X \ . \tag{D.38}$$

The relevant initial conditions are obviously:

$$v^0 = 0 \, , \tag{D.39}$$

$$a^0 = 0 \, . \tag{D.40}$$

The solution of the variation of F is constrained by the final conditions of Eq. (D.37) and Eq. (D.38):

$$v^* = \frac{2}{3}\beta \, , \tag{D.41}$$

$$a^* = 2 - \frac{X^{*2}}{2} \, . \tag{D.42}$$

where β is the reduced volume of choice.

More detailed analysis of the Euler-Lagrange equations shows a singularity point at $s = 0$. To evaluate asymptotic solutions, the general shape equation has to be determined. To do so, it is convenient to eliminate γ from the differential equations. This is done by first rewriting Eq. (D.12) as $\gamma = \gamma\left(\ddot{\psi}, \dot{\psi}, \psi, r\right)$ and then inserting the expression obtained for γ into Eq. (D.34) for h = 0. This gives the general equation of the shape in the following form:

$$\ddot{\psi} + \frac{1}{2}\dot{\psi}^2 + \left(\dot{\psi} + 2f\right)\frac{\dot{X}}{X} - \frac{1}{2}\frac{\sin^2\psi}{X^2} - \frac{\dot{X}\sin\psi}{X^2} - p \cdot \sin\psi - p\frac{\dot{X} \cdot X}{2} - \sigma = 0 \tag{D.43}$$

In the limit of $s \to 0$ and $r \to 0$, and expanding to the first order, this equation can be rewritten as:

$$\ddot{\psi} + \frac{\dot{\psi}}{X} - \frac{\psi}{X^2} = \sigma - \frac{2f}{X} \tag{D.44}$$

The solution to this differential equation can be assumed to be in the form of a Taylor expansion:

$$\psi = aX \ln X + bX + cX^2 . \tag{D.45}$$

Using the auxiliary condition Eq. (D.27), the derivatives of ψ with respect to the arclength s can be easily found and by comparison of coefficients after the substitution, it can be easily read:

$$a = -f , \tag{D.46}$$

$$c = \frac{\sigma}{3} . \tag{D.47}$$

According to presented development the coefficient b can undertake any value. But in the case of no force, the curvature at the north pole is finite in this parameterization, and equal to the principal curvature. Therefore it has to stand:

$$b = U^0 . \tag{D.49}$$

The final set of differential equations with associated boundary conditions is presented in Table D.1. It should be noticed that asymptotic solutions have to be found for most of the relevant variables. This is done by an expansion to the first order around the exact value of the coordinate at $s = 0$.

For a chosen β, the above equations have to be solved simultaneously to satisfy the given boundary conditions by adjusting the set of free parameters (s^*, p, σ, U^0, Z^0).

It is easy to see that if $s = 0$, then $X = 0$, which leads to a divergence of the second equation in the table. To avoid this singularity, in the numerical study, the asymptotic values have to be used for initial conditions. It is sufficient to take $ds^0=10^{-4}$, and consistently with this, all other values.

Table D.1: The set of equations and boundary conditions that, when solved, produce a shape of an adhered vesicle under force.

Equations	Initial Conditions Asimptotic conditions	Final Conditions
	$s = 0$ $s = 0 + \Delta s$	$s = s^*$
$\dot{\psi} = U$	0 $-fX \ln X + U^0 X$	π
$\dot{U} = -U\frac{\cos\psi}{X} + \frac{pX}{2}\cos\psi + \frac{\gamma}{X}\sin\psi - \frac{f}{X}\cos\psi + \frac{\sin\psi\cos\psi}{X^2}$	U^0 $U^0 - f(\ln X + 1) + \frac{2}{3}\sigma X$	$\sqrt{2w}$
$\dot{\gamma} = \frac{U^2}{2} - \frac{\sin^2\psi}{2X^2} + \sigma + pX\sin\psi$	0 $\sigma \cdot \Delta s$	γ^*
$\dot{X} = \cos\psi$	0 Δs	X^*
$\dot{Z} = -\sin\psi$	Z^0	0
$\dot{v} = \frac{X^2}{2}\sin\psi$	0	$\frac{2}{3}\beta$
$\dot{a} = X$	0 Δs	$2 - \frac{X^{*2}}{2}$

In the presented work, the study of the phase diagram has been restricted to the variation of the adhesion strength w, the force f, for a given reduced volume of the vesicle β.

Bibliography

Albersdörfer

A., T. Feder and E. Sackmann. 1997. *Adhesion-induced domain formation by interplay of long-range repulsion and short-range attraction force: A model membrane study*. Biophys. J. **73**:245-257.

Alberts B., D. Bray, J. Lewis, M. Raff, K. Roberts and J. D. Watson. 1994. *Molecular biology of the cell, 4th edition*. Garland Publishing, Inc. New York.

Alon R., D. A. Hammer, and T. A. Springer. 1995. *Lifetime of the P-selectin-carbohydrate bond and its response to tensile force in hydrodynamic flow*. Nature **374**:539–542.

Alon R. and S. Feigelson. 2002. *From rolling to arrest on blood vessels: leukocyte tap dancing on endothelial integrin ligands and chemokines at sub-second contacts*. Semin. Immunol. **14**:93-104.

Andelman D. 1995. *Electrostatic properties of membranes: The Poisson-Boltzman theory.* In *Handbook of biological physics*. R. Lipowsky and E. Sackmann editors. Elsevier Science. Amsterdam. 605-640.

Balaban N.Q., U. S. Schwarz, D. Riveline, P. Goichberg, G. Tzur, I. Sabanay, D. Mahalan, S. Safran, A. Bershadsky, L. Addadi, and B. Geiger. 2001. *Force and focal assembly: A close relationship studied using electric micropatterned substrates.* Nature Cell Bio. **3**:466-472.

Baeckmark T., G. Elender, D. Lasic and E. Sackmann.1995. *Conformational transitions of mixed monolayers of phospholipids and polyethylene-oxide lipopolymers and interactionforces with solid surfaces*. Langmuir **11**:3975-3987.

Bell, G. I. 1978. *Models for the specific adhesion of cells to cells*. Science **200**:618-627.

Bell, G. I., M. Dembo and P. Bongrand. 1984. *Cell adhesion: Competition between non-specific repulsion and specific bonding*. Biophys. J. **45**:1051-1064.

Berndl K., J. Käs, R. Lipowsky, E. Sackmann and U. Seifert. 1990. *Shape transformations of giant vesicles: extreme sensitivity to bilayer asymmetry*. Europhys. Lett. **13**:659-664.

Bogan B. and K. Thorn. 1998. *Anatomy of hot spots in protein interfaces*. J. Mol. Biol. **280**:1-9.

Bongrand P. 1989. *Ligand-receptor interactions*. Rep. Prog. Phys. **62**:921-968.

Boulbitch A., Z. Guttenberg and E. Sackmann. 2001. *Kinetics of membrane adhesion mediated by ligand-receptor interaction studied with biomimetic system*. Biophys. J. **81**:2743-2751.

Born M. And E. Wolff. 1999. *Principles of Optics, 7th edition*. Cambridge University Press. Cambridge.

Brian A. A. and H. M. McConnell. 1984. *Allogenic stimulation of cyto-toxic T-cells by supported planar membranes*. Proc. Nat. Acad. Sci. U.S.A. **81**:6159-6163.

Brochard-Wyart F. and P. G. de Gennes. 2002. *Adhesion induced by mobile binders: Dynamics*. Proc. Nat. Acad. Sci. U.S.A. **99**:7854-7859.

Bruinsma R., A. Behrisch and E. Sackmann. 2000. *Adhesive switching of membranes: experiment and theory*. Phys Rev E **61**: 4253-426.

Bruinsma R. and E. Sackmann. 2001. *Bioadhesion and dewetting transition*. C. R. Acad. Sci. IV-Phys. **2**:803-815.

Bukman D. J., J. H. Yao and M. Wortis.1996. *Stability of cylindrical vesicles under axial tension.* Phys. Rev. E **54**:5463–5468.

Canham P. B. 1970. *The minimum energy of bending as a possible explanation of the*

biconcave shape of the human red blood cell. J. Theoret. Biol. **26**:61-81.

Chapman D. L. 1913. *A contribution to the theory of electrocapillarity*. Philos. Mag. **25**:475.

Coakley W. T., H. Darmani and A. J. Baker. 1991. *Membrane contact induced between erythrocytes by polycations, lectins and dextran*. In *Cell and Model Membrane Interactions*. S. Ohki, editor. Plenum Press, New York. 25-46.

Coombs D., M. Dembo, C. Wofsy and B. Goldstein. *Equilibrium thermodynamics of cell-cell adhesion mediated by multiple ligand-receptor pairs*. Biophys. J. **86**:1408-1423.

Darnell J., H. Lodish, and D. Baltimore. 1990. *Molecular Cell Biology*. Scientific American Books, NY.

Dembo M., D. C. Torney, K. Saxman, and D. Hammer. 1988. *The reaction-limited kinetics of membrane-to-surface adhesion and detachment*. Proc. Roy. Soc. London B **234**:55–83.

Dimitrov D. S. and M. I. Angelova. 1988. *Lipid swelling and liposome formation mediated by electric fields*. Journal of Electroanalytical Chemistry. **253**: 323-336.

Dustin M. L. and L. B. Dustin. 2001. *The immunological relay race: B cells take antigen by synapses*. Nature Immunology **2**:480-481.

Evans E. A. 1974. Bending resistance and chemically induced moments in membrane bilayers. Biophys. J. **14**:923-931.

Evans E. A. 1994. *Physical actions in biological adhesion*. In *Handbook of Physics and Biological System*s. R. Lipowsky and E. Sackmann, editors. Elsevier Science, Amsterdam. 697-728.

Evans E. and K. Ritchie. 1997. *Dynamic strength of molecular adhesion bonds*. Biophys. J. **72**:1541–1555.

Evans E., A. Leung, V. Heinrich, and C. Zhu. 2004. *Mechanical switching and coupling between two dissociation pathways in a P-selectin adhesion bond*. Proc. Nat. Acad. Sci.

U.S. A. **101**:11281-11286.

Fisher L. 1993. *Forces between biological surfaces*. J. Chem. Soc. Faraday Trans. **89**:2567-2582.

Finger E. B., K. D. Puri, R. Alon, M. B. Lawrence, U. H. Von Andrian and T. A. Springer. 1996. *Adhesion through L-selectin requires a threshold hydrodynamic shear*. Nature **379**:266-269.

Florin E. L., V. T. Moy, and H. E. Gaub. 1994. *Adhesion forces between individual ligand-receptor pairs*. Science **264**:415–417.

Fragneto G., T. Charitat, F. Graner, K. Mecke, L. Perino-Gallice, E. Bellet-Amalric. 2001. *A fluid floating bilayer*. Europhys. Lett. **53**:100-106.

Fritz J., A. G. Katopodis, F. Kolbinger and D. Anselmetti. 1998. *Force-mediated kinetics of single P-selectin/ligand complexes observed by atomic force microscopy*. Proc. Nat. Acad. Sci. U.S.A. **95**:12283-12288.

Galla, H.-J., W. Hartmann, U. Theilen and E. Sackmann. 1979. *On two-dimensional passive random walk in lipid bilayers and fluid pathways in biomembranes.* J. Membrane Biol. **48**: 215-236.

Gege C., S. Oscarson and R. R. Schmidt. 2001. *Synthesis of fluorescence labeled sialyl-Lewis^X glycosphingolipids*. Tetrahedron Lett. **105**:5178-5185.

Gönnenwein S., M. Tanaka, B. Hu, L. Moroder and E. Sackmann. 2003. *Functional Incorporation of Integrins into solid supported membranes on ultrathin films of cellulose – Imapct on adhesion.* Biophys. J. **85**:646-655.

Gönnenwein S. 2003. *Generic and specific cell adhesion: Investigations of a model system by Micro-Interferometry*. PhD Thesis at the Physics Department of the Technical University in Munich.

Gouy G. 1910. *Sur la constitution de la charge électrique a la surface d'un électrolyte*. J. Phys. Theor. Appl. **9**:455-468.

Grakoui A, S. K. Bromley, C. Sumen, M. M. Davis, A. S. Shaw, P. M. Allen and M. L.

Dustin. 1999. *The immunological synapse: A molecular machine controlling T cell activation*. Science **285**:221-227.

Greenberg, A. W., D. K. Brunk and D. A. Hammer. 2000. *Cell-free rolling mediated by L-selectin and sialyl-Lewis^X reveals the shear threshold effect*. Biophys.l J. **79**:2391-2402.

Guttenberg Z., A. Bausch, B. Hu, R. Bruinsma, L. Moroder, and E. Sackmann. 2000. *Measuring ligand-receptor unbinding forces with magnetic beads: Molecular leverage.* Langmuir **16**:8984–8993.

Guttenberg Z., B. Lorz, E. Sackmann and A. Boulbitch. 2001. *First-order transition between adhesion states in a system mimicking cell-tissue interaction.* Europhys. Lett. **54**:826-832.

Guyton A. C. 1997. *Immunity, allergy, blood groups, and transfusion.* In *Human Physiology and Mechanisms of Disease. 6th ed.* J. E. Hall, editor. W.B. Saunders Company. Philadelphia, PA. 291-293.

Heinrich V. and R. E. Waugh. 1996. *A piconewton force transducer and its application to measurement of the bending stiffness of phospholipid membranes.* Ann. Biomed. Eng. **24**:595-605.

Helfrich W. 1973. *Elastic properties of lipid bilayers: Theory and possible experiments.* Naturforsch. C **28**:693-703.

Helmholtz H. L. 1879. *Studien über electrische Grenzschichten*. Ann. Phys. Leipzig **7**:337-382.

Hiemenz P. C. and R. Rajagopalan. 1997. *Principles of colloids and surface chemistry. 3rd edition*. Marcel Dekker, New York.

Hochmuth R. M. and W. D. Marcus. 2002. *Membrane tethers formed from blood cells with available area and determination of their adhesion energy.* Biophys. J. **82**:2964-2969.

Israelachvili J. N. and G. E. Adams. 1976. *Direct measurements of long-range forces between two mica surfaces in 10^{-4} to 1 M KNO_3 solutions*. Nature 262:774-776.

Israelachvilli J. N. 1992. *Intermolecular and Surface Forces. 2nd edition*. Academic Press. London.

Israelachvili J. N. and H. Wennerstrom. 1992. *Entropic forces between amphiphilic surfaces in liquids.* J. Phys. Chem. **96**:520-531.

Jain M. K. 1988. *Introduction to biological membranes*. John Wiley & Sons, NY.

Janiak M. J., D. M.Small, G. G. Shipley. 1979. *Temperature and compositional dependence and structure of hydrated dimyristoyl lecithin*. J. Biol. Chem. **254**:6068-6078.

Jürlicher F., U. Seifert and R. Lipowsky. 1998. *Conformal degeneracy and conformal diffusion of vesicles*. Phys. Rev. Lett. **71**:452-455.

Kalb E., S. Frey and L. Tamm.1992. *Formation of supported planar bilayers by fusion of vesicles to supported phospholipid monolayers.* Biochim. Biophys. Acta **1103**:307-316.

Käs J., and E. Sackmann. 1991. *Shape transitions and shape stability of giant phospholipid vesicles in pure water induced by area-to-volume changes.* Biophys. J. **60**:825-844.

Keller C., K. Glasmästar, V. Zhdanov and B. Kasemo. 2000. *Formation of supported membranes from vesicles. Phys*. Rev. Lett. **84**:5443-5446.

Komura S. and D. Andelman. 2000. *Adhesion-induced lateral phase separation in membranes*. Euro. Phys. J. E **3**:259-271.

Kraus M., U. Seifert, and R. Lipowsky. 1995. *Gravity-induced shape changes of bound vesicles*. Europhys. Lett. **32**:431-436.

Küchner M. and E. Sackmann. 1996. *Ultrathin hydrated dextran films grafted on glass: preparation and characterization of structural, viscous and elastic properties by quantitative micro-interferometry*. Langmuir **12**:4866-4876.

Küchner M., R. Tampé and E. Sackmann. 1994. *Lipid mono- and bilayer supported on polymer films:composite polymer-lipid films on solid substrates*. Biophys. J. **76**:217-226.

Landau L. D. and E. M. Lifshitz 1958. *Statistical Physics*, vol 5. Pergamon, London.

Langner M., D. Cafiso, S. Marcelja and S. G. L. McLaughlin. 1990. *Electrostatics of phosphoinositide bilayer membranes. Theoretical and experimental results*. Biophys. J. **57**:335-349.

Lasic D. 1993. *Liposoms*, *From Physics to Application*. Elasevier Science. Amsterdam.

Leckband D. 1995. *The surface forces apparatus - a tool for probing molecular protein interactions*. Nature **376**:617–618.

Leckband D. and J. Israelachvili. 2001. *Intermolecular forces in biology*. Quarterly Reviews of Biophysics **34**:105–267.

Leibler S. and R. Lipowsky. 1987. *Complete unbinding and quasi-long-range order in lamellar phases*. Phys. Rev. B **35**:7004-7009.

Limozin, L. and E. Sackmann. 2002. *Polymorphism of cross-linked actin networks in giant vesicles*. Phys. Rev. Lett. **89**:168103.

Lipowsky R. and S. Leibler. 1986. *Unbinding transitions of interacting membranes*. Phys. Rev. Lett. **56**:2541-2544.

Lipowsky R. 1995. *Generic Interactions of flexible membanes*. In *Handbook of Physics and Biological System*. R. Lipowsky and E. Sackmann, editors. Elsevier Science, Amsterdam. 524-596.

Lipowsky R. 1996. *Adhesion mediated via anchored stickers*. Phys. Rev. Lett. **77**:1652-1656.

Lipowsky R. 1997. *Flexible membranes with anchored polymers*. Colloids Surf. A **128**:255-264.

Lorz B. G. 2003. *Etablierung enines Modellsystems der Zelladhäsion über spezifische Bindungen geringer Affinität – eine mikrointerferometrische Studie*. PhD Thesis. Physics Department. Technische Universität München.

Lorz B. G., A.-S. Smith, C. Gege and E. Sackmann. *Adhesion of Giant Vesicles Mediated by Weak Binding of sialyl-Lewis^X to E-Selectin: Influence of Lipopolymers*. In

preparation.

Marcelja S. and N. Radic. 1976. *Repulsion of interfaces due to boundary water.* Chem. Phys. Lett. **42**:129-130.

Marra J. and J. N. Israelachvilli. 1985. *Direct measurements of forces between phosphatidylcholine and phosphatidylethanolamine bilayers in aqueous-electrolyte solutions*. Biochem. **24**:4608-4618.

Marx S., J Schilling, E. Sackmann and R. Bruinsma. *Helfrich repulsion and dynamical phase-separation of multi-component surfactant bilayers.* Phys. Rev. Lett. **88**:1380102.

Matlin K. S. And M. J. Caplan.1992. *Epithelial cell structure and polarity. In The Kidney: Physiology and Pathophysiology*. D. W. Seldin and G. Giebisch, editors. Raven Press, Ldt. NY. 447-473.

McEver R. P., K. L. Moore and R. D. Cummings. 1995. *Leukocyte trafficking mediated by selectin-carbohydrate interactions.* J. Biol. Chem. **270**:11025-11028.

Mehta A. D., M. Rief, J. A. Spudich, D. A. Smith, and R. M. Simmons. 1999. *Single-molecule biomechanics with optical methods*. Science **283**:1689–1695.

Mecke K. R., T. Charitat and F. Graner. 2002. *Fluctuating lipid bilayer in an arbitrary potential: theory and experimental determination of bending rigidity*. Langmuir **19**:2080-2087.

Merkel R., P. Nassoy, A. Leung, K. Ritchie, and Even Evans. 1999. *Energy landscapes of receptor-ligand bonds explored with dynamic force spectroscopy*. Nature **397**:50–53.

Merkel. R. 2001. *Force spectroscopy on single passive biomolecules and single biomolecular bonds.* Phys. Rep. **346**:344–385.

Michalet X. and D. Bensimon. 1995. *Observation of stable shapes and conformal diffusion in genus 2 vesicles*. Science **269**:666-668.

Moore K. L., S. F. Eaton, D. E. Lyons, H. S. Lichenstein, R. D. Cummings and R. P. McEver. 1994. *The P-selectin glycoprotein ligand from human neutrophils displays sialylated, fucosylated, O-linked poly-N-acetyllactosamine***.** J. Biol. Chem **269**:23318-23327.

Mutz M. and D. Bensimon.1991. *Observation of toroidal vesicles*. Phys.Rev. A **43**:4525-4527.

Mutz R. And W. Helfrich. 1989. *Unbinding transition of a biological model membrane*. Phys. Rev. Lett. **62**:2881-2884.

Nardi J., R. Bruinsma and E. Sackmann. 1999. *Adhesion induced reorganisation of charged fluid membranes*. Phys. Rev. E **58**:6340-6354.

Netz R. R. 2001. *Field-theoretic approaches to classical charged systems*. In *Electrostatic effects in soft matter and biophysics*. C. Holm *et al.* editors. Kluwer Academic Publishers. Dordrecht.

Netz R. R. 2001.*Electrostatics of counter-ions at and between planar charged walls: From Poisson-Boltzman to strong coupling theory.* Euro. Phys. J. E **5**:557-574.

Nguyen-Duong M., K. W. Koch and R. Merkel. 2003. *Surface anchoring reduces the lifetime of single specific bonds.* Europhys. Lett. **61**:845-851.

Noppl-Simson D. A. and D. Needham. 1996. *Avidin-Biotin interactions at vesicle surfaces: adsorption and binding, cross-bridge formation, and lateral interactions*. Biophys. J. **70**:1391-1401.

Parsegian V. A and R. P. Rand.1995. *Interaction in membrane assemblies*. In *Handbook of biological physics*. R. Lipowsky and E. Sackmann editors. Elsevier Science. Amsterdam. 645-687.

Petri, D. S. F., G. Wenz, P. Schunk and T. Schimmel. 1999. *An improved method for the assembly of amino-terminated monolayers on SiO_2 and the vapor deposition of gold layers*. Langmuir **15**:4520-4523.

Ploem J. 1975. *Reflection contrast microscopy as a tool for investigation of attachment of living cells to a glass surface*. Mononuclear Phagocytes in Immunity, Infection and Pathology. Blackwell Scientific Publications. Oxford.

Prechtel K., A. Bausch, V. Marchi-Artzner, M. Kantlehner, H. Kessler, R. Merkel. 2002. *Dynamic force spectroscopy to probe adhesion strength of living cells*. Phys. Rev. Lett. **89**:028101.

Purrucker O., A. Förtig, R. Jordan and M. Tanaka. 2004. *Supported membranes with well-defined polymer tethers – Incorporation of cell receptors*. ChemPhysChem **5**:327-335.

Rand R. P. and V. A. Parsegian. 1989. *Hydration forces between Phospholipid bilayers*. Biochim. Biophys. Acta **988**:351-376.

Sackmann E. 1995. *Physical basis of self-organization and function of membranes: Physics of vesicle*. In *Handbook of Biological Physics*. R. Lipowsky and E. Sackmann editors. Elsevier Science. Amsterdam. chap.5.

Sackmann E. 1996. *Supported membranes: Scientific and practical applications*. Science **271**:43-48.

Sackmann E. and R. F. Bruinsma. 2002. *Cell adhesion as a wetting transition?* ChemPhysChem. **3**:262-269.

Safiniya C., R. Roux, G. Smith, S. Sinha, P. Dimon, N. Clark and A. Bellocq. 1986. *Steric interaction in a model multimembrane system – a synchrotron X-ray study*. Phys. Rev. Lett. **57**:2718-2721.

Salafsky J., J. Groves and S. Boxer. 1996. *Architecture and function of membrane proteins in planar supported bilayers: A study with photosynthetic reaction centers*. Biochem. **35**:14773-14781.

Schilling J. 1999. *Entwicklung einer Echtzeit-Bildverarbeitungssoftware undi digitaler Videoaufnehmetechnik zur quantitativen Mikrorheonetie von Aktin_Netzwerken*. Diploma thesis. Physics Department. Technische Universität München.

Schwarz U. S., N. Q. Balaban, D. Riveline, A. Bershadsky, B. Geiger and S. A. Safran. 2002. *Calculation of forces at focal adhesions from elastic substrate data: the effect of localized force and the need for regularization*. Biophys. J. **83**:1380-1394.

Schwarz U. S., N. Q. Balaban, D. Riveline, L. Addadi, A. Bershadsky, S. A. Safran and B. Geiger. 2003. *Measurement of cellular forces at focal adhesions using elastic micro-*

patterned substrates. Mat. Sci. Eng. C **23**: 387-394.

Seifert U. and R. Lipowsky. 1990. *Adhesion of vesicles*. Phys. Rev. A **42**: 4768-4771.

Seifert U. 1991. *Vesicles of toroidal topology*. Phys. Rev. Lett. **66**:2404-2407.

Seifert U. 1991. *Conformal transformations of vesicles*. J Phys. A: Math. Gen. **24**:L573-L578.

Seifert U., K. Berndl and R. Lipowsky. 1991. *Shape transformations of vesicles: Phase diagrams for spontaneous-curvature and bilayer-coupling models*. Phys. Rev. A **44**:1182-1202.

Seifert U. 1997. *Configurations of fluid membranes and vesicles.* Adv. Phys. **46**:13-137.

Seifert. U. *Rupture of multiple parallel molecular bonds under dynamic loading*. 2000. Phys. Rev. Lett. **84**:2750–2753.

Sengupta K., J. Schilling, S. Marx, M. Fischer, A. Bacher and E. Sackmann. 2003. *Mimicking tissue surfaces by supported membrane thin layer of hyaluronic acid*. Langmuir **19**:1775-1781.

Simson D. A., M. Stringl, M. Hohenadl, and R. Merkel. 1999. *Statistical breakage of single protein A-IgG bonds reveals crossover from spontaneous to force-induced bond dissociation*. Phys. Rev. Lett. **83**:652–655.

Shelley C., N. Da Silva and J. M. Teodoridis. 2001. *During U937 monocyte differentiation repression of the CD43 gene promoter is mediated by the single stranded DNA binding*. British J. of Hematology **115**:159-166.

Singer S. and G. Nicolson. 1972. *The fluid mosaic model of the structure of cell membranes*. Science **175**:720-731.

Smith A.-S., B. Lorz, U. Seifert, E. Sackmann. *Antagonist-induced unbinding of specifically adhered vesicles*. Submitted for publication.

Smith A.-S., E. Sackmann and U. Seifert. 2004. *Pulling tethers from adhered vesicles*. Phys. Rev. Lett. **92**:208101.

Smith A.-S., E. Sackmann and U. Seifert. 2003. *Effects of a pulling force on the shape of a bound vesicle*. Europhys. Lett. **64**:281-288.

Smith A.-S., S. Gönnenwein, U. Seifert and E. Sackmann. *Pulling on adhered vesicles: Comparison of theory and experiment*. In preparation.

Springer T. A. 1990. *Adhesion receptors of the immune system*. Nature **346**:425-434.

Springer T. A. 1994. *Traffic signals for lymphocyte recirculation and leukocyte emigration: The multi-step paradigm*. Cell **76**:301-314.

Svetina S., A. Ottova-Leitmanova, and R. Glaser. 1982. *Membrane bending energy in relation to bilayer couples concept red blood cell transformations*. J. Theoret. Biol. **94**:13-23.

Torney D. C., M. Dembo and G. I. Bell. 1986. *Thermodynamics of cell adhesion II*. Biophys. J. **49**:501-507.

Tozeren A., K. L. P. Sung, L. A. Sung, M. L. Dustin, P. Y. Chan, T. A. Springer, and S. Chien. 1992. *Micromanipulation of adhesion of Jurkart cell to a planar membrane containing LFA-3 molecules*. Cell Biol. **116**:997-1006.

Veatch. S. L. and S. L. Keller. 2002. *Organization in lipid membranes containing cholesterol.* Phys. Rev. Lett. **89**:268101.

Voet D., J. Voet, and W. Pratt. 1995. *Biochemistry, 2nd edition*. John Wiley & Sons, Inc. New York.

Waats T., H. Gaub and H. McConnell. 1986. *T-cell mediated association of peptide antigen and major histocompatibility complex protein detected by energy transfer in an evanescent field*. Nature **320**:179-181.

Wegner G. 1992. *Ultrathin films of polymers: Architecture, characterization and properties*. Thin Solid Films **216**:105-116.

Weikl T. R. and R. Lipowsky. 2001. *Adhesion-induced phase behavior of multicomponent membranes*. Phys. Rev. E **64**:011903.

Weikl T. R., R. R. Netz and R. Lipowsky. 2000. *Unbinding transitions and phase separation of multicomponent membranes*. Phys. Rev E **62**: R45-R47.

Weiss T. F. 1998. *Cellular Biophysics. Volume 1: Transport*. A Bradford Book. The MIT Press. Cambridge, MA. Chapter 1.

Winiski A. P., M. Eisenberg, M. Langner and S. McLaughlin. 1988. *Fluorescent probes of electrostatic potential 1nm from the membrane surface*. Biochem. **27**:386-392.

Zinkl G. M., A. Zuk, P. van der Bijl, G. van Meer and S. Matlin. 1996. *An antiglycolipid antibody inhibits Madian-Darby canine kidney cell adhesion to laminin and interferes with basolateral polarization and tight junction formation*. J. Cell Biol. **133**:695-708.

Zuckerman D. M. and R. F. Bruinsma. 1995. *Statistical mechanics of membrane adhesion by reversible molecular bonds*. Phys. Rev. Lett. **74**:3900-3903.

Zuckerman D. M. and R. F. Bruinsma. 1998. *Vesicle-vesicle adhesion by lock-and-key molecules: Debye-Hückel theory and Monte Carlo simulation*. Phys. Rev. E **57**:964-977.

Curriculum Vitae

- **Personal details:**

Name:	Ana-Sunčana Smith
Birth name:	Barišić
Date of birth:	03/03/1975
Place of birth:	Zagreb, Croatia
Marital status:	married, 1 child

- **Education:**

Since Mar. 2002:	PhD student at the Institut für Biophysik E22, Technische Universität München. Germany.
Jan. 2000-Jun. 2001:	Completion of diploma work at the Institute for Physics, University of Zagreb, Croatia. Graduation.
Mar. 1999-Nov.1999:	Visiting student at Australian National University, RSPHYSSE, Department of Applied Mathematics, Canberra, A.C.T. Beginning of diploma work.
Oct. 1993-Mar. 1999:	Studies at the Faculty for Physics and Mathematics, University of Zagreb, Croatia.
Mar.1993-July 1993:	V. Gymnasium for natural sciences, Zagreb, Croatia.
Sept.1992-Mar. 1993:	Ecole Secondaire „Camille See“, Paris 14, France.
Sept. 1989-Jul. 1993:	V. Gymnasium for natural sciences, Zagreb, Croatia.
Sept. 1981-July 1989:	Primary School (OŠ „Mladost“), Zagreb, Croatia.

List of Publications

1. Effects of a Pulling Force on the Shape of a Bound Vesicle

   Smith A.-S., E. Sackmann, and U. Seifert. *Europhys. Lett*. **64**, (2003), 281-287.

2. Pulling tethers from adhered vesicles

   Smith A.-S., E. Sackmann, and U. Seifert. *Phys. Rev. Lett*. **92**, (2004), 208101/1-4.

3. Dewetting Phenomena in Specifically Adhered Vesicles Induced by Antagonists

   Smith A.-S., B. Lorz, U. Seifert, and E. Sackmann. *Biophys. J.* Submitted for publication.

4. Effective Adhesion Strength of Specifically Bound Vesicles

   Smith A.-S., and U. Seifert. *Phys. Rev. E*. Submitted for publication.

5. Pulling on Vesicles Adhered by Mobile Receptors and Ligands

   Smith A.-S., S. Goennenwein, U. Seifert and E. Sackmann. In preparation.

6. Unbinding of Specifically Adhered Giant Vesicles by Vertical Magnetic Tweezers: Comparison of Systems with High and Low Adhesion Affinities

   Goennenwein S., B. Lorz, A.-S. Smith and E. Sackmann. In preparation.

7. The influence of repelling molecules in vesicles on the adhesion processes

   Smith A.-S., and U. Seifert. In preparation.

8. Adhesion of Giant Vesicles Mediated by Weak Binding of Sialyl-LewisX to E-selectin: Influence of Lipopolymers

   Lorz B., A.-S. Smith, C. Gege and E. Sackmann. In preparation.

9. The Hydrophobic Effect: Angular Dependency of the Solute-Solvent Correlation Function

   Smith A.-S. In preparation.

List of Symbols and Abbreviations

a	area of a ligand on the vesicle surface
BSA	album bovine serum
C_v	number concentration of antibodies in solution.
DMPC	1,2-dimyristoyl-sn-glycero-3-phosphocholine
DMPE-PEG2000	1,2-dimyristoyl-sn-glycero-3 phosphoethanolamine-N-polyethylene-glycol
DN_b	absolute density of bound ligands in the contact zone
DN_f	absolute density of free ligands in the contact zone
DOPC	1,2-dioleoyl-sn-glycero-3-phosphocholine
E_a	binding strength of a ligand-receptor pair
E_b	antibody-receptor binding strength
E_{bend}	total bending energy of a shape
F	free energy
FAC	focal adhesion center
HEPES	4-(2-Hydroxyethyl)piperazine-1-ethanesulfonic acid
k_B	Boltzmann constant
N_b	number of ligands that are in the contact zone and bound to receptors
n_b	fraction of total ligands that are in the contact zone and bound to
n_b^{eq}	equilibrium fraction of bound ligands
N_f	number of ligands that are in the contact zone and free
n_f	fraction of total ligands that are in the contact zone and free
N_{free}	number of free ligands in the vesicle
N_t	total number of ligands in a vesicle
n_t	total surface concentration of ligands in a vesicle
p_a	total density of antibodies on the substrate
p_b	density of antibodies on the substrate bound to receptors
p_f	density of antibodies on the substrate not bound to receptors
RGD	amino acid sequence Arg-Gly-Asp
RICM	reflection interference contrast microscope
R_{ligand}	gyration radius of a ligand
R_{vescle}	vesicle radius
S	entropy
S_c	number of sites forming the contact zone of the vesicle.

s_c	fraction of the total vesicle area forming the contact zone:
S_c^*	critical number of sites in the contact zone
s_c^{eq}	equilibrium contact zone
$s_c^{\max}$	fraction of the total vesicle area forming a contact zone of a spherical
S_t	total number of sites in the vesicle
sLe^X	sialyl-Lewis^X
T	temperature
TEM	tunneling electron microscope
TRIS	Tris-(hydroxymethyl)-aminomethane
U	internal energy
v	reduced volume
W	adhesion energy
w	effective adhesions trength in contrinuous models
κ	bending rigidity
Π	lateral osmotic pressure of antibodies
ρ_r	density of receptors on the substrate
ω	effective adhesion strength in discrete models
ω_0	maximal effective adhesion strength